People's Democratic Republic of Algeria
Ministry of Higher Education and Scientific Research
University of El Oued
Faculty of Nature and Life Sciences
Department of Cellular and Molecular Biology

MASTER THESIS

In partial fulfilment of the requirements for the degree of Master

Major: Biological Sciences

Speciality: Toxicology

THEME

Design, Synthesis, and Multiscale Computational Evaluation of Ferrocenyl Acetylaniline Derivatives Targeting Oxidative Stress-Related Enzymes

Presented by:

- Abdallah MOUHADJER
- Mohammed Seghir MESBAHI

Jury Members:

• Dr.	Nawel HOUMRI	……	President
• Dr.	Khaoula ZEGHIB	……	Examiner
• Dr.	Elhafnaoui LANEZ	MCA	Supervisor
• Dr.	Mohammed Larbi BENAMOR	……	Co-Supervisor

Academic Year: 2025 – 2026

Acknowledgments

All praise is due to God, by whose grace good deeds are accomplished, and who granted me the strength, patience, and perseverance to complete this work and overcome the challenges encountered along the way.

With deep gratitude and sincere appreciation, I dedicate this humble work to the entire academic community, including all professors and administrative staff, whose continuous efforts, commitment, and dedication have greatly contributed to our intellectual and academic development. Their guidance and knowledge have been a constant source of inspiration throughout our journey.

I would like to express my special and heartfelt thanks to my supervisor, Dr. Elhafnaoui LANEZ, whose unwavering support, valuable guidance, and insightful remarks played a crucial role in the successful completion of this dissertation. His patience, encouragement, and academic rigor have profoundly influenced the quality of this work. I am truly grateful for his time, effort, and dedication, and I pray that he is rewarded abundantly for all that he has shared.

I also extend my sincere thanks to all my professors who have accompanied me throughout my academic journey, contributing to my education and shaping my path with their knowledge and wisdom.

My gratitude also goes to everyone who contributed, directly or indirectly, to the accomplishment of this work, whether through support, advice, or encouragement.

Finally, I dedicate this work to everyone who believed in me and supported me throughout this journey.

To all those who have taught me even a single letter, I dedicate this work.

All praise is due to God, at the beginning and the end.

Dédicaces

Dedicate this graduation to

To the Piece of my heart...

To the light of my eyes...

To the love of my life...

To the soul of my Mother

أسأل الله ان يرحمك

ويسكنك فسيح جناته

ويجعل قبرك روضة من رياض الجنة

And to whom he struggled and resisted

to get me to this point

My Father

And to all my family members,

had it not been for God's blessing,

then you would not have reached this day

And to all that the pen forgot

and the heart remembered

Thank You

Abdallah Mouhadjer

Dédicaces

Thank God who enabled me to complete this work,

dedicate the fruit of my effort and graduate this to:

To whom her prayers were the secret of my success,

the fountain of inexhaustible tenderness, my beloved mother,

God prolonged her age.

To the one who taught me patience and struggle,

and was my support at every step,

Dear Father,

may Allah protect him.

To my esteemed family members, brothers and sisters,

who have always been by my side,

I share my joy at this achievement.

To my dear friends, who accompanied me during my study career,

gave me support and encouragement.

To everyone who knew me and contributed a kind word or sincere prayer.

Mouhamed Seghir Mesbahi

Abstract

This thesis reports the synthesis, physicochemical characterisation and in silico evaluation of a series of ferrocenyl acetylaniline derivatives (FcMe2Ac, FcMe3Ac and FcMe4Ac), with the objective of elucidating the relationship between molecular structure, electronic properties and interaction behaviour. The target compounds were successfully synthesised via a nucleophilic substitution approach and isolated in good yields ranging from 48% to 80%. Structural confirmation was achieved using FT-IR, UV–Visible spectroscopy and nuclear magnetic resonance (^{1}H, ^{13}C and 2D NMR). The FT-IR spectra revealed characteristic absorption bands corresponding to N–H stretching (~3290–3445 cm^{-1}) and carbonyl groups (~1647–1651 cm^{-1}), while UV–Visible analysis showed absorption maxima in the range of 259–432 nm, associated with $\pi \rightarrow \pi^*$ and d–d transitions. NMR analysis confirmed the expected structural features, including signals for the ferrocenyl unit (~4.1–4.3 ppm) and aromatic protons (~6.6–7.8 ppm). Electrochemical investigations using cyclic voltammetry demonstrated a quasi-reversible Fe(II)/Fe(III) redox process, with formal potentials of 43.9, 51.0 and 57.5 mV for FcMe2Ac, FcMe3Ac and FcMe4Ac, respectively. Peak-to-peak separations (ΔEp = 87.8–115 mV) and current ratios close to unity confirmed quasi-reversible behaviour. Diffusion coefficients ranged from 1.11×10^{-7} to 5.74×10^{-7} $cm^2 \cdot s^{-1}$, while heterogeneous electron-transfer rate constants (k_s) varied from 0.14×10^{-3} to 0.62×10^{-3} $cm \cdot s^{-1}$, reflecting the influence of substitution on transport and kinetic properties. Density functional theory calculations revealed HOMO energies between −5.83 and −5.68 eV and HOMO–LUMO gaps ranging from 3.99 to 4.29 eV, indicating moderate chemical stability and reactivity. Global reactivity descriptors showed hardness values between 1.995 and 2.143 eV and electrophilicity indices up to 3.519 eV, while dipole moments increased from 3.82 to 5.12 D, reflecting enhanced molecular polarity. Molecular docking studies indicated favourable binding affinities, with binding energies ranging from −7.05 to −8.36 $kcal \cdot mol^{-1}$, where FcMe4Ac exhibited the strongest interaction. Molecular dynamics simulations (100 ns) confirmed the stability of the FcMe4Ac–protein complexes, with RMSD values stabilising around 0.10–0.25 nm and reduced residue fluctuations, indicating a stable binding mode. ADMET predictions demonstrated favourable pharmacokinetic profiles, including high gastrointestinal absorption, LogP values between 3.12 and 3.45, and no predicted mutagenic or hepatotoxic effects. Overall, the results demonstrate that structural modification of ferrocenyl derivatives significantly influences their electronic properties, electrochemical behaviour and interaction profiles. Among

the studied compounds, FcMe4Ac emerged as the most promising candidate, combining favourable redox properties, strong binding affinity, high dynamic stability and suitable pharmacokinetic characteristics.

Résumé

Cette thèse présente la synthèse, la caractérisation physicochimique et l'évaluation *in silico* d'une série de dérivés ferrocenyl acétylaniline (FcMe2Ac, FcMe3Ac et FcMe4Ac), dans le but d'établir des corrélations entre la structure moléculaire, les propriétés électroniques et le comportement interactionnel. Les composés cibles ont été synthétisés avec succès par une réaction de substitution nucléophile, avec des rendements compris entre 48 % et 80 %. Leur caractérisation structurale a été réalisée par des techniques spectroscopiques complémentaires, notamment FT-IR, UV–Visible et RMN (^{1}H, ^{13}C et 2D). Les spectres FT-IR ont mis en évidence des bandes caractéristiques correspondant à l'élongation N–H (~3290–3445 cm^{-1}) et au groupement carbonyle (~1647–1651 cm^{-1}). L'analyse UV–Visible a révélé des maxima d'absorption compris entre 259 et 432 nm, attribués aux transitions π→π* et d–d. Les spectres RMN ont confirmé les structures attendues, avec notamment des signaux caractéristiques du noyau ferrocenyl (~4,1–4,3 ppm) et des protons aromatiques (~6,6–7,8 ppm). L'étude électrochimique par voltampérométrie cyclique a montré un comportement quasi réversible du couple Fe(II)/Fe(III), avec des potentiels formels de 43,9, 51,0 et 57,5 mV pour FcMe2Ac, FcMe3Ac et FcMe4Ac, respectivement. Les séparations de pics (ΔEp = 87,8–115 mV) et les rapports de courant proches de l'unité confirment ce caractère quasi réversible. Les coefficients de diffusion varient de $1{,}11 \times 10^{-7}$ à $5{,}74 \times 10^{-7}$ $cm^2 \cdot s^{-1}$, tandis que les constantes de transfert électronique hétérogène (k_s) se situent entre $0{,}14 \times 10^{-3}$ et $0{,}62 \times 10^{-3}$ $cm \cdot s^{-1}$, traduisant l'influence de la substitution sur les propriétés cinétiques. Les calculs de théorie de la fonctionnelle de la densité (DFT) ont révélé des énergies HOMO comprises entre −5,83 et −5,68 eV et des écarts HOMO–LUMO de 3,99 à 4,29 eV, indiquant une stabilité chimique modérée associée à une réactivité contrôlée. Les descripteurs globaux montrent des valeurs de dureté comprises entre 1,995 et 2,143 eV et un indice d'électrophilie atteignant 3,519 eV. Le moment dipolaire augmente de 3,82 à 5,12 D, traduisant une polarité croissante avec la substitution. Les études de docking moléculaire ont mis en évidence des affinités de liaison favorables, avec des énergies comprises entre −7,05 et −8,36 $kcal \cdot mol^{-1}$, le composé FcMe4Ac présentant la meilleure interaction. Les simulations de dynamique moléculaire (100 ns) ont

confirmé la stabilité des complexes, avec des valeurs de RMSD stabilisées entre 0,10 et 0,25 nm et de faibles fluctuations résiduelles, indiquant un mode de liaison stable. Enfin, les prédictions ADMET ont révélé des profils pharmacocinétiques favorables, incluant une forte absorption gastro-intestinale, des valeurs de LogP comprises entre 3,12 et 3,45, et l'absence de toxicité mutagène ou hépatique prédite. Dans l'ensemble, cette étude démontre que la modification structurale des dérivés ferrocenyl influence significativement leurs propriétés électroniques, leur comportement électrochimique et leur capacité d'interaction. Parmi les composés étudiés, FcMe4Ac se distingue comme le candidat le plus prometteur, combinant des propriétés redox favorables, une forte affinité de liaison, une stabilité dynamique élevée et un profil pharmacocinétique adéquat.

الملخص

تتناول هذه المذكرة دراسة شاملة شملت التخليق، والتوصيف الفيزيائي-الكيميائي، والتقييم *الحاسوبي* (In silico) لسلسلة من مشتقات الفيروسينيل أسيتيـلانيلين (FcMe2Ac, FcMe3Ac, FcMe4Ac) وذلك بهدف فهم العلاقة بين البنية الجزيئية والخصائص الإلكترونية وسلوك التفاعل لهذه المركبات. تم تحضير المركبات المستهدفة بنجاح اعتماداً على تفاعل إحلال نووي، مع مردودات تراوحت بين 48% و80%. وقد تم تأكيد البنية الكيميائية باستخدام مجموعة من التقنيات الطيفية، بما في ذلك مطيافية الأشعة تحت الحمراء (FT-IR)، والأشعة فوق البنفسجية–المرئية (UV–Visible)، والرنين المغناطيسي النووي (^{1}H, ^{13}C, 2D)أظهرت أطياف FT-IR نطاقات مميزة تعود إلى اهتزازات N–H في المجال (cm^{-1} 3445–3290~) ومجموعة الكربونيل (cm^{-1} 1651–1647~) كما كشفت أطياف UV–Visible عن قمم امتصاص ضمن المجال 259–432 nmتعزى إلى انتقالات $\pi \rightarrow \pi^*$ و d–d. أما أطياف الرنين المغناطيسي فقد أكدت البنية المتوقعة، خاصة الإشارات الخاصة بنواة الفيروسين (ppm 4.3–4.1~) والبروتونات العطرية(ppm 7.8–6.6~) . أظهرت الدراسة الكهروكيميائية بواسطة الفولتمترية الدورية سلوكاً شبه انعكاسي لزوج الأكسدة-الاختزال Fe(II)/Fe(III) ، مع جهود قياسية بلغت 43.9 و51.0 و57.5 mVلكل من (FcMe2Ac, FcMe3Ac, FcMe4Ac) على التوالي. كما أن فرق الجهد بين القمتين 115–87.8 = ΔEp) (mVونسبة التيارات القريبة من الواحد تؤكد الطبيعة شبه الانعكاسية. تراوحت معاملات الانتشار بين 1.11×10^{-7} و5.74×10^{-17} $cm^2 \cdot s^{-1}$ ، بينما تراوحت ثوابت سرعة انتقال الإلكترون (k_s) بين 0.14×10^{-3} و0.62×10^{-13} $cm \cdot s^{-1}$ ، مما يعكس تأثير الاستبدال على الخصائص الحركية. كشفت حسابات نظرية دالة الكثافة (DFT) عن طاقات HOMO بين −5.83 و−5.68 eV، وفجوة طاقية (HOMO–LUMO) بين 3.99 و4.29eV ، مما يدل على استقرار كيميائي متوسط مع قابلية تفاعل ملائمة. كما أظهرت المعاملات العالمية قيم صلابة بين 1.995 و2.143eV ، ومؤشر إلكتروفيلية يصل إلى 3.519 eV. لوحظ أيضاً ازدياد في العزم ثنائي القطب من 3.82 إلى 5.12 ديباي، مما يشير إلى زيادة في قطبية الجزيئات. أظهرت دراسات الإرساء الجزيئي (Molecular Docking) طاقات ارتباط سالبة تتراوح بين −7.05 و−8.36 $kcal \cdot mol^{-1}$ ، حيث سجل المركب FcMe4Acأعلى ألفة ارتباط. كما أكدت محاكاة الديناميكا الجزيئية (100 نانوثانية) استقرار المعقدات، مع قيم RMSD مستقرة

ضمن المجال 0.10–0.25nm ، وانخفاض في تذبذب البقايا، مما يدل على ثبات التفاعل. أما نتائج التنبؤات الدوائية (ADMET)فقد أظهرت خصائص حركية دوائية ملائمة، من بينها امتصاص مرتفع على مستوى الجهاز الهضمي، وقيم LogPبين 3.12 و3.45، مع غياب السمية الطفرية والكبدية المتوقعة. بشكل عام، تُظهر هذه الدراسة أن التعديل البنيوي لمشتقات الفيروسين يؤثر بشكل واضح على خصائصها الإلكترونية وسلوكها الكهروكيميائي وقدرتها على التفاعل. ويبرز المركب FcMe4Acكأفضل مرشح ضمن هذه السلسلة، نظراً لما يتمتع به من خصائص إلكترونية ملائمة، وألفة ارتباط عالية، واستقرار ديناميكي جيد، إلى جانب خصائص دوائية واعدة.

Figure list

Table list

Contents

GENERAL INTRODUCTION

GENERAL INTRODUCTION

Ferrocene and its derivatives are among the most important classes of compounds in organometallic chemistry, owing to their remarkable structural stability and distinctive electronic properties. These features have made them a central focus in various fields, including chemistry, electrochemistry, and biological applications. Consequently, significant research efforts have been directed toward the design and development of new ferrocene-based derivatives capable of balancing stability and reactivity, particularly in the context of pharmaceutical applications. Among these, ferrocenyl acetylaniline derivatives have attracted increasing attention due to their hybrid structure, which combines an aromatic organic moiety with a redox-active ferrocene core, thereby imparting unique electronic characteristics and reactivity. [1]

In this context, there is a growing need for an integrated approach that combines chemical synthesis, spectroscopic characterization, electrochemical analysis, and advanced computational evaluation to better understand the relationship between molecular structure, physicochemical properties, and biological activity. Modern computational tools, such as Density Functional Theory (DFT), molecular docking studies, and molecular dynamics simulations, have become essential for predicting the behavior of these compounds and their interactions with biological targets, thereby accelerating drug discovery and reducing reliance on costly experimental procedures.

Accordingly, this study aims to investigate a series of ferrocenyl acetylaniline (FcMe2Ac, FcMe3Ac and FcMe4Ac) derivatives through a comprehensive methodology that integrates synthesis, structural characterization, electrochemical studies, and in silico evaluation. The objective is to elucidate the impact of structural modifications on electronic properties and reactivity, as well as to assess their potential as promising candidates for biological and pharmaceutical applications. [1]

This work is expected to contribute to a deeper understanding of this class of compounds and to open new perspectives for their utilization in various fields, particularly in the rational design of more effective and selective therapeutic agents.

This thesis is structured in two main parts as follow:

- The first part contains a bibliographical study and is divided into two chapters:
    - Chapter 1: Ferrocene Derivatives: Structure, Reactivity and Applications
    - Chapter 2: Computational Approaches in Molecular Modelling and Drug Design

- The second part concerns the experimental part and it is also divided into two chapters:
    - Chapter 1: Materials & Methods
    - Chapter 2: Results & Discussion

PART I : BIBLIOGRAPHIC STUDY

Chapter 1 : Ferrocene Derivatives : Structure, Reactivity and Applications

1. Introduction

Organometallic chemistry serves as a pivotal cognitive and structural nexus, bridging the realms of organic chemistry and coordination chemistry. Conceptually, organometallic compounds are defined by the presence of at least one direct chemical bond between a metal atom and a carbon atom belonging to an organic molecule, ion, or radical. From a physical perspective, this interaction is frequently characterized as a singular, polarized sigma bond ($M^{\delta+}-C^{\delta-}$). The nomenclature in this field is inherently hybrid, synthesizing rules from both organic and coordination systems to reflect the profound integration between these two chemical disciplines [2]. From a historical standpoint, the emergence of this field was marked by critical milestones rather than a singular event. These include the synthesis of Zeise's Salt in 1827—the first transition metal organometallic complex to be prepared—followed by the discovery of nickel carbonyl in 1890, and the revolutionary development of Grignard Reagents at the dawn of the 20th century, which significantly expanded the horizons of organic synthesis. Despite these early advances, the fundamental bonding paradigms and structural architectures of certain complex species remained a scientific enigma until the middle of the twentieth century [2 ،3].

The definitive paradigm shift occurred in 1951 with the independent discovery of ferrocene by Kealy, Pauson, and Miller [4, 3]. This discovery was far more than a mere addition to the chemical library; it represented a structural and theoretical breakthrough that deepened our comprehension of bonding, symmetry, and reactivity, effectively formalizing organometallic chemistry as an autonomous branch of science [2, 4].

Scientific progress did not terminate with ferrocene; rather, it catalyzed the development of an extensive family of "metallocenes," incorporating other transition metals such as ruthenium (ruthenocene), osmium (osmocene), cobalt (cobaltocene), and nickel (nickelocene). The exploration of ferrocene derivatives has since led to a proliferation of applications across diverse fields: these molecules function as sophisticated catalysts in asymmetric transformations, as electron-transfer mediators in electrochemical systems, and as specialized fuel additives. Furthermore, the burgeoning field of bioorganometallic chemistry has identified significant potential for ferrocene derivatives as potent anticancer agents and diagnostic biological probes, underscoring that the true essence of ferrocene lies not only in its geometric elegance but in its expansive functional utility in modern science [5, 4].

2. Structural and Electronic Properties of Ferrocene

Ferrocene, chemically identified as [$Fe(\eta5{-}C5H5)2$], represents the quintessential archetype of the metallocene family and remains a cornerstone of modern organometallic chemistry since its independent discovery in 1951 [2 ،6].

2.1. Definition and Structure

Ferrocene (Figure I-1) represents a unique "sandwich" architecture, where a central iron atom is situated between two parallel cyclopentadienyl (*Cp*) rings. It strictly adheres to the 18-electron rule, providing the iron center with a saturated electronic structure equivalent to the noble gas krypton, which accounts for its remarkable chemical and thermal stability up to 400 °C [6].

Figure I-1 Ferrocene

Geometrically, the molecule primarily exists in two conformations: eclipsed and staggered, which differ in the relative arrangement of their carbon atoms:

The eclipsed conformation follows the *D*5*h* symmetry group and represents the ground state of the molecule when it is in the gas phase. In this position, the carbon atoms in one ring are directly aligned with those in the other, making the overlap of the *p*-orbitals between carbon atom pairs in equivalent positions particularly strong [7].

In contrast, the staggered conformation follows the *D*5*d* symmetry group and represents the ground state of the compound in the condensed phase. Chemically and physically, this conformation is characterized by providing better coupling with external electrodes when ferrocene is used in molecular devices, as the overlap between the carbon orbitals and anchoring atoms (such as sulfur) is larger than in the eclipsed conformation [6] [7].

Energetically, the difference between the two conformations is very small, amounting to approximately 20 meV in an isolated molecule. These two states are separated by a rotational energy barrier of about 4 kJ/mol (equivalent to approximately 20.7 meV). This low barrier allows the molecule to transition between conformations or engage in continuous spinning depending on the available energy, making it an ideal candidate for use as a molecular oscillator in high-frequency applications, such as terahertz technology [6] [7].

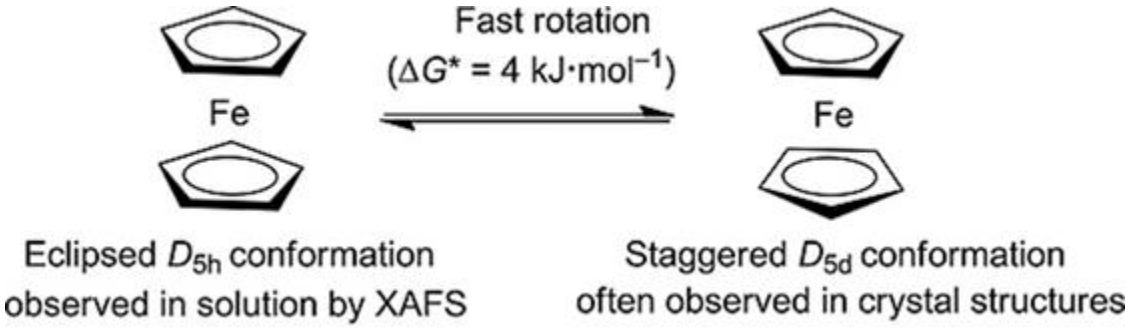

Figure I-2 The eclipsed and staggered conformation of Ferrocene

2.2. Structural Properties

When examining bond dimensions, extreme precision is found particularly in the eclipsed conformation, which is the most stable equilibrium state (Table I-1):

- The iron-carbon (Fe-C) bond length is approximately 205.6 pm computationally, which aligns strikingly with experimental measurements of 205.4 pm.
- The vertical distance between the metal and the ring center (Fe-C5) is estimated at 165.5 pm.
- The carbon-carbon (C-C) bond within the rings is 143.3 pm, while the carbon-hydrogen (C-H) bond is about 107.7 pm.
- A notable structural feature is that the hydrogen atoms do not lie in the same plane as the five carbon atoms; they are bent slightly toward the central iron atom with a tilt angle (*aC*5−*H*) estimated at 1.03° computationally and reaching 1.7° according to neutron diffraction.
- In the staggered conformation, the distance between the metal and the ring center increases slightly to 165.9 pm [7].

Table I-1 Structural Parameters of Ferrocene: Theoretical and Experimental Comparison [7]

Bond/angle	MP2	CCSD	CCSD(T)	GED	XR	ND
			eclipsed conformation (D_{5h})			
Fe–C_5	146.475	167.013[a]	165.542[b]	166.1[c]		
Fe–C	190.996	206.346	205.558	205.4(3)[d]	205.9[e]	203.1[f]
C–C	144.094	142.460[g]	143.252[h]	143.5(2)[d]	143.1[e]	141.5(2)[i]
C–H	107.589	107.480	107.723	108.0(7)[d]		107.3(3)[i]
∢C_5–H	0.33	1.21	1.03	3.7(9)[21]		1.7(2)[f]
			staggered conformation (D_{5d})			
Fe–C_5	148.658	167.616[j]	165.849[k]			
Fe–C	192.454	206.808	205.778			
C–C	143.686	142.406	143.202			
C–H	107.589	107.484	107.728			
∢C_5–H	1.39	1.48	1.34			
ΔE, E_h	0.007304	0.001339	0.001828			
ΔE/kcal mol^{-1}	4.58	0.84	1.15	0.9(3)[c]		

2.3. Electronic Properties

Ferrocene ($Fe(C_5H_5)_2$) is a classic example of the 18-electron rule, exhibiting a highly stable, saturated electronic configuration. It consists of an iron center in the +2-oxidation state sandwiched between two cyclopentadienyl (Cp) rings, each contributing six π-electrons to reach a total of 18 electrons, similar to noble gas configurations. This exceptional stability arises from Cp ring aromaticity and strong metal–ligand backbonding. [8]

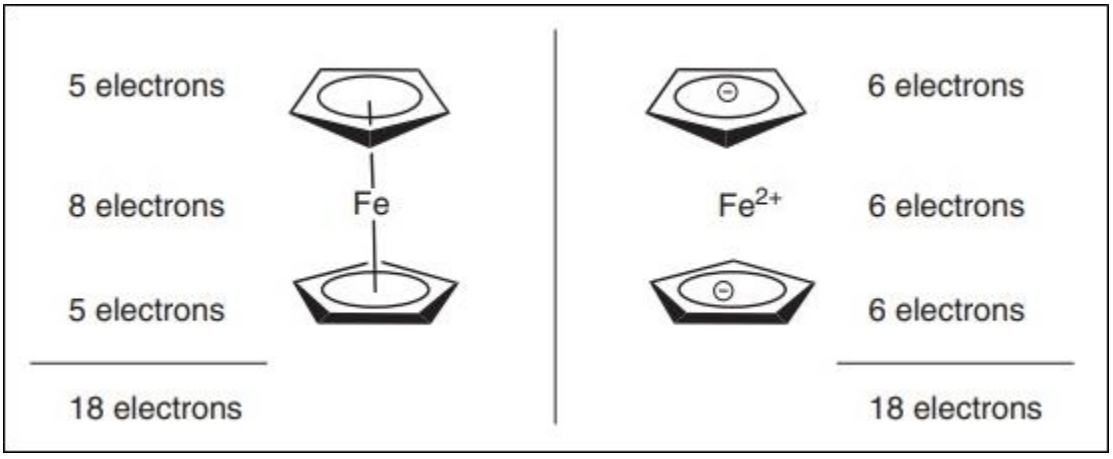

Figure I-3 The 18-electron rule exemplified on Ferrocene

From a molecular orbital (Figure I-4) perspective, ferrocene results from strong overlap between iron orbitals (3d, 4s, 4p) and the π orbitals of the cyclopentadienyl rings, involving all five carbon

atoms in each ring through η^5-coordination. This delocalized interaction creates stable bonding orbitals while leaving antibonding orbitals mostly unoccupied, which strengthens the metal–ligand bonds [9].

The compound also exhibits characteristic electronic transitions, such as $\pi \rightarrow \pi^*$ excitations, reflecting interactions between the aromatic rings and the metal center. In addition, ferrocene has highly stable and reversible redox behavior, allowing it to be oxidized to ferrocenium without structural breakdown. This redox stability makes it important in electrochemistry, nanomedicine, and bioactive compound design [9].

In the traditional case, the bonds between iron and Cp rings are of a strong covalent nature supported by aromaticity, while they tend to Ionic character when 20-electron derivatives are formed as a result of the addition of new covalent bonds. Iron can also form additional covalent bonds with electron pair donor ligands, such as nitrogen in pyridine, via the σ overlap between the metal orbital and the free electron pair [8].

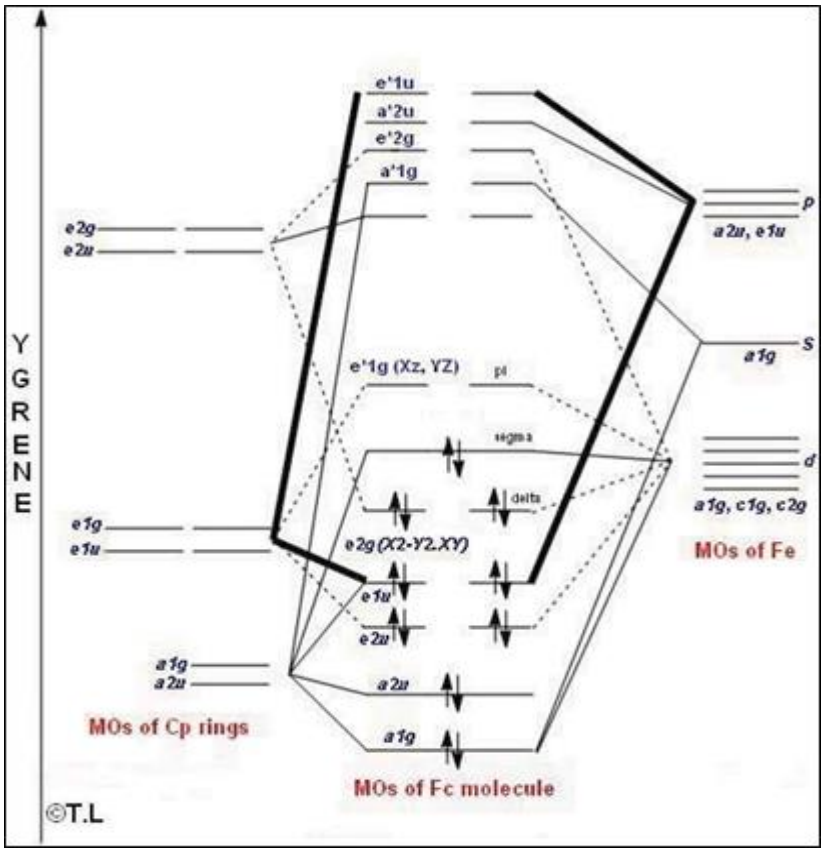

Figure I-4 Molecular orbital of ferrocene molecule [9]

2.4. Techniques Used for Study

2.4.1. Diffraction Techniques

X-ray Diffraction (XRD) for solid-state structures, GED for free molecule dimensions, and ND for precise determination of hydrogen atom positions [7].

2.4.2. Spectroscopy

- **NMR (**1*H*,13*C***):** Essential for studying chemical shifts and the fluxional rotation of the rings (Figure I-5) (Figure I-6) [10, 11].
- **IR and UV-Vis:** Used to observe characteristic bond vibrations and electronic transitions, including charge transfer and *d*−*d* bands [10 ،11].

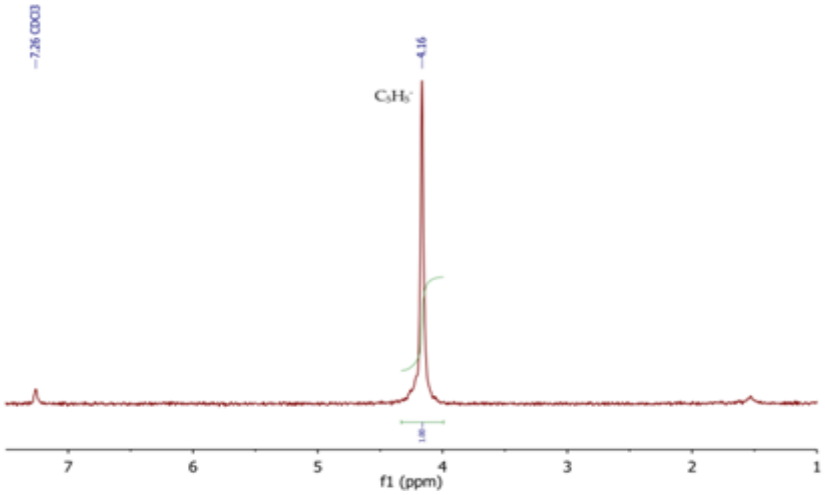

Figure I-5 NMR 1H spectrum of Ferrocene

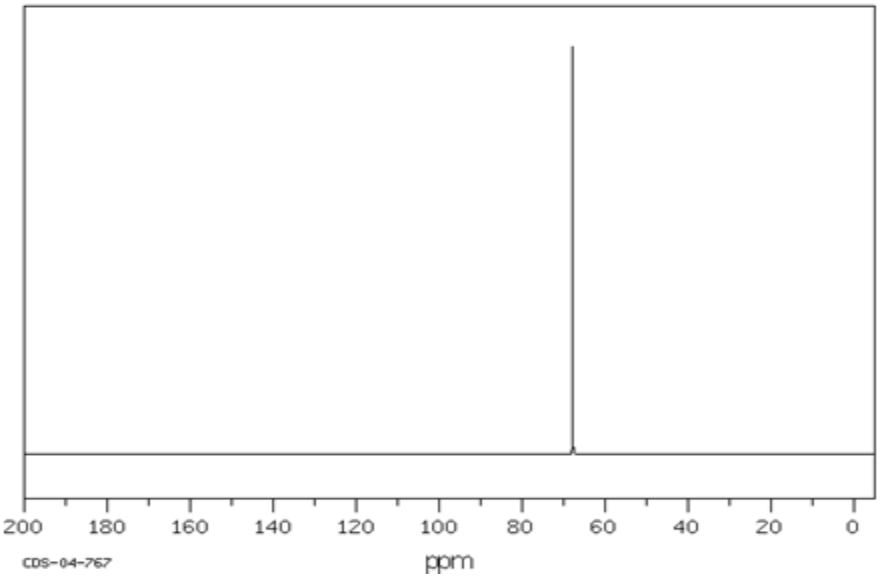

Figure I-6 NMR 13C spectrum of Ferrocene

2.4.3. Computational Chemistry

Studies have evolved from early LCAO-MO-SCF models to advanced Density Functional Theory (DFT) and high-level coupled-cluster methods like CCSD(T), which now predict equilibrium structures with accuracy comparable to experimental results [7, 10].

2.4.4. Electrochemistry

Cyclic Voltammetry (CV) and Differential Pulse Voltammetry (DPV) are standard for investigating redox behavior and electronic communication in ferrocene-containing polymers and clusters [10 ،6].

3. Synthesis and Functionalisation of Ferrocenyl Derivatives

3.1. Synthesis of Ferrocene

3.1.1. Preliminary Step: "Cracking" the Dimer

The cyclopentadiene monomer is unstable at room temperature and undergoes spontaneous Diels-Alder addition to produce dicyclopentadiene (dimer) and higher polymers.

Commercial dicyclopentadiene must be thermally degraded (cracked) at temperatures between 170-190 °C to obtain the monomer (Equation I-1).

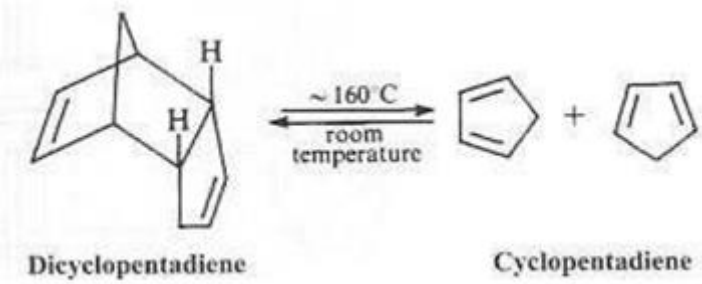

Equation I-1

The monomer is collected via distillation at 39-41 °C. It must be used immediately because it reverts to the dimer quickly; at room temperature, it is 8% dimerized within 4 hours [12].

3.1.2. Laboratory and Industrial Synthesis Methods

- **The Potassium Hydroxide (KOH) Method**

This method, described in the MIT laboratory procedures, involves reacting cyclopentadiene with a strong base:

Anion Formation: Finely powdered KOH is mixed with 1,2-dimethoxyethane (DME) under an inert nitrogen atmosphere.

Adding the Monomer: Freshly prepared cyclopentadiene is injected into the KOH slurry to form the potassium cyclopentadienide anion.

Reaction with Iron: A solution of iron (II) chloride tetrahydrate ($FeCl2{\cdot}4H2O$) dissolved in dimethyl sulfoxide (DMSO) is added gradually to the anion mixture to form ferrocene [12] (Equation I-2).

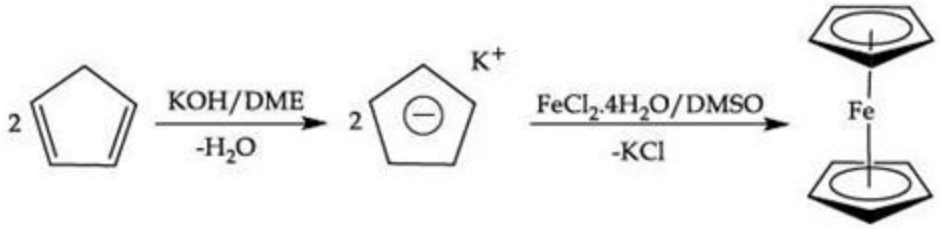

Equation I-2

- **The Metallic Sodium Method**

Used for larger-scale preparations, this method involves:

Finely dispersing metallic sodium in boiling xylene with rapid stirring (Equation I-3).

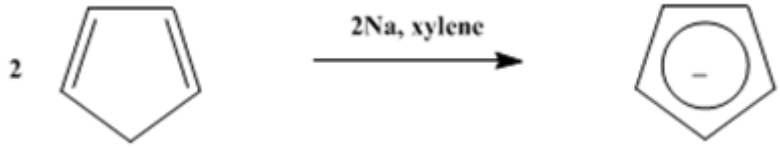

Equation I-3

Adding cyclopentadiene in tetrahydrofuran (THF) to the cooled mixture to form sodium cyclopentadienide. Reacting the resulting anion with ferrous chloride (Equation I-4) (which can be prepared by reacting ferric chloride with iron powder (Equation I-5)) [13].

Equation I-4

Equation I-5

- **The Diethylamine Method**

This is considered the simplest preparation of ferrocene. It involves the direct reaction of ferrous chloride with cyclopentadiene in the presence of diethylamine (which acts as the base) and THF (Equation I-6) [12] [13].

Equation I-6

3.1.3. Purification

Ferrocene is a crystalline material that is stable to air, moisture, and light, but sensitive to oxidizing agents.

Sublimation: This is a common purification technique where crude ferrocene is heated (below 100 °C) to transition from solid to gas and then re-condense as pure crystals on a cooled surface [12].

Recrystallization: Ferrocene can also be purified by recrystallization from solvents such as pentane, cyclohexane, hexane, or methanol [13].

3.2. Functionalisation of Ferrocenyl Derivatives

3.2.1. Substitution Reactions

Ferrocene exhibits strong aromatic properties, often more pronounced than those of benzene, allowing it to undergo various Electrophilic Aromatic Substitution (EAS) reactions [14].

- **General EAS**

Ferrocene can undergo nitration, sulfonation, and direct halogenation (Figure I-7) [14].

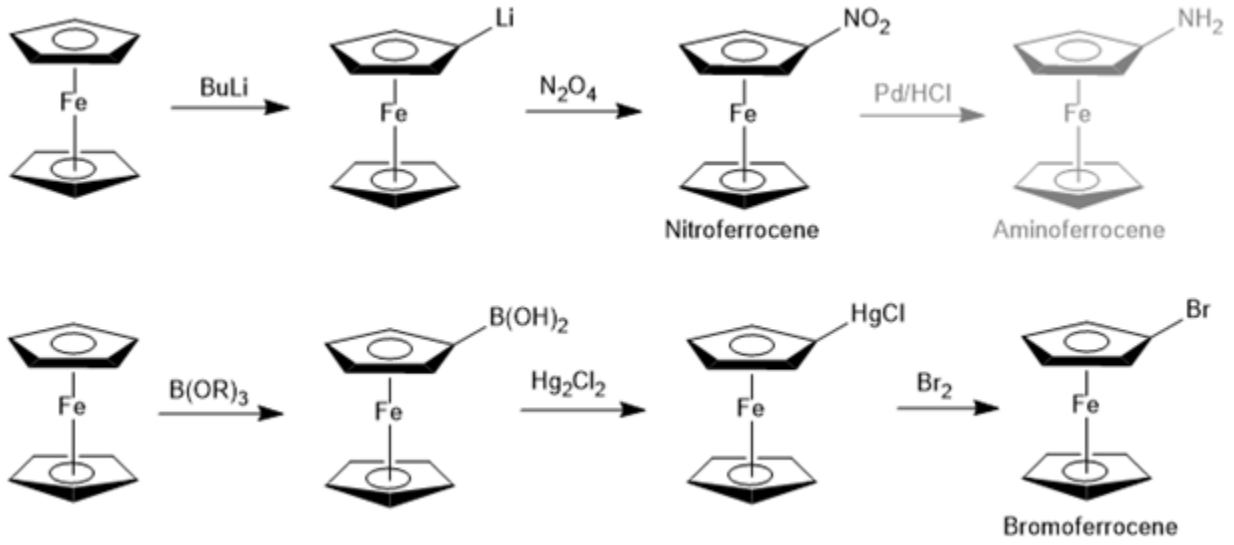

Figure I-7 Nitration and Halogenation of Ferrocene

- **Friedel-Crafts Acylation**

Ferrocene is easily acylated, such as with acetic anhydride in the presence of phosphoric acid to produce acetylferrocene (Figure I-8) [14].

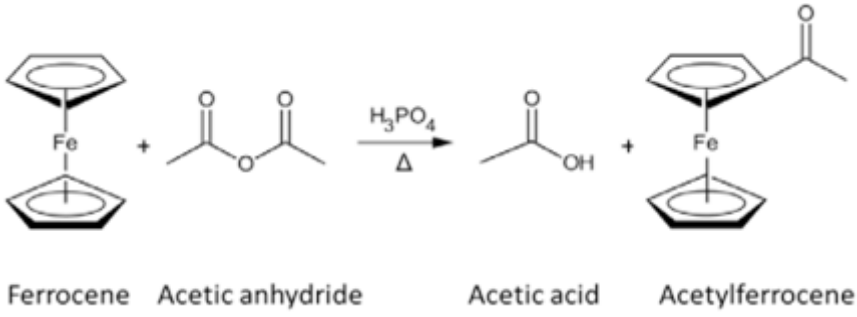

Figure I-8 Friedel-Crafts Acylation of Ferrocene

- **Friedel-Crafts Alkylation**

This process uses alkylating agents like haloalkyls or alcohols in the presence of catalysts such as *AlCl*3 or *BF*3. However, *AlCl*3 can also oxidize ferrocene to the blue ferrocenium ion, which may reduce the yield of the alkylation product (Figure I-9) [14].

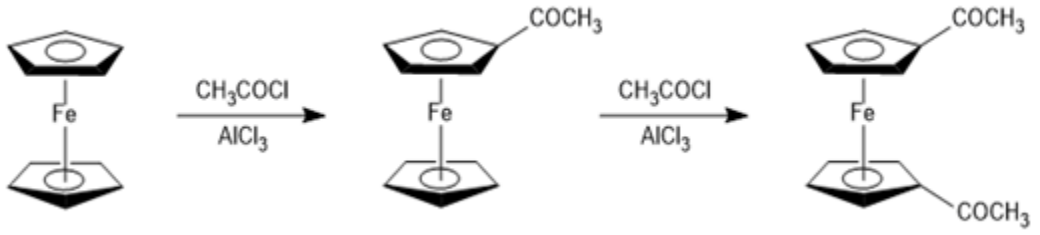

Figure I- 9 Friedel-Crafts Alkylation of Ferrocene

3.2.2. Metalation

Metalation is a foundational strategy for introducing functional groups by replacing a hydrogen atom with an active metal [15] [16].

- **Lithiation**

Ferrocene is treated with alkyllithium reagents (like n-BuLi) to generate ferrocenyl lithium, which is then quenched with electrophiles to install new functionalities (Figure I-10) [15] [16].

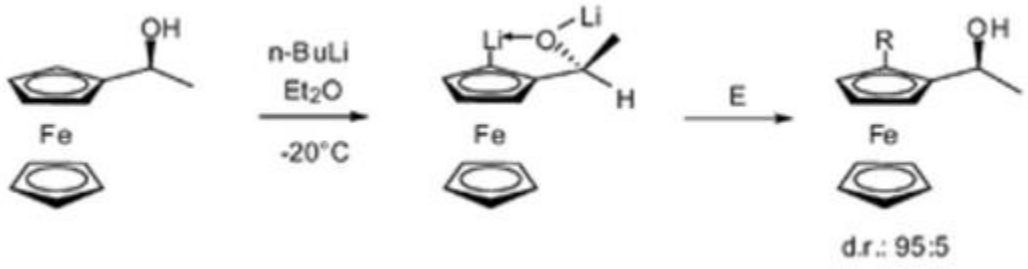

Figure I- 10 Lithiation of Ferrocene

- **Directed Metalation**

The use of directing groups (DGs) such as amines, acetals, sulfoxides, or amides allows for regioselective cleavage of neighboring C-H bonds. This is particularly useful for the synthesis of planar chiral 1,2-disubstituted ferrocenes [15] [16] [17].

3.2.3. Coupling Reactions

Transition metal-catalyzed coupling reactions have become powerful tools for linking the ferrocene backbone to complex organic motifs.

- **Suzuki and Heck Couplings**

These are used to form C-C bonds between ferrocene and aryl boronic acids or alkenes. Specialized ferrocenyl tetraphosphine ligands have demonstrated the ability to promote these reactions with very high turnover numbers (TONs) (Figure I-11) [15].

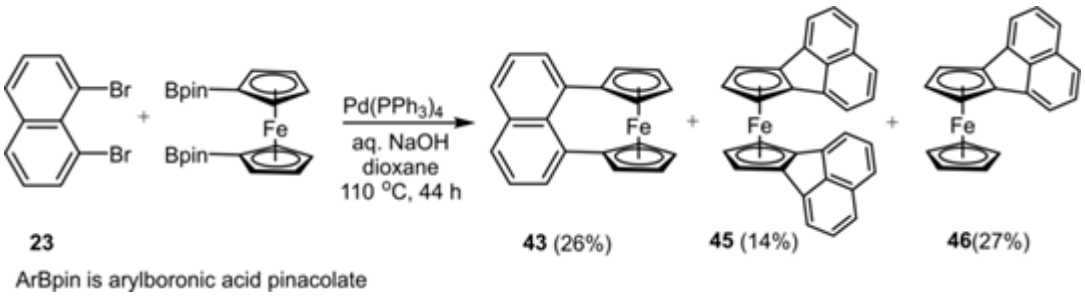

Figure I-11 Suzuki coupling method on Ferrocene

- **Sonogashira Coupling**

This method is employed to link ferrocene with terminal alkynes (Figure I-12) [17].

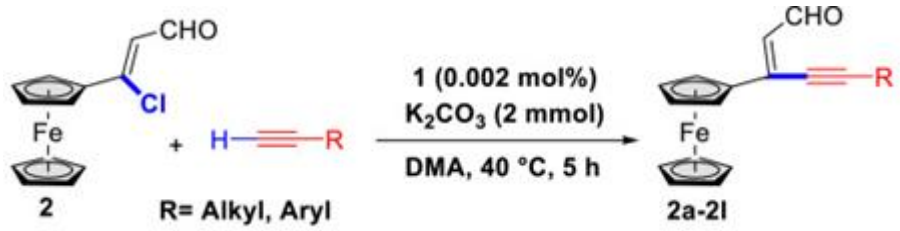

Figure I-12 Sonogashira coupling method on Ferrocene

- **C-H Bond Activation**

This modern approach allows for the transformation of non-activated C-H bonds into C-C or C-heteroatom bonds in an atom-economical way. While traditionally focused on the 1,2-position, recent template-directed approaches have successfully achieved regiospecific 1,3-functionalization (distal C-H activation), bypassing the more reactive second position [16].

3.3. Regioselectivity

Regioselectivity in ferrocene chemistry refers to the preference shown by a chemical reaction to attack a specific carbon atom or site within the ferrocene molecule or its attached groups

For example, when ferrocene is integrated with nucleobases (such as purine), regioselectivity appears in how the ferrocenoyl group attaches to the nucleobase rings (Figure I-13) [18]*:*

N7 and N9 Derivatives**:** The reaction of purine bases with ferrocenoyl chloride typically forms two types of regioisomers N7 and N9 [18].

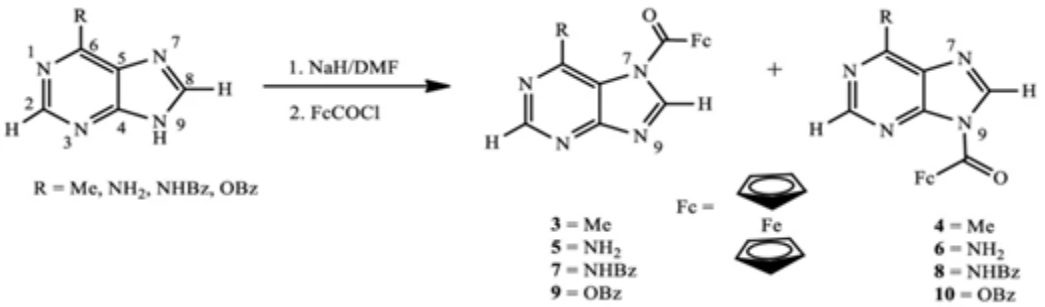

Figure I-13 Regioselective synthesis of ferrocene derivatives with differently substituted purine nucleobases [18]

Effect of Substituents: The ratio between these two types depends on the substituent at the C6 position of the purine ring. For example, in the reaction of unsubstituted purine, the N7 isomer is the major product (90%) [18].

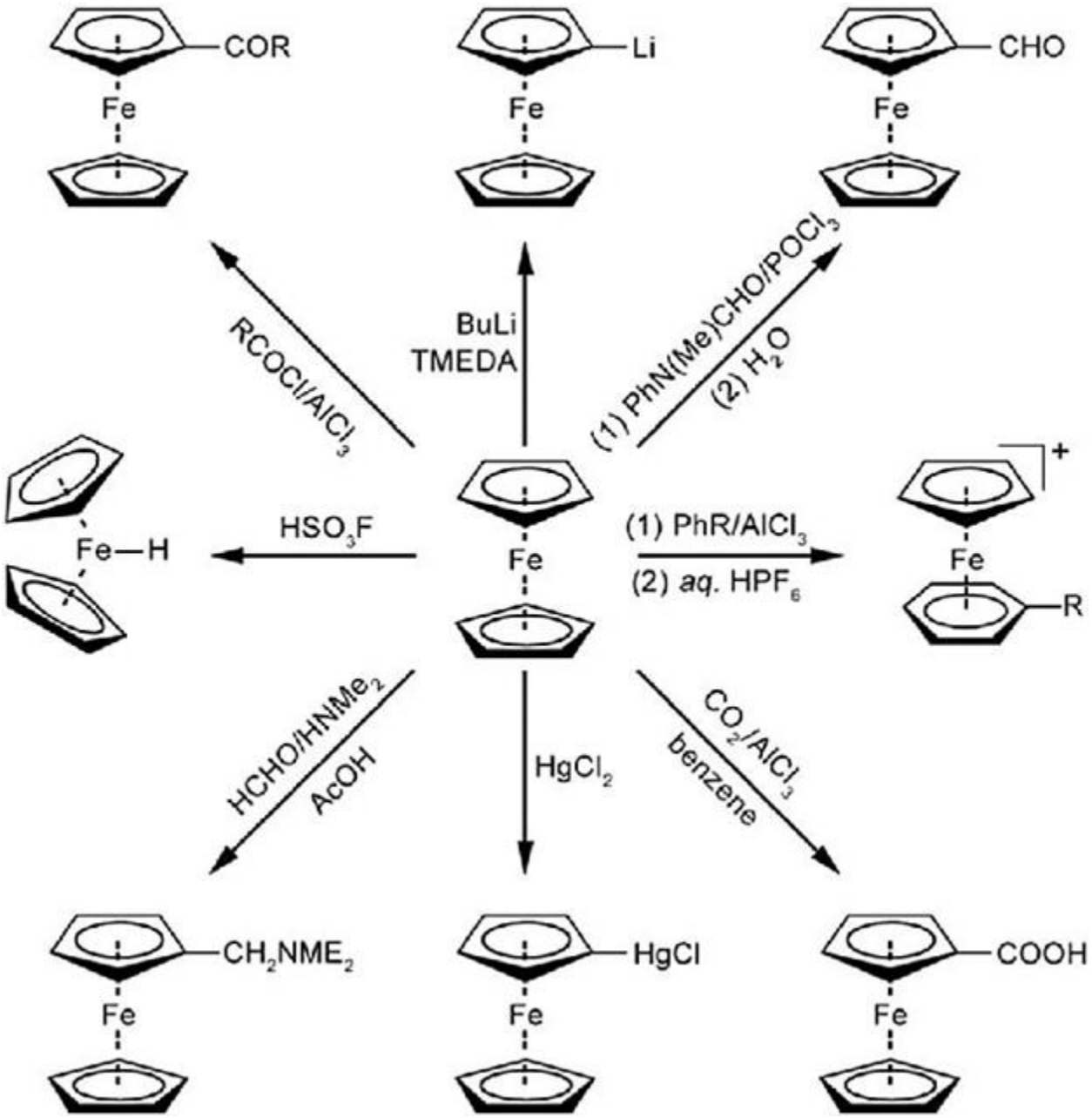

Figure I-14 Functionalisation some of Ferrocenyl Derivatives

4. Electrochemical Behaviour of Ferrocene Compounds

Ferrocene is considered a reliable redox reference in non-aqueous systems and ionic liquids due to its well-defined reversible behavior and stable formal potential within a narrow range. Its compatibility with these solvents, which exhibit wide electrochemical windows, enables accurate measurements without solvent degradation. Moreover, its use as an internal reference provides a solvent-independent potential scale, ensuring precise and thermodynamically consistent electrochemical analysis [19].

- **Redox reaction of Ferrocene**

The primary feature of ferrocene is its ability to undergo a highly stable, reversible one-electron oxidation process to form the ferrocenium cation ([*Cp*2*Fe*] +) (Figure I-14). This transformation is represented by the following equation [20] [21]:

$$Fe(C5H5)2 \rightleftharpoons [Fe(C5H5)2]^{+} + e-$$

Equation I-7

Figure I-15 Oxidation reaction of ferrocene to ferrocenium ion

The structural integrity of the molecule remains largely unchanged during this electron transfer, which accounts for its exceptional chemical stability [20].

This reaction is studied by Cyclic Voltammetry, which provides information about the oxidation state of the element and the stability of the compound under experimental conditions. It is also used to measure the standard reduction voltage (E°) of the FE III/II redox pair (Figure I-15) [22].

Ferrocene exhibits a reversible system where the peak separation (ΔEp) is approximately 59 mV for a one-electron process [22].

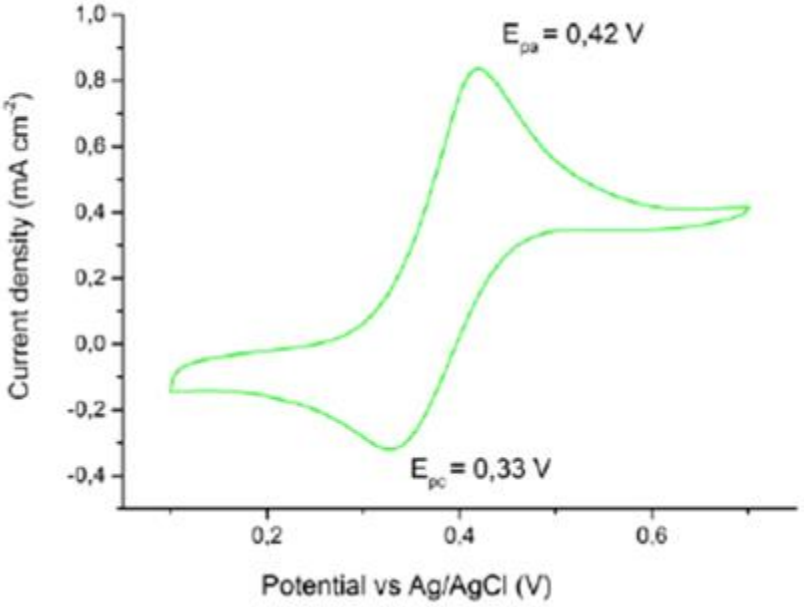

Figure I-16 Cyclic voltammogram of ferrocene oxidation performed at a scan rate of 10 mV/s

- **Diffusion-Controlled Process**

Research indicates that the redox reactions of the ferrocene/ferricenium couple are diffusion-controlled processes in both organic media (such as dichloromethane) and aqueous environments (such as ethanol with sulfuric acid) [23].

- **Stability of Current Ratios**

In cyclic voltammetry experiments, the ratio of the anodic peak current to the cathodic peak current (*ipa*/*ipc*) is close to unity (1.0), which confirms the reversible nature of the oxidation process across different studied mediums [24].

- **Influence of Substituents**

The electrochemical characteristics of ferrocene derivatives are significantly affected by functional groups; electron-withdrawing substituents (such as $-Cl$ and $-NO2$) shift the redox potential toward more positive values, making oxidation more difficult. Conversely, electron-donating groups like methyl ($-CH3$) shift it toward more negative values [24].

- **Use as a Universal Redox Probe**

Because its redox potential is only minimally affected by the choice of solvent, ferrocene is frequently selected as a standard redox probe for non-aqueous systems. It serves as an external standard for calibrating electrode potentials [23].

- **Physical Parameters**

Electrochemical parameters, specifically the diffusion coefficients (*D*), are calculated using the Randles-Sevcik equation for stationary electrodes and the Levich equation for rotating disk electrodes, based on the resulting polarization curves [23].

5. Biological and Pharmacological Relevance of Ferrocene Derivatives

Ferrocene is considered a fundamental cornerstone in bioorganometallic chemistry due to its high stability and unique properties that enable its use in various biological applications. Its importance is evident in its effective activity as an antibacterial, antifungal, and antimalarial agent, being incorporated into vital drugs such as "Ferroquine". Furthermore, its advanced medical role stands out in combating cancerous tumors as a cytotoxic agent and its use as a biological vector for the precise delivery of therapeutic molecules.

5.1. ROS (Reactive Oxygen Species) mechanism

The Reactive Oxygen Species (ROS) mechanism of ferrocene is primarily based on its unique redox behavior and its ability to transition between different chemical states. This explains its diverse applications, ranging from cancer therapy to smart wound healing [25].

5.1.1. Intracellular Production of Free Radicals

The mechanism for generating ROS within cells (such as breast cancer cells) involves the following:

Autooxidation: Once taken up by cells, ferrocene can generate hydrogen peroxide (*H*2*O*2) through a process of autooxidation, which simultaneously forms ferrocenium (Figure I-16) [25].

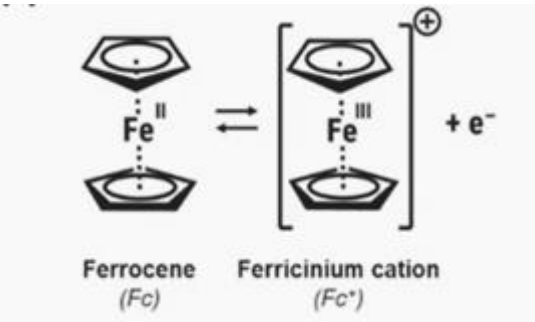

Figure I-17 Autooxidation of Ferrocene

Hydroxyl Radical Production: The cytotoxic effect of ferrocenium is specifically associated with the production of hydroxyl radicals under physiological conditions [25].

$$Fe2^{+} + H2O2 \rightarrow Fe3^{+} + OH^{-} + \bullet OH$$

Oxidative Damage: These free radicals induce oxidative damage to nuclear DNA (specifically the oxidation of guanine bases to 8-oxoguanine) and disrupt cell membranes and organelles [25].

5.1.2. Response to ROS in Smart Systems (e.g., Smart Bandages)

In other applications, ferrocene is utilized as a "sensor" for high ROS levels:

On-Demand Drug Release: In chronic wound environments characterized by high oxidative stress, elevated ROS levels oxidize the ferrocene core within nanoparticles [26].

Structural Disruption: This oxidation leads to the swelling and disassembly of the nanoparticle structure, allowing for the controlled release of encapsulated therapeutic agents, such as *Centella asiatica*, in response to the wound's oxidative state [26].

5.1.3. Oxidative Stress and Cell Death

When the ROS levels generated by ferrocene or its derivatives exceed the capacity of the cell's antioxidant defense system, the cell enters a state of persistent oxidative stress. This stress leads to the peroxidation of fatty acids (lipids), which initiates a chain reaction that disrupts the plasma and organelle membranes, ultimately resulting in cell death. This is a key strategy for targeting cancer cells, which are often more susceptible to such stimuli [25].

5.2. Medical and pharmaceutical applications

Ferrocene derivatives serve as a promising foundation in bioorganometallic chemistry due to their stability, non-toxicity, and unique redox properties. Their medical and pharmaceutical importance is centered on the development of innovative drugs that have shown exceptional effectiveness against diseases such as cancer, malaria, and HIV. Furthermore, these compounds pave the way for designing future therapies with high efficiency and fewer side effects compared to currently used traditional medications.

5.2.1. Antimalarial and Anticancer agents

Ferrocene derivatives are among the most promising compounds in the medical field. Ferrocifen compounds (Figure I-17) have shown exceptional effectiveness as anticancer agents, specifically in treating both hormone-dependent and hormone-independent breast cancer cells. Regarding malaria, the drug Ferroquine (Figure I-18) stands out as a unique innovation designed to overcome

the malaria parasite's resistance to traditional treatments, demonstrating activity 22 times higher than chloroquine in some laboratory tests [27] [28].

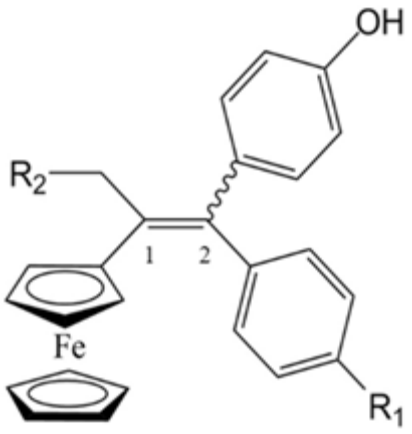

Figure I-18 General structure of Ferrocifen compound

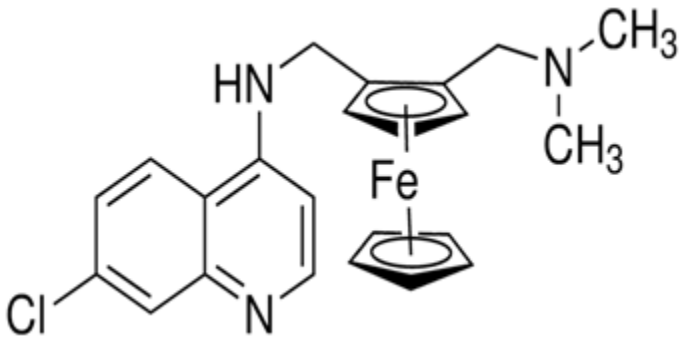

Figure I-19 General structure of Ferroquine compound

5.2.2. Anti-HIV agents

Research indicates that ferrocene derivatives possess effective activity against the Human Immunodeficiency Virus (HIV-1). The incorporation of a ferrocenemethyl moiety into certain heterocyclic bases (such as thymine) led to the production of compounds active against the virus. Furthermore, specific derivatives act as inhibitors of the topoisomerase II enzyme, helping to prevent viral replication by inhibiting proviral DNA synthesis and blocking the formation of the pre-integration complexes necessary for its integration within infected cells [27].

5.2.3. Anti-Infective agents

The mechanism of action of ferrocene derivatives as anti-infective agents primarily relies on their ability to generate Reactive Oxygen Species (ROS) within pathogenic cells. This leads to

oxidative stress, which damages DNA and proteins essential for pathogen survival, ultimately causing cell death. This strategy is employed in the development of advanced therapies targeting a wide range of infectious diseases, including parasites, bacteria (including antibiotic-resistant strains), as well as fungi [29].

5.2.4. Antioxidant agents

Ferrocene derivatives, specifically those containing the tetrahydropyrimidin-2(1H)-one ring, demonstrate a remarkable capacity as antioxidant agents. Studies have established that these derivatives possess high efficacy in neutralizing ABTS radical cations (ABTS•+); notably, certain compounds such as 7a, 7c, and 7m surpassed the reference compound Trolox in their inhibitory potential. This activity is primarily attributed to the ability of the ferrocene nucleus and the tetrahydropyrimidinone core to donate electrons or hydrogen atoms to free radicals, leading to their stabilization. However, these compounds were found to be more effective against ABTS than DPPH radicals, which may be linked to structural factors and steric hindrance effects from substituents [30].

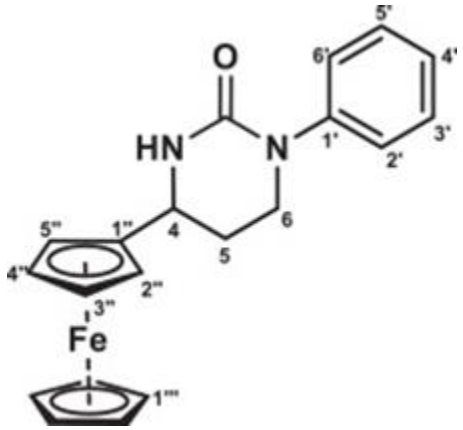

Figure I-20 General structure of Ferrocene-containing tetrahydropyrimidin-2(1H)-ones

6. Conclusion

Ferrocene serves as a cornerstone of modern organometallic chemistry, representing a unique paradigm that harmonizes exceptional structural stability with high chemical versatility. The singularity of this compound is rooted in its "sandwich" architecture, where a central iron atom in the +2-oxidation state is situated between two parallel cyclopentadienyl (Cp) rings.

This assembly achieves remarkable thermodynamic stability by adhering to the 18-electron rule, a result of the overlap between the iron d-orbitals and the π-orbitals of the aromatic rings, yielding an electronic configuration analogous to that of an inert gas.

This structural robustness is further characterized by the molecule's ability to adopt distinct conformations—eclipsed (*D*5*h*) or staggered (*D*5*d*)—facilitated by a negligible rotational energy barrier around the Fe-Cp axis, which allows for precise structural modification.

Regarding its reactivity, ferrocene emulates the behavior of electron-rich aromatic systems, often surpassing benzene in its susceptibility to electrophilic aromatic substitution reactions. The Friedel-Crafts acylation serves as a quintessential example, where the cyclopentadienyl rings host diverse functional groups under relatively mild conditions, thereby enabling the design of sophisticated functional derivatives.

Beyond ring reactivity, the compound's unique electrochemical signature—defined by the reversible ferrocene/ferricenium redox couple—is a pivotal attribute for numerous sensitive applications in analytical chemistry and nanomedicine.

The significance of ferrocene derivatives stems from their diverse utility across strategic scientific and industrial sectors. In the biomedical arena, these derivatives function as redox mediators in amperometric blood glucose biosensors and are at the forefront of oncology research, utilizing ferrocenium salts and medicinal scaffolds such as ferrocenyl-tamoxifen. In materials science, they serve as crucial fuel additives to enhance combustion and as building blocks in conductive polymers and cathodic battery materials.

Furthermore, ferrocene acts as a nanoscale template for producing ultra-high molecular weight polyethylene fibers and serves as a vital ligand scaffold, such as 1,1′-Bis (diphenylphosphino) ferrocene (dppf), in transition-metal catalyzed reactions for pharmaceutical and agrochemical synthesis. In summary, the distinctive convergence of structural integrity, tunable reactivity, and multi-functional applicability positions ferrocene derivatives as an ideal model for the integration of fundamental chemistry with advanced technological innovation.

Chapter 2: Computational Approaches in Molecular Modelling and Drug Design

1. Introduction

Molecular modeling is broadly defined as any process that requires the use of a computer to paint, describe, or evaluate any aspect of the properties of a molecule's structure. It is a field concerned with using various strategies to model and deduce information about a system at the atomic level, with computational chemistry serving as its core nucleus. The fundamental goal of modeling is to help humans understand phenomena occurring on a submicroscopic scale by simulating this activity in familiar, observable forms [31].

Historically, the discipline began with the quantum chemical description of molecules, but its transition into a routine research tool is credited to the development of molecular mechanics and advanced computer graphics.

Before the digital era, scientists relied on physical kits, such as Dreiding models, to gain a three-dimensional impression of crystal structures. By the 1970s, the emergence of fast processors allowed for the creation of "virtual Dreiding models"—color-coded, rotatable 3D descriptions on a computer screen that could handle complex systems like proteins containing thousands of atoms [31].

Modern molecular modeling relies on two primary mathematical approaches to calculate a system's energy:

Quantum Mechanics: A procedure based on first principles that solve the Schroedinger equation to describe electronic density.

Molecular Mechanics: A faster computational model that treats atoms as spheres of different sizes connected by "springs" (bonds), using the laws of classical mechanics [32].

Ultimately, molecular modeling is more than just the creation of "pretty pictures" or "colored graphics". It is a systematic way of thinking designed to gain new insights and develop reliable working hypotheses regarding molecular interactions. By understanding these interactions, modeling becomes a vital component of computer-aided drug design, enabling scientists to optimize the complementarity between ligands and their biological receptors [33].

2. Density Functional Theory (DFT) and Electronic Descriptors

2.1. Definition of Density Functional Theory (DFT)

Density Functional Theory (DFT) is a computational quantum mechanical modeling tool widely used in materials science and drug design to study the electronic structure of atoms and molecules.

The theory is based on the fundamental principle that the electron density of any system uniquely determines the ground-state energy and all other physical and molecular properties.

The true power of this theory lies in its ability to bypass the complexities of the traditional "wavefunction," which depends on (3N) variables for N electrons, and replace it with electron density, which depends on only three spatial variables.

This significantly reduces computational requirements and makes it more practical and conceptually accessible. Mathematically, DFT is based on the Hohenberg-Kohn theorems, which prove that energy is a "functional" of the electron density.

In practical applications, it often relies on the Kohn-Sham approach, which simplifies the problem by using a fictitious system of non-interacting electrons. Due to its efficiency, DFT has become the dominant method for simulating molecular energy surfaces and predicting spectral properties and reaction mechanisms in bioinorganic chemistry [34] [35].

2.2. Theory and Methods OF Density Functional Theory

The density functional theory is based on the basic idea of using electron density ρ (r) as an axial variable Instead of a complex wave function to determine the properties of the ground state of the system

2.2.1. Density Functional Theory (Theory)

- **Hohenberg–Kohn Theorems:**

First Theorem: Proved that the external potential $v(r)$ is a unique functional of the ground-state electron density. This implies that the density contains all the information needed to determine the system's Hamiltonian and its properties.

$$\boldsymbol{Ev\,[\rho(r)] = \int v(r)\rho(r)dr + FHK[\rho(r)]}$$

Second Theorem (Variational Principle): Established that the total energy functional reaches its minimum value if and only if the input density is the true ground-state density.

$$\boldsymbol{Ev\,[\rho 0(r)] \leq Ev\,[\rho\sim(r)]}$$

- **Kohn–Sham Method:**

To address the difficulty of calculating kinetic energy, Kohn and Sham introduced a fictitious system of non-interacting particles that yields the same density as the real, interacting system.

This approach allows the exact calculation of the major part of the kinetic energy, while all complex many-body effects (exchange and correlation) are grouped into a single term: the Exchange-Correlation Functional (*Exc*).

- **Levy's Constrained Search:**

This provides a more rigorous theoretical foundation by defining the universal functional through a search over all wavefunctions that yield a specific density. It resolves issues like *v*-representability and extends the theory to degenerate ground states.

2.2.2. DFT Methodology (Methods)

Methods in DFT focus on approximating the unknown exchange-correlation functional and solving the resulting equations numerically.

- **Approximating the Exchange-Correlation Functional (*Exc*)**

Since the exact form of *Exc* is unknown, several levels of approximation (often called "Jacob's Ladder") are used:

Local Spin Density Approximation (LSDA): Assumes the density at each point behaves like a uniform electron gas.

Generalized Gradient Approximation (GGA): Incorporates both the density and its gradient (rate of change) to account for inhomogeneities, such as the PW86 and B88 functionals.

meta-GGA: Adds dependence on the Laplacian of the density or the kinetic energy density to provide more detail, such as the LAP or VSXC functionals.

Hybrid Functionals**:** Mix a portion of "exact" exchange from Hartree–Fock theory with DFT functionals; B3LYP is a prominent example.

Optimized Effective Potential (OEP): A method to calculate exchange exactly while maintaining a local potential.

- **Solving the Kohn–Sham Equations**

Practical implementation requires several technical choices:

Basis Sets (LCAO): Orbitals are typically represented as a Linear Combination of Atomic Orbitals. Common types include Gaussian Type Functions (GTF) and Slater Type Functions (STF).

Potentials: The Coulomb potential can be calculated exactly or through fitting procedures using auxiliary basis sets to save computational time.

Numerical Integration: Because *Exc* functionals are mathematically complex, they are integrated numerically over a spatial grid.

Core Potentials: To speed up calculations, the inner "core" electrons are often replaced by Pseudopotentials or Effective Core Potentials (ECP), allowing the simulation to focus only on the chemically active valence electrons [36].

2.3. The Importance and Role of Density Functional Theory (DFT)

Density Functional Theory (DFT) is a dominant computational quantum mechanical modeling tool in the fields of materials science, bioinorganic chemistry, and drug design.

Its fundamental importance lies in its ability to simplify complex problems by replacing the wavefunction—which depends on a vast number of variables (3N)—with electron density, which depends on only three spatial variables, making it more efficient and suitable for both practical and conceptual applications.

Its primary role is to serve as an accurate means for calculating ground-state energy, predicting molecular geometries, and simulating molecular energy surfaces and complex reaction mechanisms.

In the context of medical research, DFT contributes to accelerating drug development, particularly for antimicrobials, by simulating interaction energies and identifying the electronic properties that grant molecules stability and strong inhibitory activity.

Furthermore, it acts as a powerful complementary tool for experimental research, providing access to a wide range of spectroscopic and magnetic properties (such as Infrared, X-ray Absorption, and Electron Paramagnetic Resonance), which aids in validating laboratory results or exploring regions that remain experimentally uncharted [35].

3. Molecular Docking and Ligand–Protein Interactions

3.1. Definition of Molecular Docking

Molecular docking is a computational approach and modeling technique used to predict how small molecules, known as ligands, bind to appropriate receptor proteins or biological macromolecules [37]. This structure-based technique primarily focuses on determining the optimal

binding orientation (pose) and predicting the affinity or strength of attraction between the ligand and the target [38].

By simulating these interactions at the atomic level, it allows researchers to study molecular behavior and understand the fundamental biochemical processes governing the interaction [38]. The process typically involves two key steps: sampling possible poses of the ligand within the receptor's active site and using mathematical scoring functions to evaluate and rank these poses based on their energetic stability [39].

This approach has become an essential tool in drug discovery and development, making the process faster and more cost-effective by identifying promising compounds before proceeding to wet lab experiments [37] [39].

3.2. Representation of Molecular Docking

Generally, the Docking process can be represented in a flowchart as shown in Figure I-21

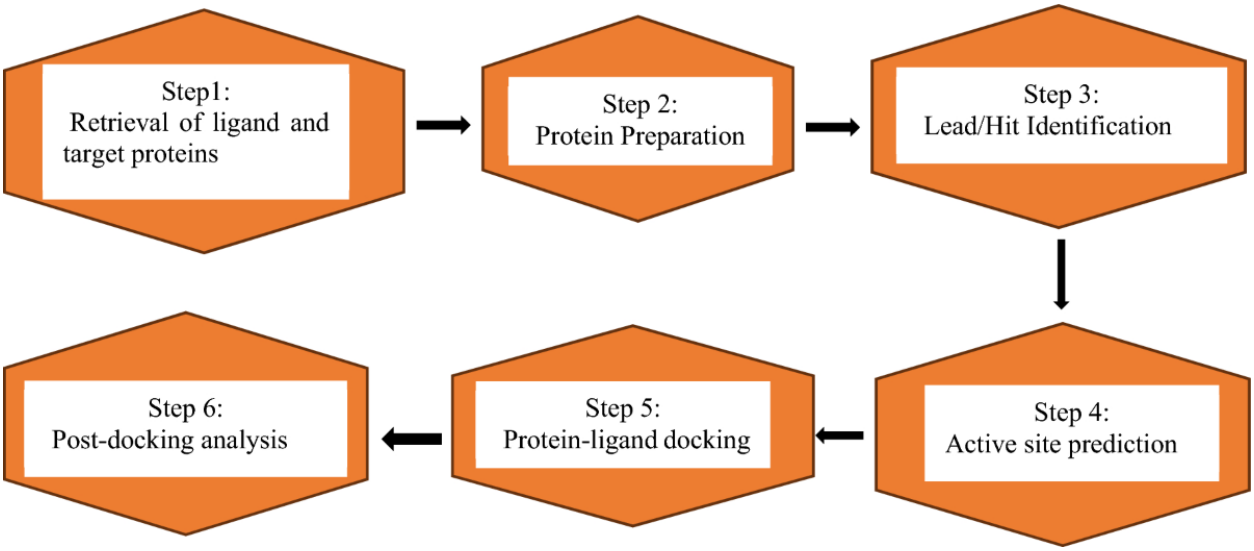

Figure I-21 A prototype flow chart of a Molecular Docking study

- **Retrieval of protein and ligand structure**

Finding practical target proteins and ligands is crucial for carrying out docking. Thus, one must check to see if the target protein has been stored in the Swiss UniProt knowledge base or the Protein Data Bank (PDB) database. Homology modeling may be done utilizing the Swiss model repository, modeller programs like I-TASSER, etc. if the target protein is not in the database but comparable sequences are. The next step is to locate the ligand using the PubChem database, Zinc,

ChmBl, or if none of these databases include the ligand, ChemDraw or ChemSketch can be used to synthesize the ligand from scratch

- **Protein preparation**

The process of optimizing the protein structure and getting it ready for precise docking simulations is known as protein preparation, and it is an essential stage in the molecular docking process. The protein structure is first obtained from a database like Protein Databank (PDB) or created using molecular modeling tools like SWISS MODELLER. The structure is then completed by adding any extra atoms or residues.

The protein is subsequently put through energy minimization to loosen up the structure and get rid of any steric interference

The protonation states of ionizable residues are then established to provide proper electrostatic interactions during docking. To further simplify the system, water molecules, and extraneous ligands are eliminated from the protein structure.

To appropriately reflect the protein's behavior during docking simulations, the proper force field parameters are lastly supplied to it. Through these preparation steps, the protein structure is optimized and refined, providing a suitable starting point for successful molecular docking studies.

- **Lead or hit identification**

The ligands to be docked are selected based on various criteria, such as their chemical diversity, their known biological activity, or their potential for drug development. The ligands are then prepared for docking by assigning charges, generating conformers, and optimizing their geometry.

- **Active site prediction**

During molecular docking, the binding pockets can be initially specified or identified after docking. Consequently, to validate the binding pocket of interest during molecular docking three different approaches can be conceived as highlighted below.

i. Site-directed docking: Here, first, identify the protein–ligand binding site and then dock the ligand.

ii. Blind docking: Here, the docked ligand is directly onto the complete receptor structure without prior knowledge of the binding site.

iii. Docking with a standard: Here, you dock the protein with the test ligands and/or standard small molecule(s). The standard ligand facilitates the prediction of the relevant binding pocket.

Additionally, calculating the inhibition constant for docked ligands and proteins is an important step in evaluating the binding affinity and potential inhibitory activity of the ligands. However, it is not always necessary or applicable in all cases. The decision to calculate the inhibition constant depends on the specific research question, experimental design, and the objectives of the study.

- **Protein–ligand docking**

Ligand is docked against the protein and the interactions are analyzed. The scoring function gives a score based on the best-docked ligand complex picked out.

- **Post-docking analysis**

After the ligands have been docked to the protein, the results are analyzed to identify the most promising candidates for further study. The binding affinity of each ligand is calculated based on the predicted interaction energy, and the ligands are ranked based on their affinity scores. The docked structures are also analyzed to identify key interactions between the ligands and the protein, such as hydrogen bonds, hydrophobic interactions, and electrostatic interactions. These interactions can provide insights into the mechanism of action of the ligands and guide further optimization of their structure [38].

3.3. Applications of Molecular Docking

The applications of molecular docking extend across various vital fields, prominently in drug discovery and development through hit identification and lead optimization to enhance drug potency and selectivity [37].

It is widely used in virtual screening to scan large molecular databases and in drug repurposing to find new therapeutic uses for approved drugs, a role that was particularly evident in efforts to combat COVID-19 [39].

Additionally, this technique contributes to predicting ADMET properties (Absorption, Distribution, Metabolism, Excretion, and Toxicity) and identifying potential side effects by detecting off-target interactions [37] [39].

Its applications further include studying drug-DNA interactions and exploring polypharmacology to design molecules that interact with multiple targets simultaneously.

Recently, it has become a fundamental tool in nutraceutical research to identify molecular targets for managing chronic diseases like cancer, cardiovascular diseases, and neurodegenerative disorders, as well as in bioremediation and elucidating unknown protein structures [38].

4. Molecular Dynamics Simulation

4.1. Definition of Molecular Dynamics

Molecular Dynamics (MD) simulations provide precise atomic-level insights into the dynamic evolution of a system and the movement of atoms and molecules as a function of time [40].

These simulations offer detailed information regarding the structural fluctuations and conformational changes of the proteins and nucleic acids under study, which is essential for understanding complex biological functions [40].

Functioning as a "computational microscope," MD allows researchers to observe and analyze the movements of every atom in a biomolecule over time insights that are often difficult or impossible to obtain using traditional experimental methods alone.

Beyond its crucial role in drug discovery, where it helps identify "lead compounds" and analyze their interactions, MD provides vital data on thermodynamics, binding free energy, and molecular kinetics.

Furthermore, it aids in uncovering the mysteries of protein folding and understanding molecular behavior in complex environments like cell membranes, as well as developing drug delivery systems using nanoparticles.

Consequently, MD serves as a bridge between modern technological advancements and conventional laboratory experiments, significantly saving time, cost, and human labor in scientific research [40].

4.2. Methods for Molecular Dynamics Simulations

4.2.1. Key Steps of the Simulation Method

MD simulations are generally performed in three main stages, each consisting of specific sub-steps:

- Model Selection**:** Choosing the molecular system of interest, securing missing segments, and conditioning protonation states.
- Energy Minimization, Heating, and Equilibration**:** Equilibrating the structure with the chosen Force Field by solving Newton’s equations of motion. The system is heated by rescaling velocities until it reaches a specific temperature and its properties no longer change with time.

- Production Run and Analysis: Running the simulation for a relevant period to obtain trajectories, which are then analyzed to determine the desired physical and chemical properties.

4.2.2. MD Simulation Algorithms (Integration Algorithms)

These algorithms are used to integrate the classical equations of motion using the finite difference method:

- Verlet Algorithm: The most basic and widely used algorithm; it calculates new positions based on current and previous positions without using explicit velocities.
- Velocity Verlet Algorithm: A more precise version that considers positions, velocities, and accelerations simultaneously at a particular time.
- Leap Frog Algorithm: Positions and velocities are calculated at interleaved time intervals to control errors found in the Velocity Verlet algorithm.
- Beeman's Algorithm: Closely related to the Verlet algorithm but provides a more accurate expression for velocities and better energy conservation, though it is computationally more expensive.

4.2.3. Molecular Modelling Methods

If ready-made structures (from X-ray or NMR) are unavailable, three major computational methods are used to deduce them:

- Ab-initio method.
- Threading.
- Homology modelling.

4.2.4. Energy Minimization Algorithms

These are used to find lower energy conformations and include:

Steepest descent: Used for highly restrained systems.

Conjugate gradient: Efficient for large systems.

BFGS (Broyden-Fletcher-Goldfarb-Shanno): A quasi-Newton method.

Newton-Raphson: Calculates both the slopes of energy and the rate of change.

4.2.5. Solvation Methods

Since most biological processes occur in aqueous environments, two methods are used for solvation:

- Explicit treatment: Real solvent molecules are added to the system.
- Implicit treatment: The solvent is modelled as a continuum dielectric.

4.2.6. General Classes of Simulation Techniques

here are two primary classes of simulation: Molecular Dynamics (MD) and Monte Carlo (MC). Monte Carlo is often preferred for low-density systems like gases, while MD is the technique of choice for simulating liquids [40].

4.3. The role of Molecular Dynamics

Molecular Dynamics (MD) simulations have emerged as a fundamental pillar within modern structure-based drug design (SBDD) frameworks.

The primary utility of MD resides in its capacity to transcend the inherent limitations of static structural representations by explicitly integrating macromolecular flexibility and entropic contributions into the energetic landscape.

Dynamically, MD provides a high-fidelity physical description of atomic interactions and trajectories governed by Newtonian mechanics, enabling a comprehensive characterization of the free-energy landscape associated with ligand-target association.

This shift from the rigid "lock-and-key" model toward "induced-fit" and "conformational selection" paradigms allows for the precise quantification of essential thermodynamic and kinetic observables, including binding free energy and drug residence time, which are critical metrics for assessing drug efficacy in vivo.

Moreover, MD serves a strategic function in lead optimization through rigorous methodologies like free-energy perturbation (FEP). It further provides a robust computational window into identifying transient allosteric pockets and characterizing the thermodynamic behavior of solvation water molecules, thereby facilitating the rational design of therapeutics with enhanced selectivity and potency [41].

5. ADMET Prediction and Drug-Likeness Evaluation

5.1. ADMET prediction

5.1.1. Definition

ADMET prediction is defined as the process of estimating and evaluating five core properties of chemical compounds—such as drugs, pesticides, food additives, or environmental pollutants: Absorption, Distribution, Metabolism, Excretion, and Toxicity.

This evaluation is crucial for assessing the effects or risks these compounds may have on the human body.

Because approximately 50% of drug failures in late development stages are attributed to unacceptable ADMET properties, filtering and optimizing these characteristics during the early stages of drug discovery has become a necessity to reduce high attrition rates.

To overcome the high costs, labor, and time required for traditional experimental evaluations conducted in vivo (inside living organisms) or in vitro (in a controlled environment outside a living organism), "in silico" (computational) techniques are now widely used to estimate these properties.

These computational predictions primarily rely on two categories of methods: molecular modeling, which studies interactions based on the three-dimensional structures of involved proteins, and data-derived modeling, such as Quantitative Structure-Activity Relationships (QSAR) and machine learning algorithms [42].

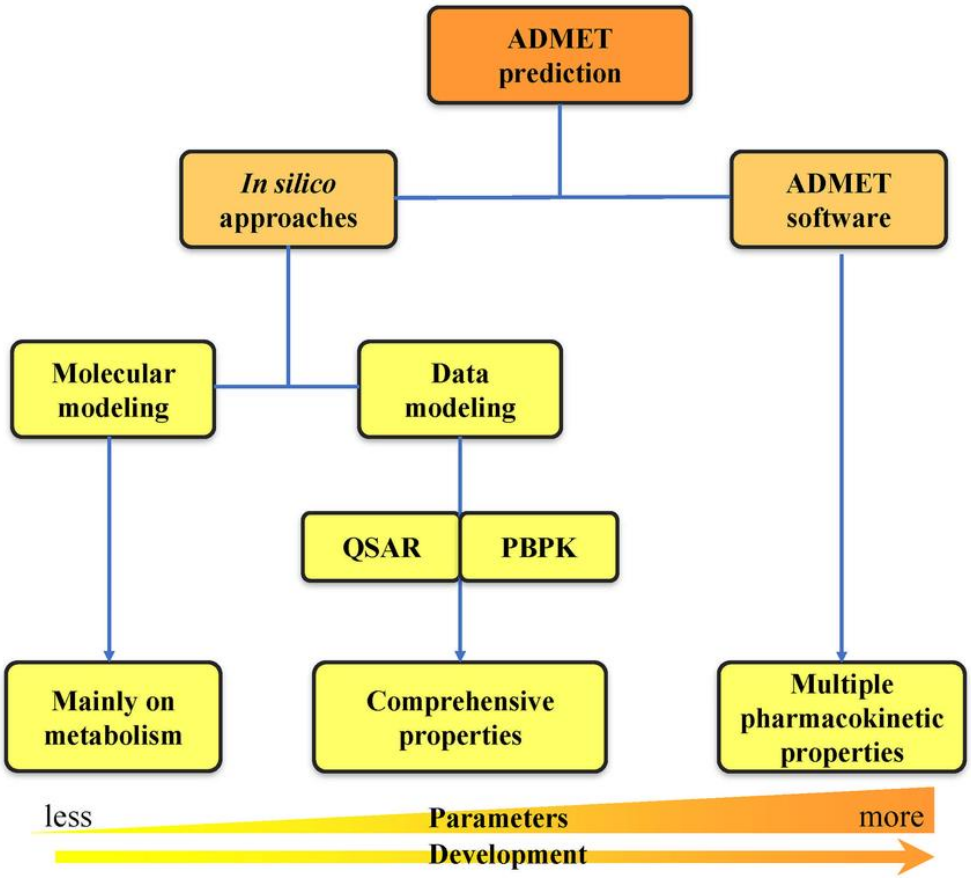

Figure I-22 Classification of ADMET prediction strategies.

5.1.2. Strategies of ADMET prediction

these strategies are classified into two main categories:

5.1.2.1. Molecular Modeling

This approach is based on the three-dimensional structures of proteins and is primarily used to analyze metabolic properties, it is further divided into:

Ligand-Based Methods: These derive information about protein active sites based on the shapes, chemical structures, and electronic properties of known inhibitors or substrates. Key techniques include Pharmacophore modeling, Quantum Mechanics (QM) calculations, and Shape-focused methods.

Structure-Based Methods: These focus on the specific interactions and binding modes between small molecules and ADMET proteins. This involves techniques like Molecular docking and Molecular Dynamics (MD) simulation to account for the flexible nature of protein binding cavities.

5.1.2.2. Data Modeling

Data modeling is used to predict a comprehensive range of ADMET properties by utilizing existing biochemical and physical data. It includes [43]:

5.1.2.3. Quantitative Structure-Activity Relationship (QSAR):

Quantitative Structure–Activity Relationship (QSAR) is a critical computational technique in modern drug discovery aimed at predicting the biological activity of chemical compounds based on their molecular structures. This technique establishes quantitative mathematical relationships between "descriptors" of chemical structure and measured biological activities, which significantly reduces the cost, time, and resources required for traditional experimental screening.

The fundamental principle of QSAR is that molecular structure determines biological activity. Structural features, such as functional groups, electronic distribution, and molecular size, influence how a compound interacts with its biological targets. The general workflow follows a specific sequence:

Chemical Structure → Molecular Descriptors → Mathematical Model → Biological Activity Prediction.

QSAR models are classified based on the dimensionality and types of descriptors used:

1D-QSAR: Uses simple physicochemical properties such as molecular weight, pKa, and lipophilicity (LogP).

2D-QSAR: Relies on structural information derived from molecular connectivity and topological descriptors.

3D-QSAR: Incorporates the three-dimensional structure of molecules to analyze steric and electrostatic interactions between the compound and its biological target.

Developing a reliable QSAR model involves several steps: collecting a dataset with known biological activities, computationally optimizing molecular structures, calculating descriptors, and using statistical methods to select the most relevant ones for model building. Validation is a vital step to ensure the model's reliability; this is done internally through cross-validation or externally using an independent dataset.

Beyond its role in drug discovery and lead optimization, QSAR is widely used in toxicity prediction and environmental chemistry. Modern approaches now integrate Artificial Intelligence and Machine Learning (such as neural networks and random forests) to improve prediction accuracy and analyze complex non-linear relationships between molecular structure and activity [44].

5.1.2.4. Physiologically Based Pharmacokinetic (PBPK) Modeling

Physiologically Based Pharmacokinetic (PBPK) modeling is a quantitative mechanistic framework used to describe the absorption, distribution, metabolism, and excretion (ADME) of drugs. These models utilize mathematical equations parameterized with known physiological variables to predict drug concentration-time profiles in the body.

- **Classical vs. PBPK Models**

Classical Models: Typically consist of a central compartment (plasma) linked to one or two peripheral compartments via rate constants. These parameters generally lack physiological meaning and are more empirical.

PBPK Models: Consist of a larger number of compartments that correspond directly to actual organs or tissues (e.g., liver, kidney, brain) connected by blood flow rates that parallel the real circulatory system.

- **Model Parameters**

PBPK models are built using two main categories of input data:

System-Specific Parameters: These are demographic and physiological variables such as tissue volumes and organ blood flow rates. These can be adjusted to represent different species (mouse, rat, human) or specific populations, such as the elderly, pediatrics, or patients with renal or hepatic impairment.

Drug-Specific Parameters: These include physicochemical properties (pKa, solubility, lipophilicity) and biological data such as plasma protein binding and intrinsic clearance (CLint),. A critical drug-specific parameter is the tissue-to-plasma partition coefficient (Kp), which characterizes how a drug moves into different tissues.

- **In Vitro-In Vivo Extrapolation (IVIVE)**

A core component of PBPK modeling is IVIVE, a technique that allows scientists to take data measured in laboratory settings (in vitro) and scale it up to predict drug behavior in a living organism (in vivo). For example, metabolic rates measured in liver microsomes can be scaled using physiological factors to predict hepatic clearance in humans.

- **Tissue Distribution Kinetics**

Drug movement into tissues is typically modeled in one of two ways:

Perfusion Rate-Limited: Assumes the drug equilibrates rapidly across the tissue; the blood flow rate is the limiting factor. This is common for small, lipophilic molecules.

Permeability Rate-Limited: Used for larger or polar molecules where the cell membrane acts as a barrier. This model accounts for passive diffusion and active transport processes [45].

5.1.2.5. ADMET software

ADMET software (standing for Absorption, Distribution, Metabolism, Excretion, and Toxicity) are essential computational tools in the drug discovery and design process, used to predict the behavior of drug-like molecules within living systems,

The importance of these tools lies in their ability to evaluate pharmacokinetic and toxicity parameters during early research stages, which significantly contributes to reducing overall innovation costs and decreasing the risk of failure in late clinical phases.

These tools function by filtering out compounds with poor properties and selecting the safest and most effective candidates. They are available in several forms, including commercial software packages like "QikProp" and "ADMET Predictor," as well as free web-based options such as "FAF-Drugs2" and "SwissADME".

It is noteworthy that integrating ADMET profiling into the early stages of drug development accelerates the discovery process and ensures that resources are directed toward compounds with a high probability of therapeutic success [46].

5.2. Drug-likeness evaluation

Drug-likeness evaluation is a comprehensive assessment used to determine the likelihood that a chemical compound will succeed in clinical trials and eventually become an approved drug. This process is essential for economizing research expenditures by filtering out compounds with unfavorable properties or poor development potential in the early stages of drug discovery.

the evaluation of drug-likeness has evolved through several key approaches:

5.2.1. Physicochemical Property-Based Rules

The earliest and most established method involves setting acceptable thresholds for a compound's physical and chemical properties. The most famous of these is Lipinski’s Rule of Five (RO5), which identifies four criteria common to many successful oral drugs:

- Molecular weight ≤ 500.
- Octanol/water partition coefficient (logP) ≤ 5.
- Number of hydrogen bond donors ≤ 5.

- Number of hydrogen bond acceptors ≤ 10. Compounds meeting at least three of these rules are generally considered "drug-like" and likely to be well-absorbed orally.

5.2.2. Structural Feature-Based Assessment

This approach defines drug-likeness by comparing the structural patterns or "building blocks" of a new compound to those of known successful drugs. It analyzes the presence of specific frameworks or moieties (functional groups) to determine if the molecule aligns with preferred chemical architectures used in medicine.

5.2.3. Quantitative Estimate of Drug-likeness (QED)

Unlike simple "yes/no" filters, QED provides a continuous measurement of drug-likeness. It uses "desirability functions" to integrate eight common physicochemical properties into a single score. This allows for a more nuanced and flexible assessment, often referred to as quantifying the "chemical beauty" of a drug.

5.2.4. Machine Learning (ML) and Deep Learning (DL)

To handle the vast and complex chemical space that simple rules cannot cover, advanced computational models have been introduced:

- **Traditional ML**

Includes methods like Support Vector Machines (SVM), Decision Trees (DT), and early Artificial Neural Networks (ANN).

- **Novel Deep Learning**

Modern techniques use Graph Neural Networks (GNNs) to process molecular graphs directly and Recurrent Neural Networks (RNNs) to analyze SMILES strings (text-based representations of molecules). These models have significantly improved classification accuracy.

Current Challenges

- Generalizability: Models often struggle to predict the behavior of molecules that are substantially different from those in their training data.
- Interpretability: Many deep learning models are considered "black boxes," making it difficult for medicinal chemists to understand *why* a compound was flagged as drug-like. Improving interpretability is crucial for building trust in these tools and guiding the design of new, effective compounds [47].

6. Conclusion

Molecular modelling and computational approaches in drug design represent a paradigm shift in scientific methodology, providing advanced tools to understand the microscopic world of atoms and molecules.

These approaches enable researchers to model, analyze, and accurately predict the behavior of molecular systems. Their fundamental strength lies in bridging theory and experiment, offering scientists a flexible "computational playground" to explore complex problems that may be costly or difficult to address using traditional experimental methods.

These strategies rely on a range of advanced techniques, including molecular mechanics for studying structural and energetic aspects of drug–target interactions, molecular docking as a virtual platform to predict how small molecules bind to target proteins, and virtual screening to rapidly evaluate large libraries of compounds and identify promising candidates.

Furthermore, artificial intelligence and machine learning have emerged as transformative tools, accelerating drug discovery, enabling de novo drug design, and predicting pharmacological properties and toxicity prior to clinical testing.

This progress has significantly improved the efficiency of drug development, making it faster, more accurate, and less costly compared to conventional approaches.

Computational simulations facilitate the rapid identification and optimization of lead compounds and support the advancement of personalized medicine by enabling the design of therapies tailored to individual genetic profiles.

Moreover, these tools promote rational drug design based on precise structural and electronic complementarity between molecules and their biological targets, rather than relying on trial-and-error methods.

Despite these remarkable achievements, challenges remain, including issues related to data quality, the complexity and interpretability of artificial intelligence models, and the need for substantial computational resources.

Nevertheless, future prospects are highly promising, particularly with the advancement of quantum computing and emerging technologies such as organ-on-a-chip systems, which enhance the realism and accuracy of biological simulations.

Consequently, molecular modelling continues to play a central role in medical innovation, contributing to the development of more efficient and precise healthcare systems.

PART II:

EXPERIMENTAL

Chapter 01:

Materials & Methods

1. General Introduction

This chapter presents the experimental procedures and computational methodologies employed for the synthesis, structural characterisation, and in silico investigation of the ferrocenyl acetylaniline derivatives. The adopted approach integrates synthetic organic chemistry, advanced spectroscopic and electrochemical techniques, and state-of-the-art computational modelling in order to achieve a comprehensive understanding of the structural, electronic and potential antioxidant properties of the studied compounds.

The synthesis of the target derivatives was carried out at the Laboratory of Valorisation and Technology of Saharian Resources (VTRS), Faculty of Technology, University of El Oued, under controlled experimental conditions. The same laboratory hosted all computational investigations, including density functional theory (DFT) calculations, molecular docking, molecular dynamics simulations and MM-PBSA analyses, thereby ensuring a coherent and consistent interpretation of both experimental and theoretical data.

Structural characterisation was performed in collaboration with the Centre de Recherche Scientifique et Technique en Analyses Physico-Chimiques (CRAPC), University of Ouargla, using complementary analytical techniques including FT-IR, UV–visible spectroscopy, and one- and two-dimensional NMR experiments. In addition, cyclic voltammetry was employed to investigate the electrochemical behaviour of the ferrocenyl core, which plays a crucial role in its redox activity and antioxidant potential.

Furthermore, in silico pharmacokinetic and toxicity properties (ADMET) were predicted using validated computational tools in order to assess the drug-likeness, bioavailability and safety profile of the synthesised compounds. This additional analysis provides a preliminary evaluation of their potential suitability as bioactive agents.

Overall, this multidisciplinary strategy ensures the reliability, reproducibility and scientific robustness of the obtained results, while establishing a solid foundation for the interpretation of the physicochemical behaviour and biological relevance of the ferrocenyl derivatives.

2. Chemicals and Reagents

All chemicals and solvents used in this study were of analytical grade and were employed without further purification unless otherwise stated. The selection of reagents was based on their

suitability for organometallic synthesis and compatibility with subsequent spectroscopic and electrochemical analyses.

Ferrocene (Fc, 99%) and orthophosphoric acid (85%) were obtained from Alfa Aesar. The o-, m-, and p-aminoacetophenone isomers (99%), as well as tetrabutylammonium tetrafluoroborate (Bu_4NBF_4, electrochemical grade, 99%), used as supporting electrolyte in electrochemical measurements, were purchased from Sigma-Aldrich. Iodomethane and anhydrous magnesium sulfate (97%) were supplied by Acros Organics. Acetic acid (99–100%) and ethanol (95%) were obtained from Biochem Chemopharma.

The ferrocenylmethyl-based quaternary ammonium intermediate was prepared according to previously reported procedures and used without further modification [1]. All aqueous solutions were prepared using double-distilled water, and solvents used for spectroscopic and electrochemical measurements were of appropriate purity to ensure reproducibility.

Stock solutions were freshly prepared when required and handled under standard laboratory conditions to minimise contamination and degradation.

3. Instrumentation and Experimental Conditions

A combination of spectroscopic and electrochemical techniques was employed to confirm the structural integrity and to investigate the physicochemical properties of the synthesised ferrocenyl acetylaniline derivatives. All measurements were carried out under controlled experimental conditions using calibrated instruments to ensure accuracy, reproducibility and reliability of the obtained data.

3.1. Spectroscopic Analysis

3.1.1. FT-IR Spectroscopy

Fourier-transform infrared (FT-IR) spectra were recorded using a Shimadzu 8000S spectrophotometer over the wavenumber range of 4000–400 cm^{-1}. The samples were prepared in the solid state using KBr pellets.

This technique was primarily used to identify the characteristic functional groups present in the synthesised compounds, including N–H stretching vibrations, carbonyl (C=O) groups, and aromatic C–H bonds. The observed absorption bands allowed confirmation of the successful formation of the ferrocenyl acetylaniline framework [2].

3.1.2. UV–Visible Spectroscopy

UV–visible absorption spectra were obtained using a Shimadzu UV-1800 spectrophotometer in the wavelength range of 200–900 nm. Measurements were performed in dimethyl sulfoxide (DMSO) using quartz cuvettes with a path length of 1 cm.

This analysis enabled the investigation of electronic transitions associated with both the ferrocenyl moiety and the conjugated aromatic system. In particular, π–π* and n–π* transitions, as well as metal-centred d–d transitions, were identified, providing insight into the electronic structure of the compounds [3].

3.2. Nuclear Magnetic Resonance (NMR)

3.2.1. ^{1}H NMR Analysis

Proton nuclear magnetic resonance (^{1}H NMR) spectra were recorded on a Bruker ARX-500 spectrometer operating at 400 MHz. The samples were dissolved in deuterated dimethyl sulfoxide (DMSO-d_6), and chemical shifts (δ) were reported in parts per million (ppm) relative to tetramethylsilane (TMS) as an internal standard.

This technique was used to identify the different proton environments corresponding to the ferrocenyl unit, aromatic protons, methylene bridge (–CH_2–), and acetyl group (–$COCH_3$), thus confirming the structural features of the synthesised derivatives [4].

3.2.2. ^{13}C NMR Analysis

Carbon-13 nuclear magnetic resonance (^{13}C NMR) spectra were acquired under similar conditions using the same spectrometer. The spectra provided detailed information on the carbon framework of the compounds, including the identification of carbonyl carbons, aromatic carbons, cyclopentadienyl rings, and methylene carbons.

This analysis was essential for confirming the molecular structure and verifying the successful functionalisation of the ferrocenyl core [5].

3.2.3. Two-Dimensional NMR (HSQC/HMBC)

Two-dimensional NMR experiments, including heteronuclear single quantum coherence (HSQC) and heteronuclear multiple bond correlation (HMBC), were performed to establish proton–carbon connectivity.

HSQC spectra enabled the identification of direct one-bond correlations between protons and their attached carbon atoms, while HMBC provided long-range (two- and three-bond) correlations.

These complementary techniques allowed unambiguous assignment of the molecular structures and confirmation of the substitution pattern on the aromatic ring [6].

3.3. Electrochemical Measurements (Cyclic Voltammetry)

Electrochemical characterisation was carried out using a PGZ301 potentiostat/galvanostat (Radiometer Analytical SAS, France) in dimethyl sulfoxide (DMSO) under an inert nitrogen atmosphere at 298 K.

A conventional three-electrode system was employed, consisting of a glassy carbon working electrode (surface area 0.013 cm^2), a platinum wire counter electrode (0.05 cm^2), and a saturated Hg/Hg_2Cl_2 reference electrode.

Tetrabutylammonium tetrafluoroborate (Bu_4NBF_4, 0.1 M) was used as the supporting electrolyte. Prior to each measurement, the solution was purged with nitrogen to remove dissolved oxygen and ensure stable electrochemical conditions.

Cyclic voltammetry measurements were performed within an appropriate potential window to investigate the reversible Fe(II)/Fe(III) redox behaviour of the ferrocenyl derivatives. The obtained electrochemical parameters, including anodic and cathodic peak currents and potentials, provided valuable insight into the electron transfer properties of the compounds, which are closely associated with their antioxidant activity [7].

4. Synthesis of Ferrocenyl Acetylaniline Derivatives

This section describes the synthetic strategy employed for the preparation of the target ferrocenyl acetylaniline derivatives. The adopted methodology is based on a nucleophilic substitution reaction involving a ferrocenylmethyl quaternary ammonium intermediate, enabling efficient formation of the C–N bond under relatively mild and environmentally favourable conditions. This approach ensures good selectivity and reproducibility for the preparation of the three regioisomeric compounds.

The overall synthetic pathway leading to the formation of the target compounds is presented in Figure 1, which illustrates the formation of the ferrocenylmethyl intermediate followed by its reaction with the corresponding aminoacetophenone isomers.

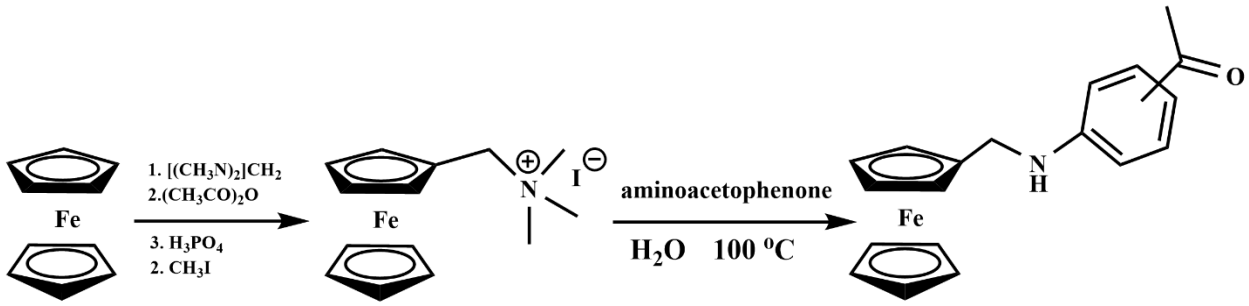

Figure II-1 Synthetic route for the preparation of N-[(ferrocenyl)methyl]acetylaniline derivatives (FcMe2Ac, FcMe3Ac and FcMe4Ac).

4.1. General Synthetic Procedure

The synthesis of N-[(ferrocenyl)methyl]acetylaniline derivatives was achieved through a nucleophilic substitution reaction between trimethylferrocenylmethylammonium iodide and the corresponding aminoacetophenone isomers (ortho, meta and para), as illustrated in Figure 1.

In a typical procedure, the appropriate aminoacetophenone (3.84 mmol) was added gradually to a well-stirred aqueous solution of trimethylferrocenylmethylammonium iodide (2.56 mmol) in distilled water (60 mL). The reaction mixture was refluxed for 4 hours under continuous stirring to ensure complete conversion.

Upon completion of the reaction, the mixture was allowed to cool to room temperature, leading to the formation of a yellow precipitate. The crude product was isolated by vacuum filtration and thoroughly washed with distilled water to remove residual inorganic salts and unreacted species.

The obtained solid was purified by recrystallisation from a 90% ethanol/water mixture. In the case of the meta-substituted derivative, additional purification by column chromatography (chloroform/methanol, 99:1 v/v) was performed to achieve higher purity.

This synthetic methodology presents several advantages, including the use of aqueous medium, operational simplicity, and avoidance of harsh reaction conditions, making it suitable for reproducible preparation of ferrocenyl derivatives [8].

4.2. Synthesis of Individual Compounds

4.2.1. N-[(ferrocenyl)methyl]-2-acetylaniline (FcMe2Ac)

Yield: 650 mg (77%).

Appearance: Yellow crystalline solid.

Melting point: 148–150 °C.

^{1}H NMR (500 MHz, DMSO-d_6): δ 2.60 (3H, m, CH_3), 3.40 (2H, t, α-C_5H_4), 4.05 (2H, t, β-C_5H_4), 4.15 (5H, s, C_5H_5), 4.30 (2H, d, CH_2N), 6.62 (1H, m, Ar-H), 6.84 (1H, d, Ar-H), 7.40 (1H, m, Ar-H), 7.85 (1H, d, Ar-H), 9.01 (1H, s, NH).

^{13}C NMR (500 MHz, DMSO-d_6): δ 29 (CH_3), 42 (CH_2N), 67, 68 (C_5H_4), 69 (C_5H_5), 87 (ipso-C), 112, 116, 118, 134, 138, 150 (aromatic carbons), 210 (C=O).

FT-IR (KBr, ν, cm^{-1}): 3426, 3291 (N–H), 3082 (Ar–C–H), 1647 (C=O), 1566, 1516 (C=C), 1454, 1416, 1146, 1003, 617.

UV–Vis (DMSO): λmax = 259 nm (π–π*), 380 nm (d–d).

Cyclic voltammetry (DMSO, Fc^+/Fc): Ipa = 29.13 μA, Ipc = −28.52 μA, Epa = 2.17 mV, Epc = −85.60 mV, ΔE = 87.8 mV, E° = 43.9 mV, Ipa/Ipc = 1.02.

4.2.2. N-[(ferrocenyl)methyl]-3-acetylaniline (FcMe3Ac)

Yield: 480 mg (48%).

Appearance: Yellow–orange crystalline solid.

Melting point: 138–140 °C.

^{1}H NMR (500 MHz, DMSO-d_6): δ 2.45 (3H, s, CH_3), 3.42 (2H, t, α-C_5H_4), 4.08 (2H, t, β-C_5H_4), 4.18 (5H, s, C_5H_5), 4.32 (2H, d, CH_2N), 6.70–7.20 (3H, m, Ar-H), 7.65 (1H, d, Ar-H), 8.95 (1H, s, NH).

^{13}C NMR (500 MHz, DMSO-d_6): δ 28 (CH_3), 43 (CH_2N), 66, 68 (C_5H_4), 69 (C_5H_5), 86 (ipso-C), 114, 118, 125, 131, 136, 152 (aromatic carbons), 205 (C=O).

FT-IR (KBr, ν, cm^{-1}): 3432, 3338 (N–H), 2925, 1650 (C=O), 1582, 1510, 1450, 1365, 1170, 820.

UV–Vis (DMSO): λmax = 268 nm, 402 nm.

Cyclic voltammetry (DMSO, Fc^+/Fc): Ipa = 52.4 μA, Ipc = −51.9 μA, Epa = 10 mV, Epc = −92 mV, ΔE = 102 mV, E° = 51.0 mV, Ipa/Ipc = 1.01.

4.2.3. N-[(ferrocenyl)methyl]-4-acetylaniline (FcMe4Ac)

Yield: 690 mg (80%).

Appearance: Deep yellow crystalline solid.

Melting point: 162–164 °C.

^{1}H NMR (500 MHz, DMSO-d_6): δ 2.35 (3H, m, CH_3), 3.41 (2H, t, α-C_5H_4), 4.10 (2H, t, β-C_5H_4), 4.20 (5H, s, C_5H_5), 4.31 (2H, d, CH_2N), 6.65 (2H, d, Ar-H), 6.78 (1H, t, NH), 7.76 (2H, d, Ar-H).

^{13}C NMR (500 MHz, DMSO-d_6): δ 28 (CH_3), 43 (CH_2N), 66 (C_5H_4), 68 (C_5H_5), 87 (ipso-C), 112, 125, 132, 154 (aromatic carbons), 194 (C=O).

FT-IR (KBr, ν, cm^{-1}): 3445, 3345 (N–H), 2932, 1651 (C=O), 1589, 1562, 1369, 1281, 1173, 822.
UV–Vis (DMSO): λmax = 432 nm.
Cyclic voltammetry (DMSO, Fc^{+}/Fc): Ipa = 71.07 µA, Ipc = −71.66 µA, Epa = 16 mV, Epc = −99 mV, ΔE = 115 mV, E° = 57.5 mV, Ipa/Ipc = 0.99.

5. Computational Methodology

Computational investigations were conducted to provide a comprehensive understanding of the electronic properties, antioxidant potential and molecular interactions of the synthesised ferrocenyl acetylaniline derivatives. The adopted in silico strategy integrates density functional theory (DFT) calculations, molecular docking, molecular dynamics (MD) simulations and MM-PBSA binding free energy analysis, complemented by ADMET predictions to evaluate pharmacokinetic and toxicity profiles.

This combined approach enables correlation between molecular structure, electronic behaviour and biological relevance, particularly in relation to oxidative stress modulation.

5.1. Density Functional Theory (DFT) Calculations

Density functional theory calculations were performed using Gaussian 16 [9] to investigate the electronic structure and reactivity of FcMe2Ac, FcMe3Ac and FcMe4Ac.

All molecular geometries were optimised at the B3LYP level of theory using the 6-311++G(d,p) basis set for C, H, N and O atoms, while the Stuttgart–Dresden (SDD) effective core potential was applied for the iron centre [10]. Frequency calculations were carried out at the same level to confirm that the optimised geometries correspond to true minima, characterised by the absence of imaginary frequencies.

The optimised structures were used to determine frontier molecular orbitals (HOMO and LUMO), energy gaps, electronegativity, chemical hardness, softness and electrophilicity index. Particular emphasis was placed on HOMO distribution, given its direct relevance to electron-donating capacity and radical scavenging behaviour.

Molecular electrostatic potential (MEP), electron localisation function (ELF), localised orbital locator (LOL), and reduced density gradient (RDG) analyses were also performed to characterise charge distribution and weak intramolecular interactions. Visualisation and analysis were carried out using GaussView and Multiwfn [11].

5.2. Molecular Docking Studies

Molecular docking simulations were performed to investigate the binding affinity and interaction mechanisms of the synthesised compounds with key oxidative stress-related enzymes: xanthine oxidase (PDB ID: 1FIQ) and NADPH oxidase (PDB ID: 8WEJ).

5.2.1. Protein Preparation

The three-dimensional structures of the target enzymes used in this study are presented in Figure 2, illustrating the structural organisation of xanthine oxidase and NADPH oxidase prior to preparation.

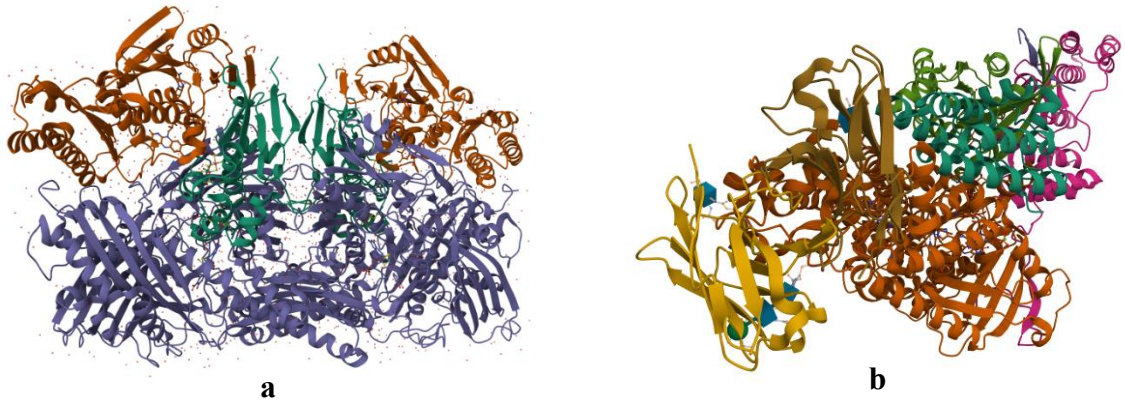

Figure II-2 Three-dimensional structures of the target proteins used in docking studies: (a) xanthine oxidase (PDB ID: 1FIQ) and (b) NADPH oxidase (PDB ID: 8WEJ).

The crystallographic structures were retrieved from the Protein Data Bank (https://www.rcsb.org/) [12], and prepared using AutoDock Tools (ADT 1.5.7) [13]. All crystallographic water molecules, co-crystallised ligands and non-essential heteroatoms were removed to prevent interference with ligand binding and to ensure accurate representation of the active site.

Polar hydrogen atoms were added, and Kollman charges were assigned. The prepared proteins were then converted into PDBQT format.

5.2.2. Ligand Preparation

The optimised molecular structures of the ferrocenyl derivatives used as ligands are shown in Figure 3, highlighting their geometry prior to docking calculations.

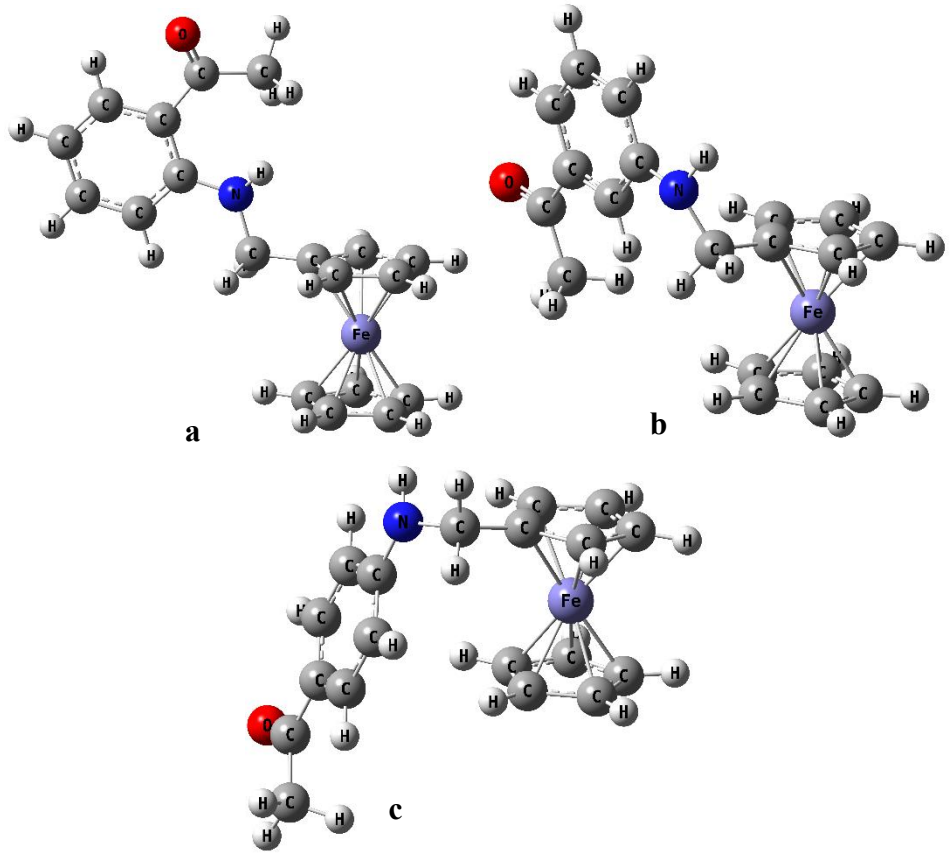

Figure II-3 Optimised molecular structures of ferrocenyl derivatives used as ligands: FcMe2Ac (a), FcMe3Ac (b) and FcMe4Ac (c).

The ligands were prepared using AutoDock Tools by assigning Gasteiger charges and defining rotatable bonds. The structures were then saved in PDBQT format.

5.2.3. Docking Protocol and Validation

The overall docking workflow adopted in this study is illustrated in Figure 4, showing the sequence of protein preparation, ligand preparation, grid generation, docking and interaction analysis.

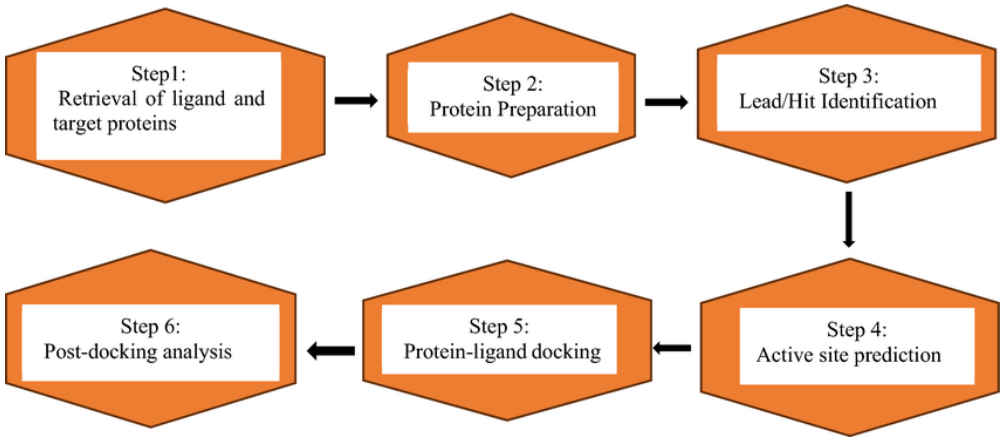

Figure II-4 Molecular docking workflow illustrating protein and ligand preparation, grid generation, docking execution and interaction analysis.

Docking calculations were carried out using AutoDock 4.2 with the Lamarckian genetic algorithm. A grid box of 60 × 60 × 60 Å with a spacing of 0.375 Å was centred on the coordinates of the co-crystallised ligand within the active site.

For each system, 100 independent docking runs were performed. The most stable conformation was selected based on the lowest binding energy and cluster population.

Validation of the docking protocol was performed by redocking the native ligand into the active site, in order to confirm the robustness and reliability of the docking procedure [14].

5.3. Molecular Dynamics (MD) Simulations

Molecular dynamics simulations were performed to evaluate the stability and dynamic behaviour of the selected protein–ligand complexes using GROMACS [15].

5.3.1. System Setup and Solvation

The solvation of the protein–ligand complex within an explicit water box is presented in Figure 5, which illustrates the simulation environment prior to energy minimization.

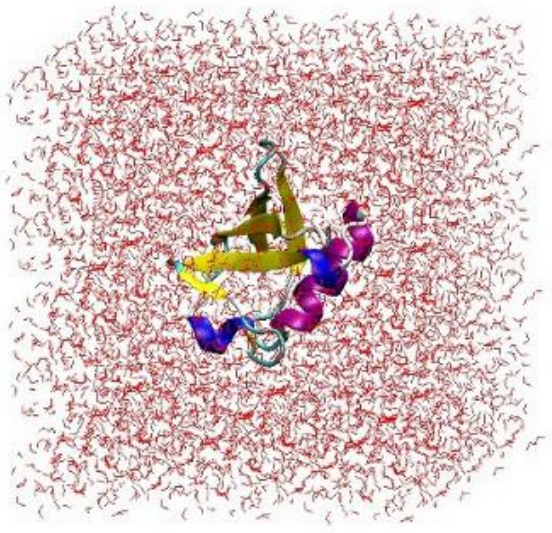

Figure II-5 Solvated protein–ligand complex showing the explicit water box used for molecular dynamics simulations.

The selected complexes were parameterised using the CHARMM36 force field [16], and ligand parameters were generated using the CGenFF protocol [17]. Each system was placed in a cubic simulation box with a minimum distance of 10 Å from the protein surface to the box boundary and solvated using the TIP3P water model. Counter ions were added to neutralise the system.

5.3.2. Energy Minimisation and Equilibration

The general molecular dynamics simulation protocol, including minimisation, equilibration and production stages, is summarised in Figure 6.

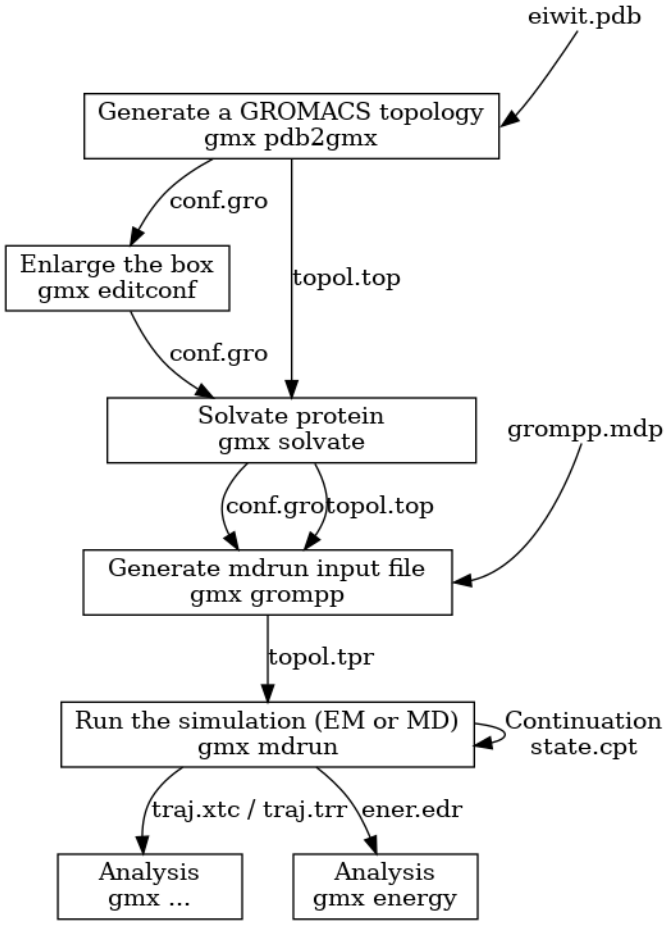

Figure II-6 Molecular dynamics simulation workflow including system preparation, energy minimisation, equilibration and production phases.

Energy minimisation was performed using the steepest descent algorithm. The system was then equilibrated under NVT conditions (300 K, 500 ps) followed by NPT conditions (1 atm, 500 ps) using the V-rescale thermostat and Parrinello–Rahman barostat.

5.3.3. Production Run Parameters

Production simulations were conducted for 100 ns with a time step of 2 fs. Periodic boundary conditions were applied in all directions, and long-range electrostatic interactions were treated using the Particle Mesh Ewald (PME) method. Covalent bonds involving hydrogen atoms were constrained using the LINCS algorithm.

Trajectory analyses were carried out using GROMACS built-in tools, including RMSD, RMSF, radius of gyration (Rg), and solvent surface accessibility area (SASA).

5.4. MM-PBSA Binding Free Energy Calculations

Binding free energy calculations were performed using the g_mmpbsa tool [18]. Snapshots extracted from the last 20 ns of equilibrated trajectories were used.

The total binding free energy (ΔG_bind) was estimated as the sum of van der Waals, electrostatic, polar solvation and non-polar solvation contributions.

5.5. ADMET Prediction

ADMET predictions were performed using ADMETlab 2.0 [19] and ProTox-II [20] to evaluate pharmacokinetic and toxicity profiles of the synthesised compounds.

Parameters assessed included gastrointestinal absorption, blood–brain barrier permeability, cytochrome P450 interactions, plasma protein binding, hepatotoxicity and acute toxicity (LD_{50}).

Chapter 02:

Results & Discussion

1. General Introduction

This chapter presents and discusses the experimental and computational results obtained for the synthesised ferrocenyl acetylaniline derivatives. The analysis aims to establish clear relationships between molecular structure, electronic properties and potential antioxidant behaviour through a comprehensive interpretation of both experimental data and in silico findings.

The discussion begins with the evaluation of the synthetic outcomes, including reaction efficiency and substituent effects, followed by detailed structural characterisation using FT-IR, UV–visible spectroscopy, nuclear magnetic resonance (^{1}H, ^{13}C and 2D NMR) and cyclic voltammetry. These techniques provide complementary information allowing confirmation of the molecular structures and insight into the electronic properties of the ferrocenyl core.

Subsequently, computational investigations are presented to support and extend the experimental observations. Density functional theory calculations are used to analyse electronic descriptors and charge distribution, while molecular docking and molecular dynamics simulations provide insight into the interaction of the compounds with oxidative stress-related enzymes. Finally, MM-PBSA and ADMET analyses are discussed to evaluate binding stability and pharmacokinetic potential.

2. Synthesis of Ferrocenyl Acetylaniline Derivatives

The ferrocenyl acetylaniline derivatives (FcMe2Ac, FcMe3Ac and FcMe4Ac) were successfully synthesised via a nucleophilic substitution reaction involving a ferrocenylmethyl quaternary ammonium intermediate and the corresponding aminoacetophenone isomers. The adopted synthetic approach proved to be efficient and reproducible, yielding the desired compounds as yellow to orange crystalline solids under relatively mild experimental conditions.

The reaction mechanism is illustrated in Figure 7, which highlights the key steps involved in the formation of the C–N bond through nucleophilic substitution at the ferrocenylmethyl position.

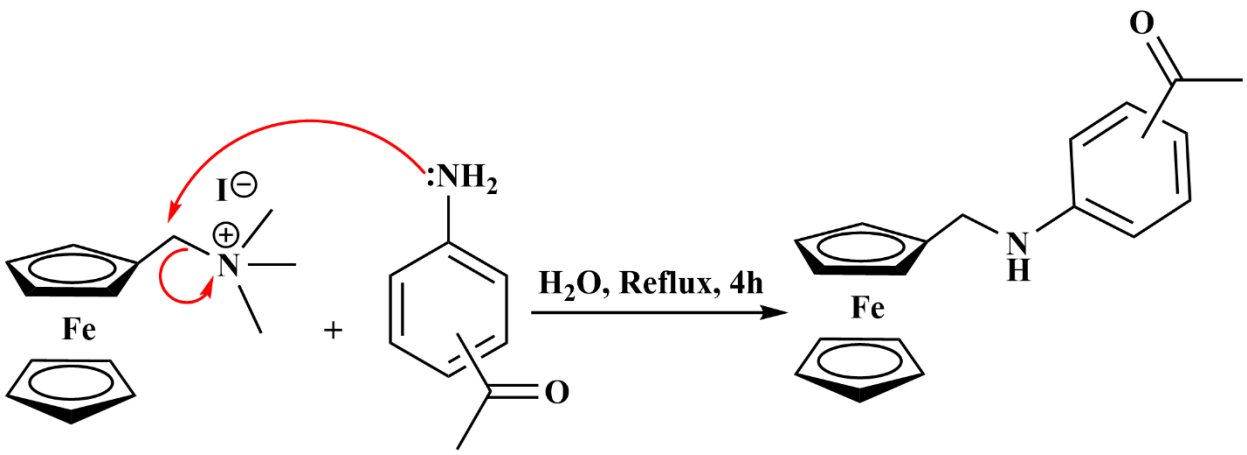

Figure II-7 Proposed reaction mechanism for the formation of N-[(ferrocenyl) methyl] acetylaniline derivatives via nucleophilic substitution.

As shown in Figure 7, the reaction proceeds via an SN2-type mechanism in which the lone pair of electrons on the amino group attacks the electrophilic methylene carbon attached to the quaternary ammonium moiety [21]. This results in the displacement of trimethylamine as a leaving group and formation of the desired ferrocenylmethylamine linkage [21].

The efficiency of this transformation can be attributed to several factors. First, the ferrocenyl unit acts as an electron-donating group, which stabilises the transition state and enhances the electrophilicity of the methylene carbon [22]. Secondly, the quaternary ammonium group constitutes an excellent leaving group, facilitating bond cleavage under aqueous conditions. Such behaviour is well documented in the literature for ferrocenylmethyl derivatives, where nucleophilic substitution reactions proceed readily due to the combined electronic and structural features of the ferrocenyl system [23,24].

The chemical structures of the synthesised compounds are presented in Figure 8, highlighting the positional variation of the acetyl substituent on the aromatic ring.

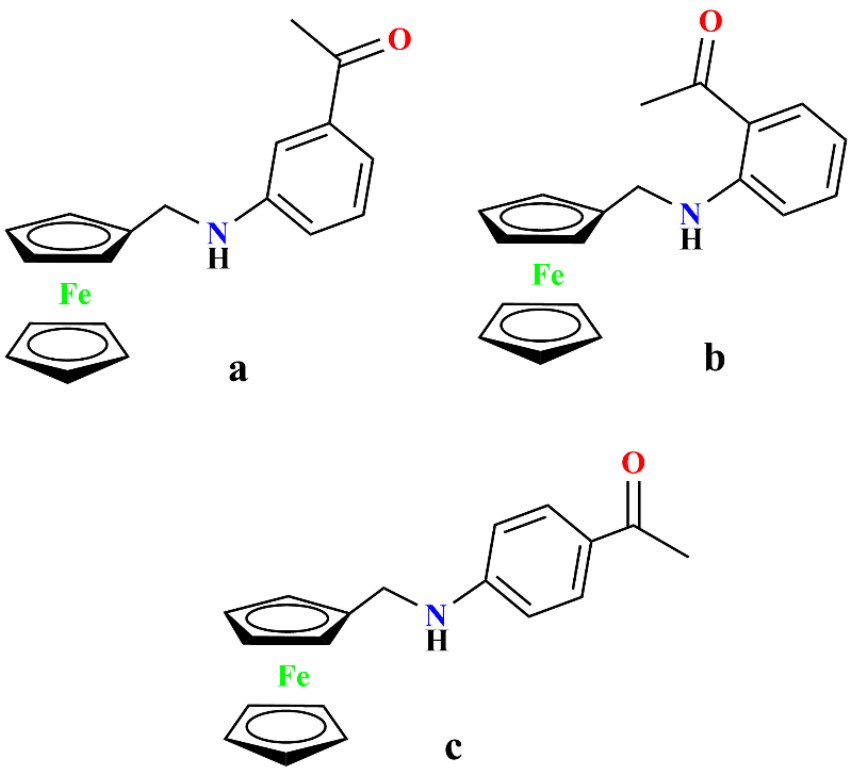

Figure II-8 Chemical structures of the synthesised ferrocenyl acetylaniline derivatives: (a) FcMe2Ac (ortho), (b) FcMe3Ac (meta), and (c) FcMe4Ac (para).

As illustrated in Figure 8, the three derivatives differ only by the position of the acetyl group (ortho, meta or para), which is expected to influence both steric accessibility and electronic distribution. These factors play a crucial role in determining the reactivity of the amino group during the substitution process [25].

To better evaluate the synthetic efficiency, the yields and physical characteristics of the obtained compounds are summarised in Table 1.

Table II-1. Yields and physical properties of the synthesised ferrocenyl acetylaniline derivatives.

Compound	Substituent Position	Yield (%)	Appearance	Melting Point (°C)
FcMe2Ac	Ortho	77	Yellow crystalline solid	148–150
FcMe3Ac	Meta	48	Yellow–orange solid	138–140
FcMe4Ac	Para	80	Deep yellow solid	162–164

As shown in **Table 1**, the reaction yields follow the order: FcMe4Ac > FcMe2Ac > FcMe3Ac

This trend can be rationalised by considering both steric and electronic effects, which are known to govern nucleophilic substitution reactions in aromatic amines. The para-substituted derivative (FcMe4Ac) exhibited the highest yield (80%), reflecting minimal steric hindrance and favourable resonance interaction between the acetyl group and the amino functionality. This electronic delocalisation enhances the nucleophilicity of the amine, thereby facilitating the substitution process [26].

In contrast, the meta derivative (FcMe3Ac) showed a significantly lower yield (48%), which can be attributed to the absence of resonance interaction between the substituents. In the meta position, the acetyl group exerts mainly an inductive electron-withdrawing effect, reducing the electron density on the amino group and consequently its nucleophilicity.

The ortho derivative (FcMe2Ac) presented intermediate behaviour (77%), where steric hindrance between adjacent substituents partially limits the accessibility of the nucleophilic site, despite favourable electronic effects.

These observations are in good agreement with previously reported studies on substituted aniline derivatives, where both steric congestion and electronic factors significantly influence reactivity. Furthermore, the results confirm that the adopted synthetic strategy is robust and well adapted for the preparation of ferrocenyl derivatives with controlled structural variation [27].

3. FT-IR Spectral Analysis

The structural features of the synthesised ferrocenyl acetylaniline derivatives were first examined by Fourier-transform infrared spectroscopy. The recorded FT-IR spectra for FcMe2Ac, FcMe3Ac and FcMe4Ac are presented in Figure 9, while the main absorption bands and their assignments are summarised in Table 2.

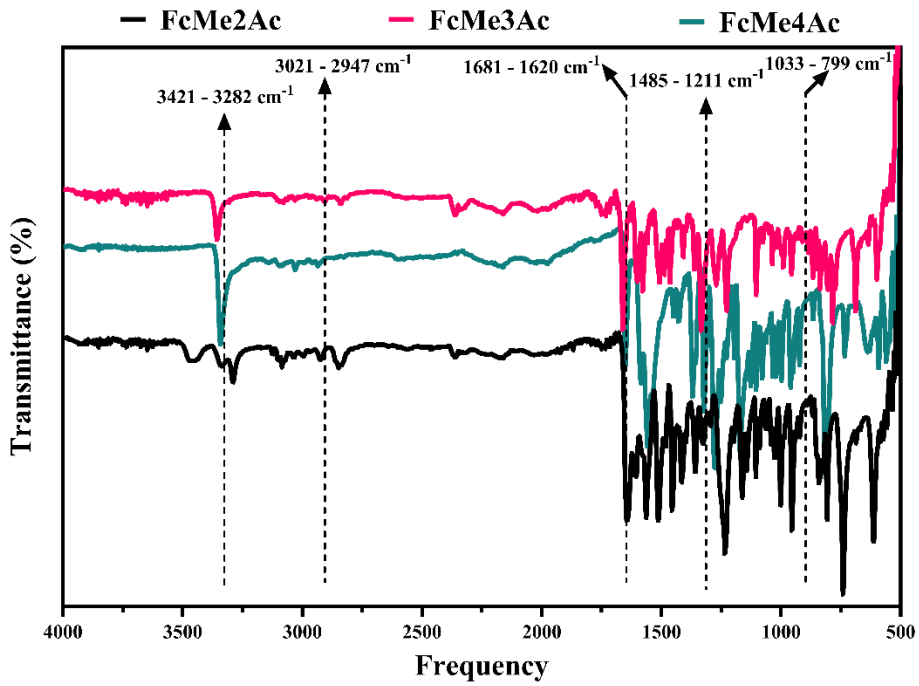

Figure II-9 FT-IR spectra of the synthesised ferrocenyl acetylaniline derivatives.

Table II-2. Characteristic FT-IR absorption bands (cm^{-1}) and their assignments for the synthesised compounds.

Assignment	FcMe2Ac (cm^{-1})	FcMe3Ac (cm^{-1})	FcMe4Ac (cm^{-1})	Description
N–H stretching	3426, 3291	3432, 3338	3445, 3345	Secondary amine vibration
Ar–C–H stretching	3082	—	—	Aromatic C–H
C=O stretching	1647	1650	1651	Acetyl carbonyl group
C=C (aromatic)	1566, 1516	1582, 1510	1589, 1562	Aromatic ring vibrations
C–N stretching	1146	1170	1173	Amine linkage
C–H bending	1454, 1416	1450, 1365	1369	Methyl/aromatic bending
Out-of-plane C–H	1003, 617	820	822	Aromatic substitution pattern

As shown in Figure 9, all three compounds exhibit similar spectral profiles, confirming the preservation of the ferrocenyl acetylaniline framework across the series, with only minor variations attributable to substituent position [28].

The presence of broad absorption bands in the region 3445–3291 cm^{-1} is characteristic of N–H stretching vibrations, confirming the formation of the secondary amine linkage resulting from the nucleophilic substitution reaction. The slight variation in band positions among the three derivatives reflects differences in hydrogen bonding interactions and local electronic environments [29].

A strong absorption band observed around 1651–1647 cm^{-1} corresponds to the stretching vibration of the carbonyl (C=O) group of the acetyl moiety. The consistency of this band across all compounds confirms the preservation of the acetyl functionality during the synthetic process.

The aromatic C=C stretching vibrations appearing in the region 1589–1510 cm^{-1} further support the presence of the substituted benzene ring. Additionally, the bands observed in the range 1173–1146 cm^{-1} can be attributed to C–N stretching vibrations, providing direct evidence for the successful formation of the C–N bond between the ferrocenylmethyl group and the aniline derivative.

The out-of-plane C–H bending vibrations observed between 820 and 617 cm^{-1} are particularly informative, as they reflect the substitution pattern on the aromatic ring. Differences in these bands among the ortho, meta and para derivatives further confirm the positional variation of the acetyl group.

Overall, the FT-IR analysis confirms the successful synthesis of the target ferrocenyl acetylaniline derivatives, with all characteristic functional groups clearly identified. The obtained spectral data are in good agreement with previously reported values for structurally related ferrocenyl and aniline-based compounds, further supporting the structural assignment [30].

4. UV–Visible Spectral Analysis

The electronic absorption properties of the synthesised ferrocenyl acetylaniline derivatives were investigated by UV–visible spectroscopy in DMSO. The recorded spectra are presented in Figure 10, while the corresponding absorption maxima are summarised in Table 3.

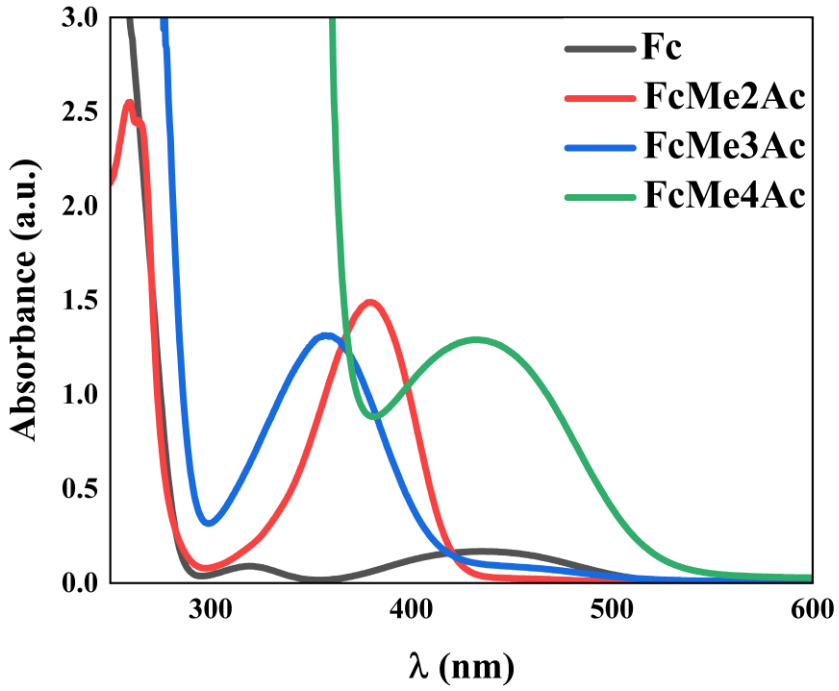

Figure II-10 UV–visible absorption spectra of the synthesised ferrocenyl acetylaniline derivatives.

Table II-3. UV–visible absorption maxima (λmax) of the synthesised ferrocenyl acetylaniline derivatives.

Compound	λmax (nm)	Assignment
FcMe2Ac	259	π → π* (aromatic system)
	380	d–d (Fe^{2+} centre)
FcMe3Ac	268	π → π*
	402	d–d transition
FcMe4Ac	432	d–d / charge transfer

As shown in Figure 10, all compounds exhibit characteristic absorption bands associated with both the aromatic system and the ferrocenyl moiety. The presence of intense absorption bands in the ultraviolet region (259–268 nm) is attributed to π → π* transitions within the conjugated aromatic system. These transitions arise from electron excitation within the benzene ring and are commonly observed in substituted aniline derivatives [31].

In the visible region, the absorption bands observed between 380 and 432 nm are associated with transitions involving the ferrocenyl iron centre. These bands can be attributed to metal-centred d–d transitions and, in some cases, ligand-to-metal charge transfer (LMCT), reflecting the interaction between the iron atom and the surrounding π-electron system.

A notable bathochromic shift is observed from FcMe2Ac (380 nm) to FcMe4Ac (432 nm), indicating an increase in conjugation and electronic delocalisation in the para-substituted derivative. This behaviour can be explained by the more effective resonance interaction between the acetyl group and the aromatic system in the para position, which enhances electron delocalisation and lowers the energy gap between molecular orbitals [32].

In contrast, the meta derivative (FcMe3Ac) exhibits intermediate behaviour, as the meta position does not allow efficient resonance interaction between substituents, leading to less pronounced electronic delocalisation. The ortho derivative (FcMe2Ac), although capable of resonance interaction, is affected by steric hindrance, which may slightly distort planarity and reduce conjugation efficiency.

These observations are consistent with previously reported studies on ferrocenyl and substituted aromatic systems, where substituent position significantly influences electronic transitions and absorption behaviour.

Overall, the UV–visible analysis confirms the presence of the ferrocenyl chromophore and highlights the impact of substituent position on the electronic structure of the compounds, which is directly related to their redox and potential antioxidant properties [33].

5. NMR Spectral Analysis

The structural elucidation of the synthesised ferrocenyl acetylaniline derivatives was comprehensively achieved using ^{1}H NMR, ^{13}C NMR and two-dimensional NMR techniques. In order to ensure clarity and facilitate interpretation, the spectra are presented separately for each compound, allowing direct correlation between spectral features and molecular structure.

5.1. ^{1}H NMR Analysis

The ^{1}H NMR spectra of the three derivatives are presented in Figure 11.

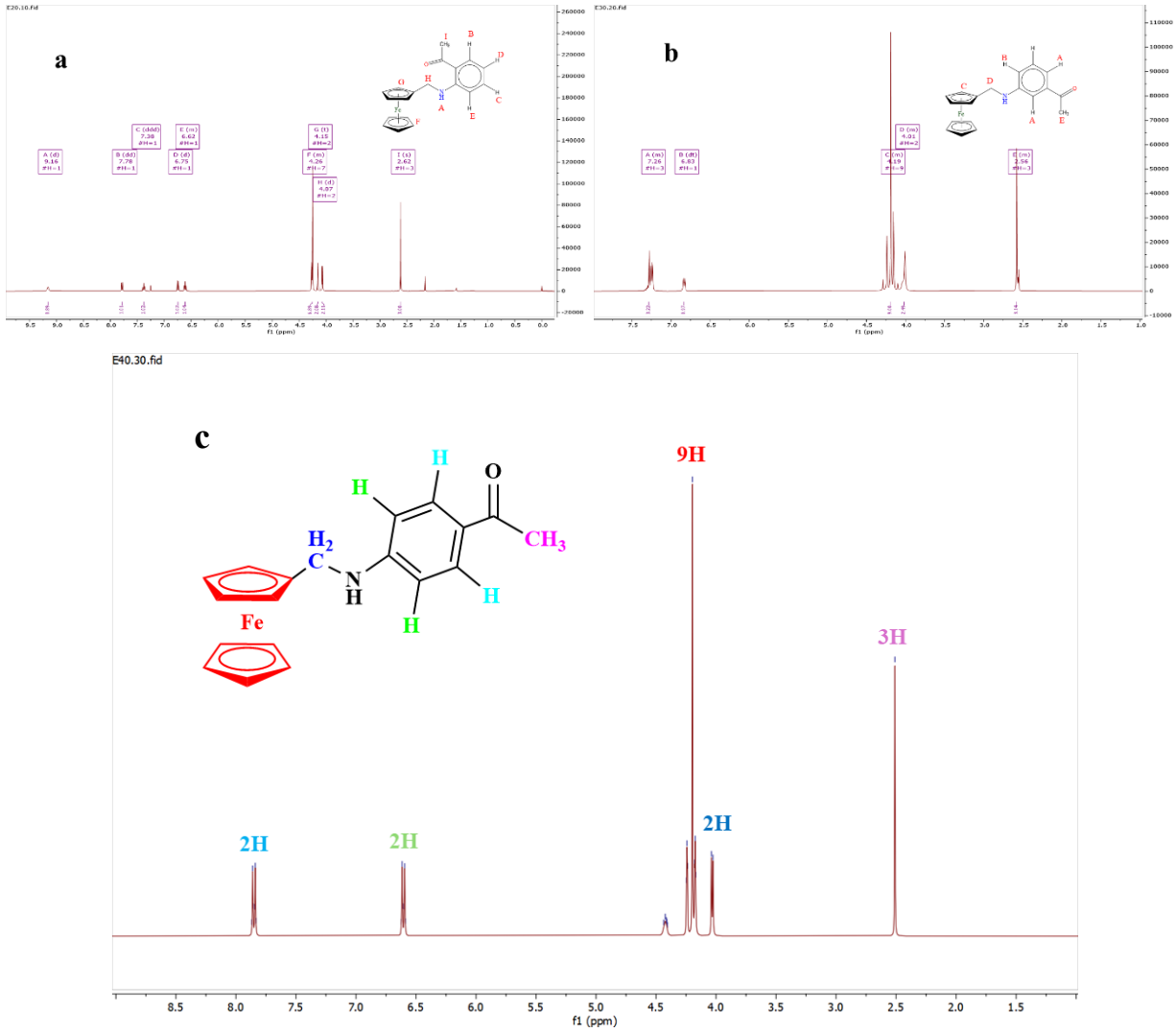

Figure II-11 ^{1}H NMR spectra of the synthesised ferrocenyl acetylaniline derivatives: (a) FcMe2Ac, (b) FcMe3Ac, and (c) FcMe4Ac.

As shown in Figure 11, all compounds exhibit characteristic proton signals confirming the successful formation of the target structures.

The methyl group of the acetyl moiety (–$COCH_3$) appears as a singlet in the region 2.35–2.60 ppm. The methylene bridge (–CH_2–N–), which links the ferrocenyl unit to the aromatic ring, is observed as a doublet around 4.30 ppm, confirming the formation of the C–N bond [34].

The ferrocenyl unit displays its typical spectral signature. The unsubstituted cyclopentadienyl ring (C_5H_5) appears as a singlet at approximately 4.15–4.20 ppm, while the substituted Cp ring (C_5H_4) gives rise to multiplet signals in the region 3.40–4.10 ppm. This splitting pattern reflects the loss of symmetry upon substitution, which is a well-established feature in ferrocenyl chemistry.

The aromatic protons are observed in the region 6.6–7.8 ppm, with distinct patterns depending on the substitution position. The ortho, meta and para isomers exhibit clearly different splitting behaviours, allowing unambiguous differentiation between the three compounds.

The NH proton appears as a downfield signal (≈ 8.9–9.0 ppm) in FcMe2Ac and FcMe3Ac, indicating possible hydrogen bonding interactions. In FcMe4Ac, a slight upfield shift is observed, which may be attributed to differences in electronic delocalisation in the para-substituted system [35].

5.2. ^{13}C NMR Analysis

The ^{13}C NMR spectra of the synthesised compounds are shown in Figure 12.

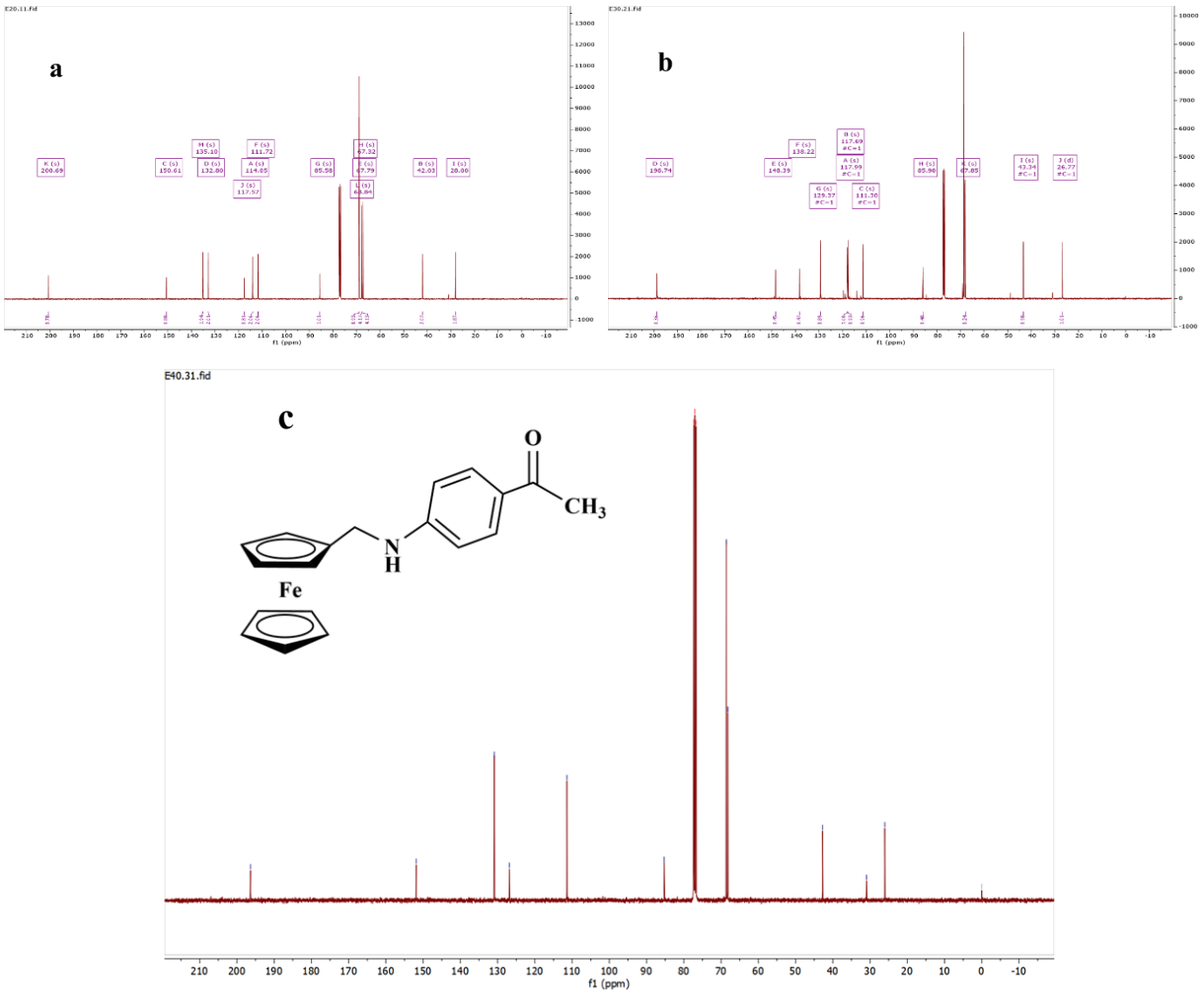

Figure II-12. ^{13}C NMR spectra of the synthesised ferrocenyl acetylaniline derivatives: (a) FcMe2Ac, (b) FcMe3Ac, and (c) FcMe4Ac.

As illustrated in Figure 12, the spectra provide clear evidence for the carbon framework of the compounds.

The carbonyl carbon (C=O) is observed in the downfield region between 194 and 210 ppm, confirming the presence of the acetyl group. The variation in chemical shift among the three derivatives reflects differences in electronic environment due to substituent position.

The methylene carbon (CH_2–N) appears consistently around 42–43 ppm, confirming the linkage between the ferrocenyl moiety and the aromatic system.

The ferrocenyl carbons are detected in the range 66–69 ppm, corresponding to the cyclopentadienyl rings. The ipso carbon bonded to the substituent appears slightly downfield due to its distinct electronic environment.

Aromatic carbons are distributed between 112 and 154 ppm, with slight variations depending on substitution pattern, which is consistent with substituted benzene derivatives [36].

5.3. Two-Dimensional NMR Analysis (HSQC and HMBC)

Two-dimensional NMR spectroscopy was employed to achieve unambiguous structural assignment and to confirm the connectivity within the synthesised ferrocenyl acetylaniline derivatives. The HSQC and HMBC spectra are presented separately to allow a clear interpretation of both direct and long-range correlations.

The HSQC spectra of FcMe2Ac, FcMe3Ac and FcMe4Ac are shown in Figure 13, while the corresponding HMBC spectra are presented in Figure 14.

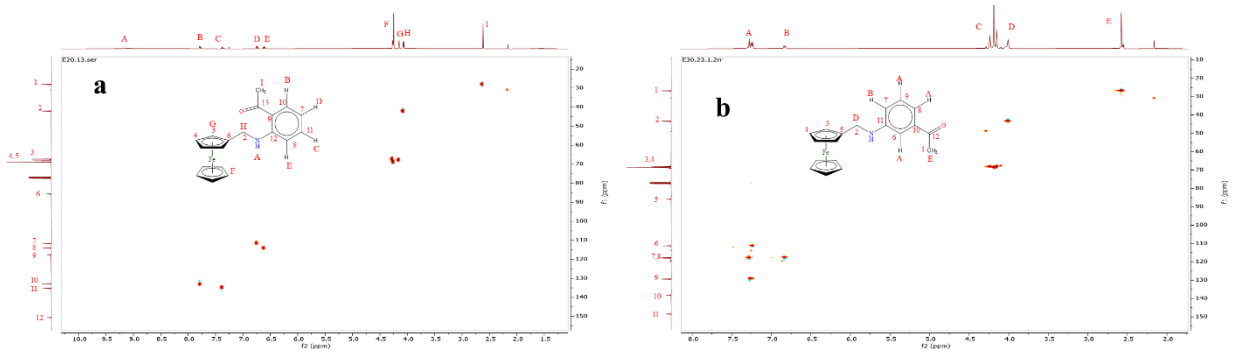

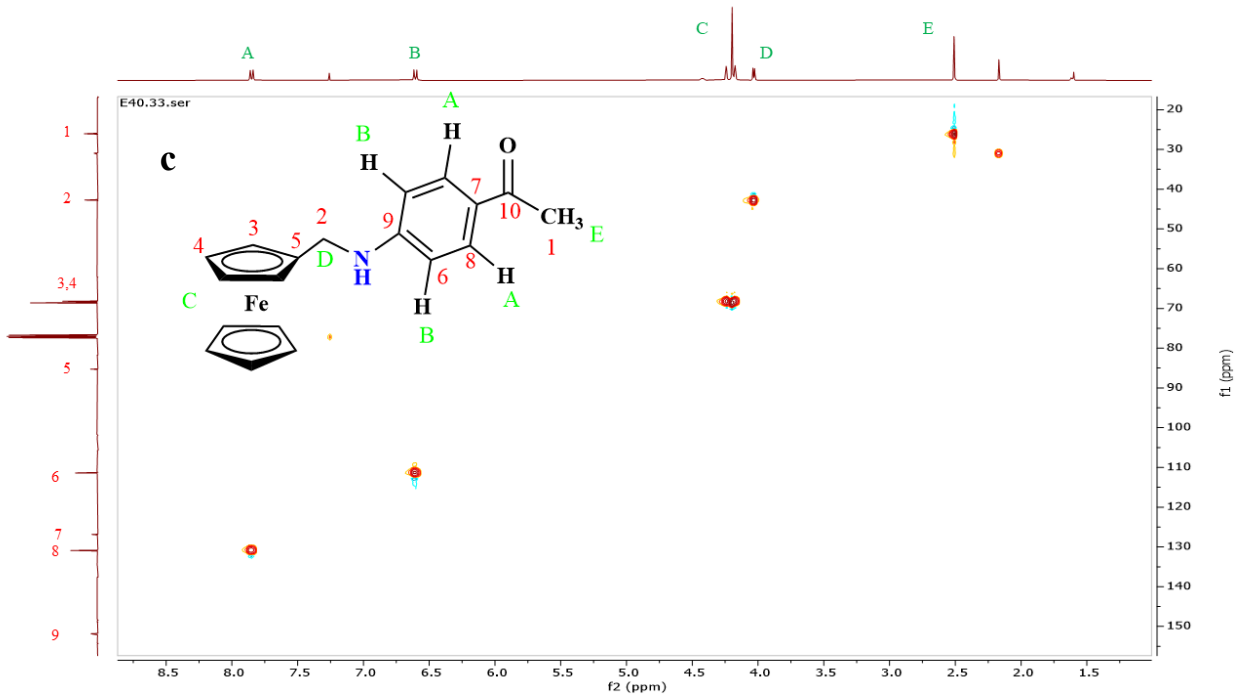

Figure II-13 HSQC spectra of the synthesised ferrocenyl acetylaniline derivatives: (a) FcMe2Ac, (b) FcMe3Ac, and (c) FcMe4Ac.

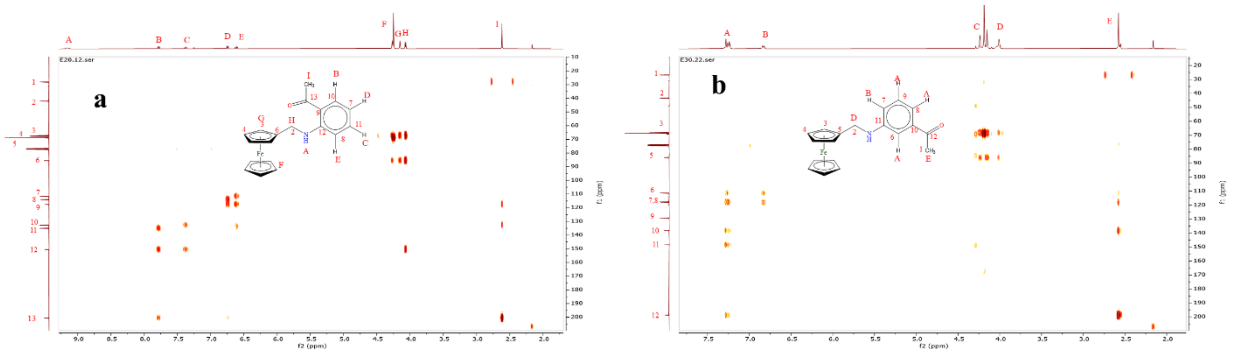

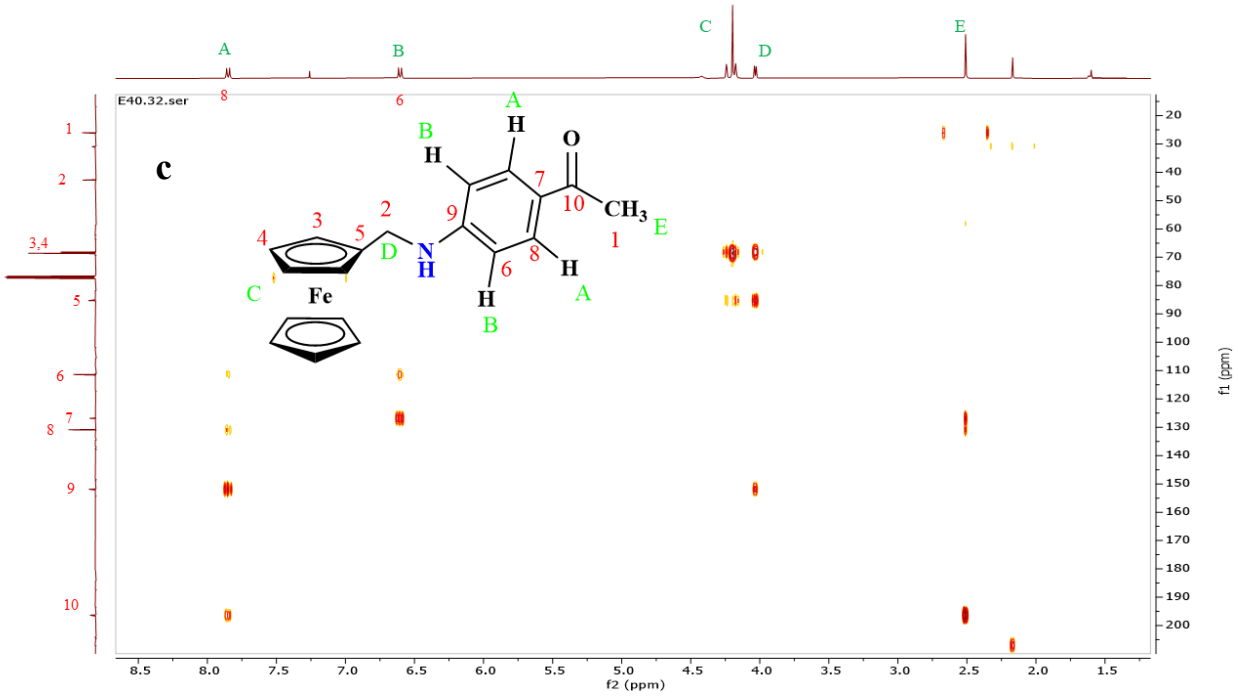

Figure II-14 HMBC spectra of the synthesised ferrocenyl acetylaniline derivatives: (a) FcMe2Ac, (b) FcMe3Ac, and (c) FcMe4Ac.

As illustrated in Figure 13, the HSQC spectra provide direct one-bond correlations between proton and carbon nuclei (^{1}JCH), allowing precise assignment of all protonated carbon atoms. The methylene protons (–CH$_2$–N–), observed around 4.30 ppm in the ^{1}H NMR spectra, show clear cross-peaks with their corresponding carbon signals at approximately 42–43 ppm, confirming the presence of the ferrocenylmethyl linkage.

Similarly, the signals corresponding to the cyclopentadienyl rings exhibit well-defined correlations. The unsubstituted Cp ring (C_5H_5) shows a single correlation pattern consistent with its symmetry, whereas the substituted Cp ring (C_5H_4) displays multiple correlations reflecting the loss of equivalence upon substitution. These observations are characteristic of monosubstituted ferrocenyl systems and further confirm the structural integrity of the organometallic core.

The aromatic proton signals also show distinct HSQC correlations with their corresponding carbon atoms in the region 112–140 ppm, enabling clear assignment of the benzene ring protons. The differences observed between the ortho, meta and para derivatives further support the positional variation of the acetyl substituent [37,38].

In contrast, the HMBC spectra (Figure 14) provide long-range correlations (^2JCH and ^3JCH), which are essential for confirming the connectivity between different fragments of the molecule. In particular, strong correlations are observed between the methylene protons (–CH_2–N–) and the aromatic carbons, confirming the formation of the C–N bond linking the ferrocenyl unit to the aniline moiety.

Additional long-range correlations between aromatic protons and the carbonyl carbon (C=O) are observed, allowing precise localisation of the acetyl group on the aromatic ring. These correlations are especially important for distinguishing between the regioisomers, as the HMBC patterns differ significantly depending on the substitution position (ortho, meta or para).

Furthermore, correlations involving the ferrocenyl carbons provide additional confirmation of the substitution pattern on the cyclopentadienyl ring. The combined HSQC and HMBC data therefore establish a complete mapping of proton–carbon connectivity within the molecules [39,40].

Overall, the two-dimensional NMR analysis provides definitive structural confirmation of the synthesised ferrocenyl acetylaniline derivatives. The observed correlation patterns are fully consistent with the proposed structures and are in excellent agreement with literature reports on related ferrocenyl compounds, where HSQC and HMBC techniques are commonly used to validate substitution patterns and molecular connectivity.

6. Cyclic Voltammetry Characterization

6.1. Redox Properties and Voltammetric Response

The electrochemical behaviour of FcMe2Ac, FcMe3Ac and FcMe4Ac was investigated by cyclic voltammetry in DMSO (1 mM) containing 0.1 M Bu_4NBF_4 as supporting electrolyte, using Hg/Hg_2Cl_2 as the reference electrode. The measurements were performed within a potential window of −0.60 to +0.60 V at a scan rate of 100 $mV \cdot s^{-1}$. Ferrocene (Fc/Fc^+) was employed as an internal reference ($E° = 0.00$ V).

The corresponding cyclic voltammograms are presented in Figure 15, where the electrochemical responses of the substituted derivatives are compared with that of ferrocene.

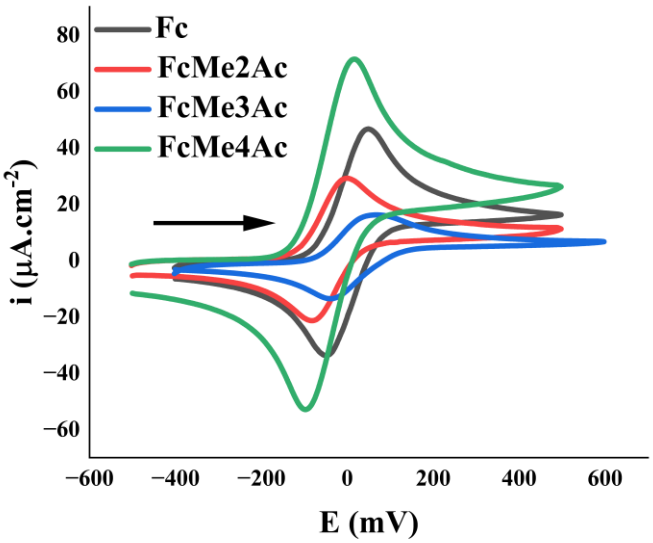

Figure II-15 Cyclic voltammograms of Fc, FcMe2Ac, FcMe3Ac and FcMe4Ac recorded in DMSO containing 0.1 M Bu_4NBF_4 at a scan rate of 100 $mV \cdot s^{-1}$ (referenced to Fc^+/Fc).

As observed in Figure 15, all compounds exhibit a single, well-defined redox couple corresponding to the Fe(II)/Fe(III) transition of the ferrocenyl centre. This confirms that the electroactive ferrocene unit retains its characteristic reversible behaviour after functionalisation [41].

A progressive anodic shift of the formal potential (E°) is observed upon substitution: FcMe2Ac (43.9 mV) < FcMe3Ac (51.0 mV) < FcMe4Ac (57.5 mV). This shift indicates a modulation of the electronic environment of the ferrocenyl core by the acetylaniline substituent. The increase in oxidation potential suggests a relative stabilisation of the Fe(II) state and/or a decreased electron density at the metal centre. Such behaviour is commonly reported in substituted ferrocenes, where electron-withdrawing groups induce anodic shifts in redox potentials [42].

The anodic-to-cathodic peak current ratios (Ipa/Ipc ≈ 1) confirm that the redox process is chemically reversible. However, the peak-to-peak separation (ΔEp = 87.8–115 mV) exceeds the theoretical value for a fully reversible one-electron transfer (59 mV), indicating a quasi-reversible system. This deviation may arise from kinetic limitations of electron transfer, uncompensated resistance in the medium, or structural reorganisation associated with oxidation [43].

6.2. Scan Rate Dependence and Mass Transport Regime

The influence of scan rate on the electrochemical response was examined in the range 100–500 $mV \cdot s^{-1}$. The resulting voltammograms are shown in Figure 16, while the dependence of anodic peak current on the square root of scan rate is presented in Figure 17.

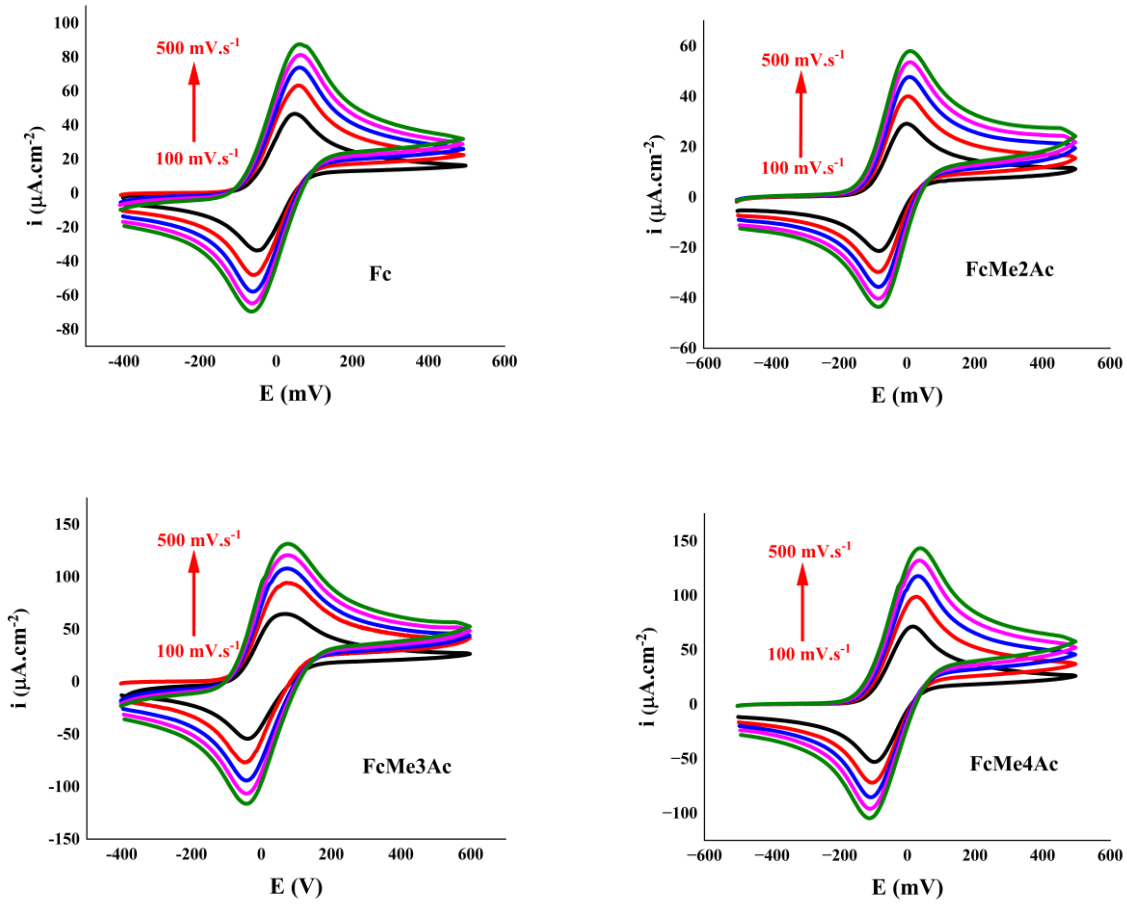

Figure II-16 Cyclic voltammograms of Fc, FcMe2Ac, FcMe3Ac and FcMe4Ac at different scan rates (100–500 $mV \cdot s^{-1}$).

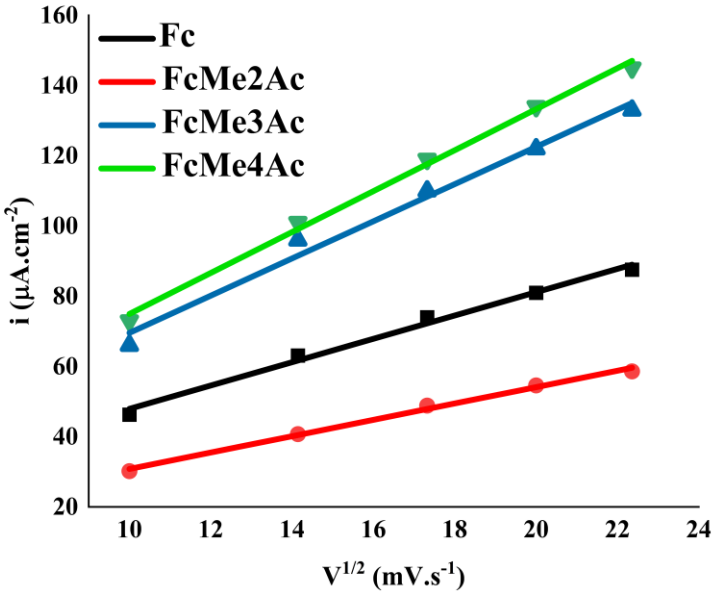

Figure II-17 Linear variation of anodic peak current (i_{pa}) as a function of the square root of scan rate ($\nu^{1/2}$).

As illustrated in Figure 16, increasing the scan rate results in a proportional increase in both anodic and cathodic peak currents, without significant distortion of peak shape. This behaviour indicates that the redox process is not governed by adsorption phenomena [44].

A linear relationship between anodic peak current (i_{pa}) and $\nu^{1/2}$ is clearly observed in Figure 17 for all compounds. The corresponding linear regression equations (Table 4) exhibit high correlation coefficients (R^2 = 0.980–0.994), confirming excellent linearity [45].

The high R^2 values demonstrate that the experimental data closely follow the Randles–Ševčík model, thereby confirming that the electron transfer process is diffusion-controlled. Slight deviations from ideal linearity, particularly for FcMe3Ac (R^2 = 0.980), may reflect minor contributions from kinetic limitations or increased solution resistance [46].

6.3. Diffusion Coefficients and Transport Properties

The diffusion coefficients of the electroactive species were determined using the Randles–Ševčík Equation 1 for a reversible system, which relates the peak current to the square root of the scan rate:

$$ip_a = 2.69\times10^5 \left(\sqrt{n}\right)^3 SC\sqrt{D}\sqrt{v}$$ **Equation 1**

where i_p is the peak current (A), $n$is the number of electrons transferred, A is the electrode surface area (cm²), C is the concentration of the electroactive species (mol.cm⁻³), D is the diffusion coefficient (cm²·s⁻¹), and v is the scan rate (V·s⁻¹).

The diffusion coefficients (D) were calculated using the Randles–Ševčík equation, and the results are presented in Table II-4.

Table II-4 Diffusion coefficients and linear regression parameters obtained from Randles–Ševčík analysis.

Compound	Equation	R^2	D × 10^{-7} ($cm^2 \cdot s^{-1}$)
Fc	y = 3.321x + 14.727	0.987	6.952
FcMe2Ac	y = 2.328x + 7.539	0.993	1.108
FcMe3Ac	y = 5.298x + 16.578	0.980	5.738
FcMe4Ac	y = 5.831x + 16.638	0.994	2.255

As shown in Table II-4, the diffusion coefficients of the substituted derivatives are significantly lower than that of ferrocene. This decrease can be attributed to several physicochemical factors:

- Increased molecular volume, leading to reduced translational mobility
- Enhanced solute–solvent interactions in polar DMSO medium
- Greater structural complexity and conformational flexibility

FcMe2Ac exhibits the lowest diffusion coefficient (1.11 × 10^{-7} $cm^2 \cdot s^{-1}$), suggesting stronger intermolecular interactions and possibly a more hindered diffusion pathway. In contrast, FcMe3Ac retains a relatively higher diffusion coefficient, which may be associated with a more favourable molecular geometry and reduced steric constraints [47,48].

6.4. Electron Transfer Kinetics

The heterogeneous electron-transfer rate constants were estimated using Nicholson's method, which relates the peak-to-peak separation to the kinetic parameter Ψ and the standard rate constant as described in Equation 2:

$$\psi = \frac{K_s}{\sqrt{\pi D \frac{nFv}{RT}}}$$ **Equation 2**

where k_s is the standard heterogeneous electron-transfer rate constant (cm.s^{-1}), D is the diffusion coefficient (cm^2.s^{-1}), n is the number of electrons transferred, F is the Faraday constant (96,500 C.mol^{-1}), ν is the scan rate (V.s^{-1}), R is the gas constant (8.314 J.mol^{-1}.K^{-1}), and T is the absolute temperature (K).

The heterogeneous electron-transfer rate constants (k_s) were estimated using Nicholson's method, and the results are summarised in Table II-5.

Table II-5. Nicholson kinetic parameters (Ψ, ΔEp) and heterogeneous electron-transfer rate constants (k_s).

Compound	Ψ	ΔEp (mV)	$k_s \times 10^3$ (cm·s^{-1})
Fc	1.51	73	2.88
FcMe2Ac	0.323	124	0.62
FcMe3Ac	0.074	263	0.14
FcMe4Ac	0.100	223	0.19

The obtained kinetic parameters clearly indicate a decrease in electron-transfer rates upon substitution. The order: Fc > FcMe2Ac > FcMe4Ac > FcMe3Ac, reflects the increasing complexity of the molecular structure and its impact on electron-transfer dynamics [49].

The relatively high k_s value for ferrocene confirms its well-known fast and reversible electron-transfer behaviour. In contrast, the substituted derivatives exhibit slower kinetics, which can be explained by:

- Increased **steric hindrance**, limiting effective interaction with the electrode surface
- Higher **reorganisation energy** associated with structural changes during oxidation
- Reduced **electronic coupling** between the ferrocenyl centre and the electrode

The particularly low k_s value for FcMe3Ac suggests that the meta substitution pattern is least favourable for efficient electron transfer, likely due to suboptimal electronic communication within the molecule [49].

7. Density Functional Theory (DFT) Analysis

The electronic structure and intrinsic reactivity of the synthesised ferrocenyl acetylaniline derivatives were investigated using density functional theory (DFT). These calculations provide a quantitative and molecular-level interpretation of electronic distribution, orbital interactions and

physicochemical properties, allowing a deeper understanding of the behaviour of the compounds beyond experimental characterisation [51].

7.1. Frontier Molecular Orbitals and Electronic Structure

The frontier molecular orbitals (HOMO and LUMO) constitute fundamental descriptors of molecular reactivity, as they govern electron donation and acceptance processes. The calculated orbital energies for FcMe2Ac, FcMe3Ac and FcMe4Ac are presented in Table 6, while the corresponding orbital distributions are illustrated in Figure 18.

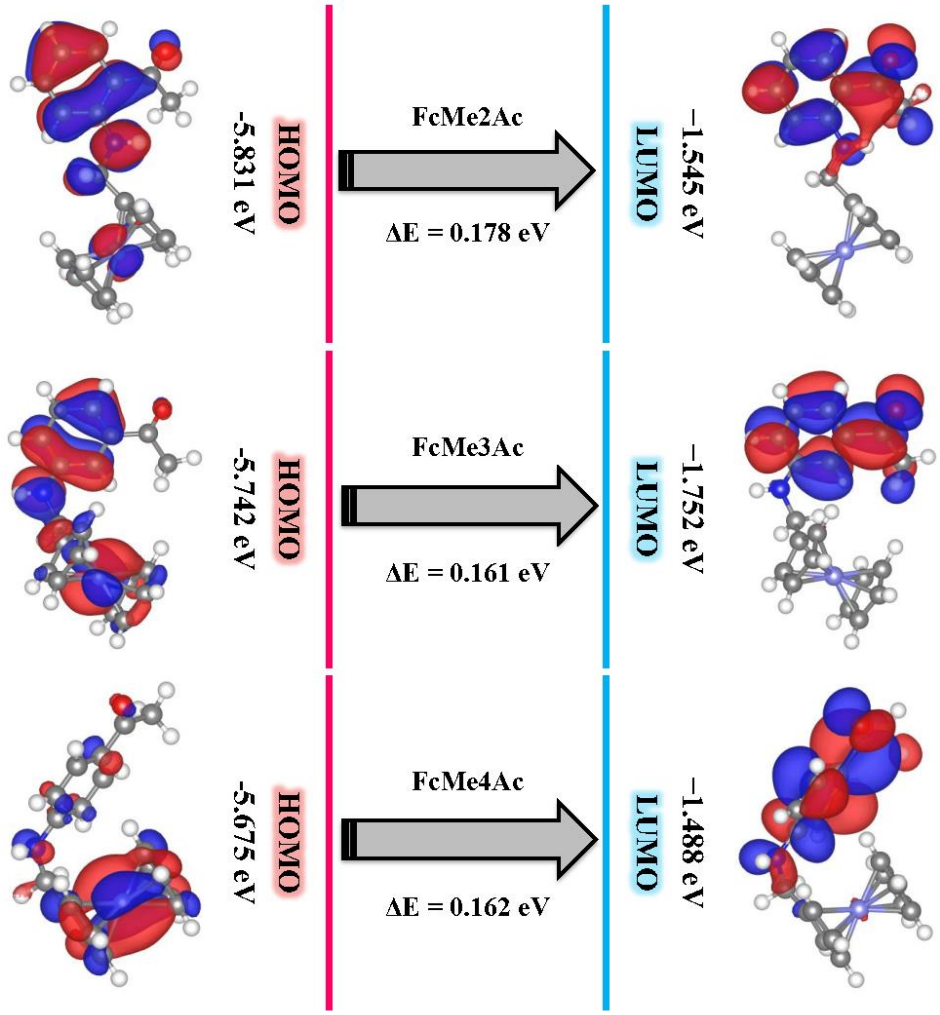

Figure II-18 Frontier molecular orbitals of ferrocenyl acetylaniline derivatives: HOMO and LUMO surfaces.

Table II-6. Frontier molecular orbital energies (eV) of the synthesised compounds.

Compound	EHOMO (eV)	ELUMO (eV)	ΔE (eV)
FcMe2Ac	−5.8306	−1.5453	4.285
FcMe3Ac	−5.7421	−1.7521	3.990
FcMe4Ac	−5.6752	−1.4882	4.187

As shown in Table II-6, a gradual increase in HOMO energy is observed from FcMe2Ac to FcMe4Ac. This trend indicates a progressive enhancement of electron-donor character with increasing substitution, which can be attributed to the influence of the acetylaniline moiety on the electronic density of the ferrocenyl system.

The HOMO–LUMO energy gap (ΔE) ranges from 3.990 to 4.285 eV, suggesting a balance between chemical stability and electronic flexibility. Notably, FcMe3Ac exhibits the smallest energy gap (3.990 eV), indicating relatively higher softness and enhanced reactivity compared to the other derivatives. In contrast, FcMe2Ac presents the largest gap, reflecting slightly higher kinetic stability [52].

The spatial distribution of the orbitals (Figure 18) reveals a clear electronic separation within the molecule. The HOMO is predominantly localised on the ferrocenyl unit and partially on the amine bridge, highlighting the role of the iron centre and cyclopentadienyl rings as electron-rich regions. Conversely, the LUMO is mainly concentrated on the aromatic ring and the carbonyl group, identifying these regions as electron-accepting sites.

This spatial separation of frontier orbitals indicates an intramolecular charge-transfer character, where electron density can be transferred from the ferrocenyl core towards the substituted aromatic system. Such behaviour is commonly observed in donor–acceptor systems and is strongly influenced by substituent position and electronic effects [53].

7.2. Global Reactivity Descriptors and Thermodynamic Parameters

To further quantify the reactivity and stability of the compounds, global reactivity descriptors derived from frontier orbital energies were calculated. The results are summarised in Table II-7.

Table II-7. Global reactivity descriptors and thermodynamic parameters of the synthesised derivatives at 298.15 K.

Parameter	FcMe2Ac	FcMe3Ac	FcMe4Ac
Hardness, η (eV)	2.143	1.995	2.094
Electronegativity, χ (eV)	3.688	3.747	3.582
Chemical potential, μ (eV)	−3.688	−3.747	−3.582
Softness, S (eV^{-1})	0.233	0.251	0.239
Electrophilicity, ω (eV)	3.174	3.519	3.064
Nucleophilicity, N	2.829	2.918	2.985
Dipole moment (D)	3.82	4.46	5.12
Polarizability ($Å^3$)	38.5	42.7	47.3
Enthalpy ($kJ \cdot mol^{-1}$)	−1245.6	−1388.2	−1531.4
Entropy ($J \cdot mol^{-1} \cdot K^{-1}$)	412.5	448.9	486.7
Heat capacity ($J \cdot mol^{-1} \cdot K^{-1}$)	236.4	258.7	281.3

The calculated hardness (η) values confirm that all compounds exhibit moderate chemical stability, consistent with their HOMO–LUMO gaps. Among them, FcMe3Ac shows the lowest hardness (1.995 eV) and highest softness (0.251 eV^{-1}), reinforcing its relatively higher reactivity.

The electrophilicity index (ω) follows the order: FcMe3Ac > FcMe2Ac > FcMe4Ac, indicating that FcMe3Ac has a stronger tendency to accept electrons, whereas FcMe4Ac displays higher nucleophilicity. This dual behaviour highlights the subtle balance between electron-donating and electron-accepting capacities within the series [54].

The negative chemical potential values for all compounds indicate thermodynamic stability and a spontaneous tendency for charge redistribution. Additionally, the progressive increase in dipole moment from FcMe2Ac to FcMe4Ac reflects an increase in molecular polarity, which is directly related to the asymmetry and electronic distribution within the molecule.

A similar increasing trend is observed for polarizability, suggesting that the electronic cloud becomes more easily deformable with increasing substitution. This behaviour is associated with enhanced intermolecular interaction potential and increased responsiveness to external electric fields.

Thermodynamic parameters, including entropy and heat capacity, also increase across the series, indicating greater molecular flexibility and a higher number of accessible vibrational states.

This can be attributed to the increasing structural complexity and conformational freedom of the substituted derivatives [55].

7.3. Molecular Electrostatic Potential (MEP) Analysis

The molecular electrostatic potential maps provide valuable insight into charge distribution and reactive sites. The calculated MEP surfaces are presented in Figure 19.

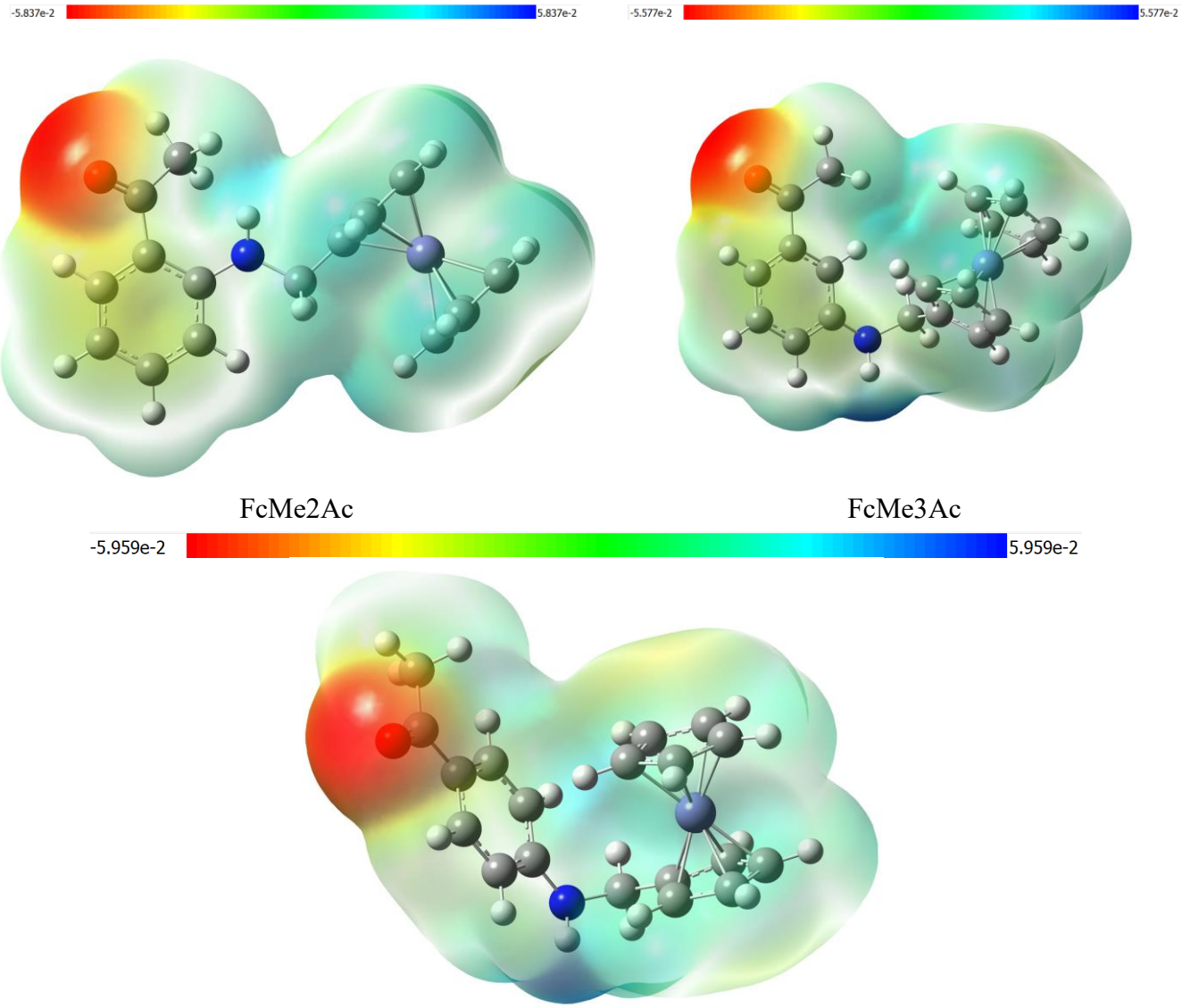

Figure II-19 Molecular electrostatic potential (MEP) maps of ferrocenyl acetylaniline derivatives showing charge distribution.

The MEP surfaces reveal that the most negative electrostatic potential regions are localised around the carbonyl oxygen atoms, indicating high electron density and strong nucleophilic

character. These regions are therefore expected to be preferential sites for electrophilic interactions or hydrogen bonding [56].

In contrast, positive electrostatic potential regions are mainly distributed over hydrogen atoms and partially over the ferrocenyl unit, reflecting electron-deficient zones.

The similarity of electrostatic patterns across the three derivatives suggests that substitution does not drastically alter the overall charge distribution, although subtle differences in intensity and localisation are observed, particularly in the para derivative, which exhibits more delocalised electronic distribution [57].

7.4. Electron Localisation and Non-Covalent Interaction Analysis

To further investigate electronic behaviour, ELF, LOL and RDG analyses were performed. Representative maps are presented in Figure 20 and 21.

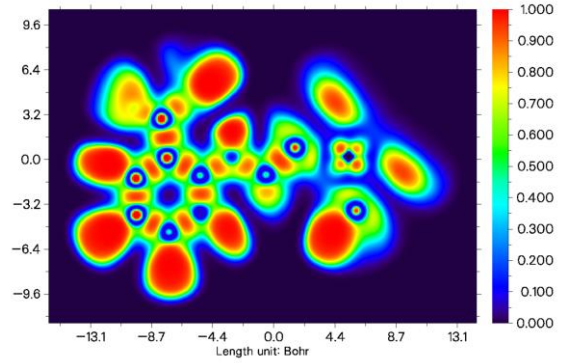

ELF_ **FcMe2Ac**

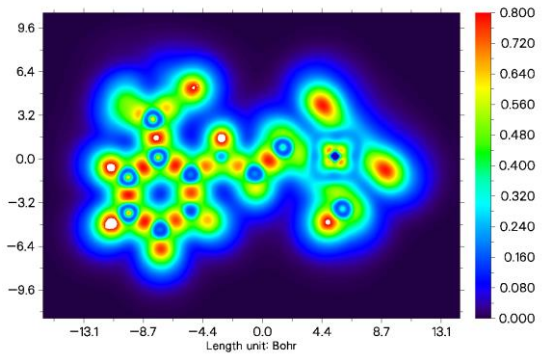

LOL_ **FcMe2Ac**

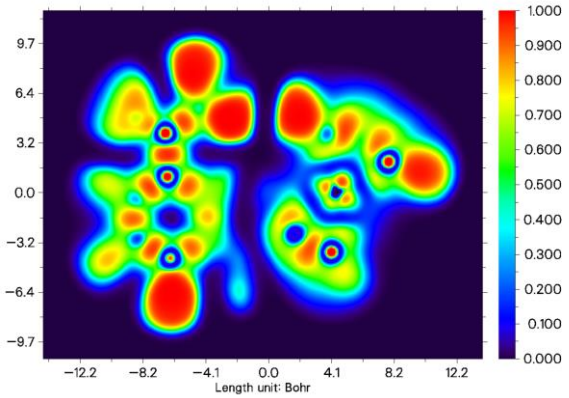

ELF_ **FcMe3Ac**

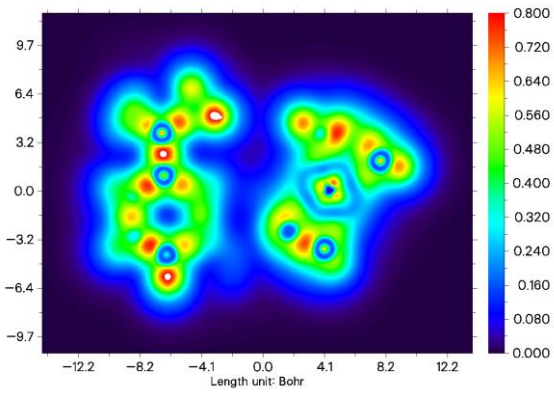

LOL_ **FcMe3Ac**

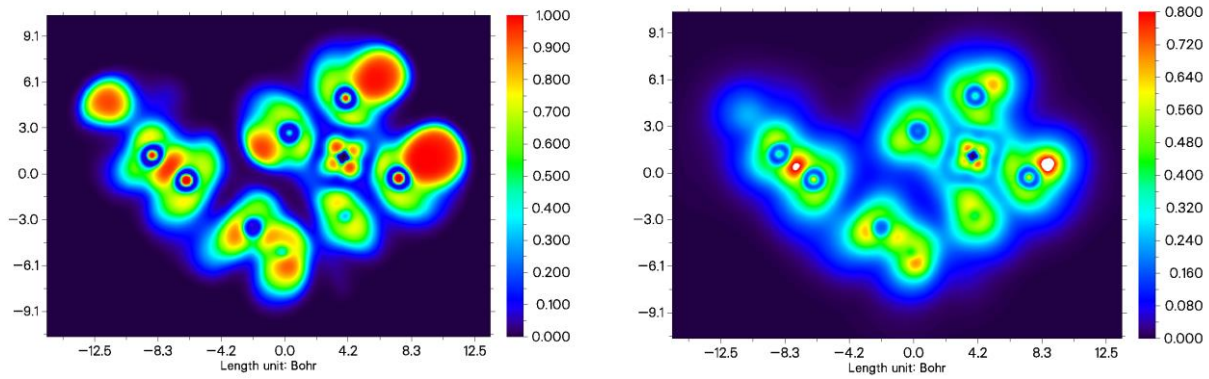

ELF_ **FcMe4Ac** LOL_ **FcMe4Ac**

Figure II-20 Electron localisation (ELF and LOL) analyses of FcMeAc.

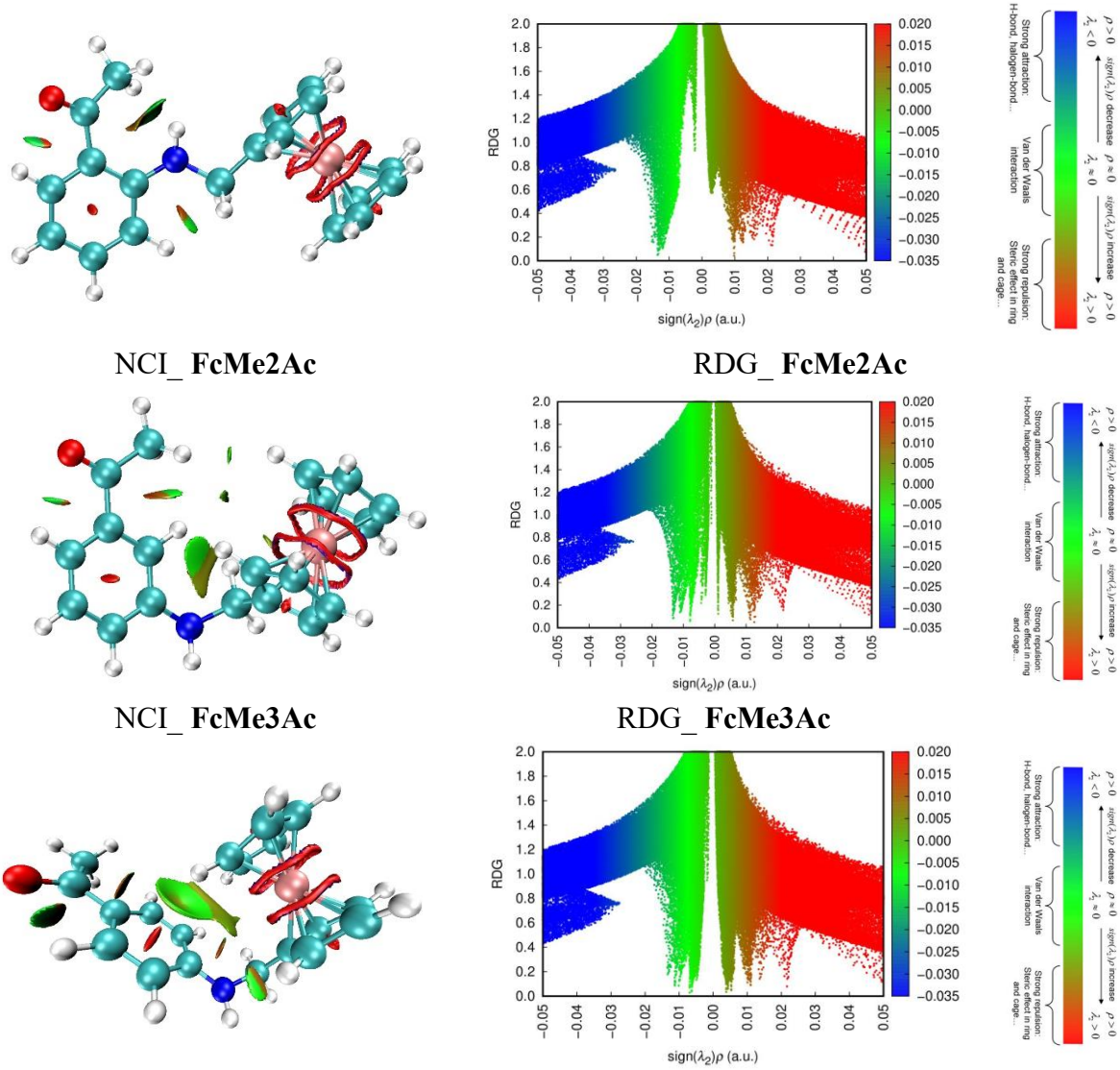

NCI_ **FcMe2Ac** RDG_ **FcMe2Ac**

NCI_ **FcMe3Ac** RDG_ **FcMe3Ac**

NCI_ **FcMe4Ac** RDG_ **FcMe4Ac**

Figure II-21 Non-covalent interaction (RDG/NCI) analyses of FcMeAc.

The ELF and LOL maps clearly show strong electron localisation within the cyclopentadienyl rings and the aromatic system, reflecting extensive π-electron delocalisation. Localised electron density around nitrogen and oxygen atoms corresponds to lone-pair regions, which are important for intermolecular interactions.

The RDG analysis highlights weak non-covalent interactions, including van der Waals contacts and steric repulsion zones. These interactions contribute to the overall stability and conformational behaviour of the molecules.

The consistency of these features across the series indicates that the fundamental electronic structure of the ferrocenyl core is preserved, while substitution mainly modulates peripheral electronic properties [58,59].

8. Molecular Docking Study

To investigate the molecular recognition and binding behaviour of the synthesised ferrocenyl acetylaniline derivatives, molecular docking simulations were performed. The study aimed to evaluate the affinity, binding modes and interaction patterns of the compounds within the active site of the selected target enzyme.

8.1. Docking Protocol Validation

Prior to analysing ligand–protein interactions (Xanathine and NADPH Oxidase), the reliability of the docking protocol was assessed through a redocking procedure of the co-crystallised ligand into the active site of the target protein. The superposition between the crystallographic and predicted binding conformations is presented in Figure 22.

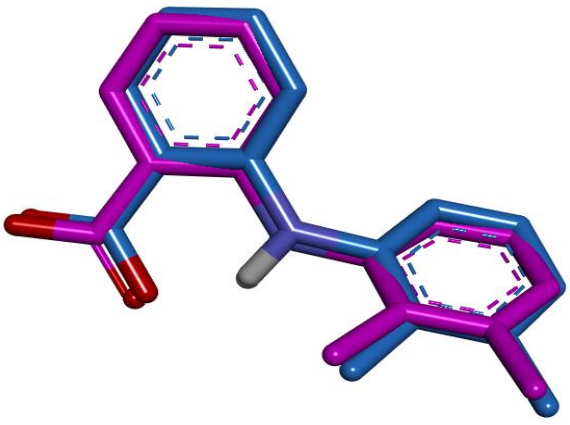

Figure II-22 Superposition of the co-crystallised ligand and the redocked pose within the active site (validation of docking protocol).

The calculated root-mean-square deviation (RMSD) between the experimental and redocked conformations was found to be 0.339 Å, which is significantly lower than the commonly accepted threshold of 2.0 Å. This result demonstrates excellent agreement between predicted and experimental ligand orientations, confirming the accuracy of the docking parameters, grid definition and scoring function.

The low RMSD value indicates that the adopted docking protocol is highly reliable for reproducing the native binding mode and can therefore be confidently applied to the ferrocenyl derivatives [60].

8.2. Binding Affinity and Energetic Analysis

The docking results, including the estimated free binding energies and energetic contributions, are summarised in Table II-8.

Table II-8. Molecular docking results of ferrocenyl acetylaniline derivatives.

Compound	Intermolecular Energy (kcal·mol^{-1})	Internal Energy (kcal·mol^{-1})	Torsional Energy (kcal·mol^{-1})	Binding Energy (kcal·mol^{-1})
FcMe2Ac	−7.84	−0.62	+0.78	−7.05
FcMe3Ac	−8.21	−0.74	+0.91	−7.68
FcMe4Ac	−9.05	−0.88	+1.02	−8.36
Reference ligand	—	—	—	−7.42

As shown in Table II-8, all compounds exhibit negative binding energies, indicating spontaneous and favourable interactions within the enzyme active site. Among the studied derivatives, FcMe4Ac displays the most negative binding energy (−8.36 kcal·mol^{-1}), suggesting the strongest binding affinity.

A clear trend is observed: FcMe4Ac > FcMe3Ac > FcMe2Ac, This behaviour reflects the influence of substitution pattern on molecular recognition and interaction strength.

The intermolecular energy contributions dominate the binding process, indicating that stabilisation arises mainly from ligand–protein interactions rather than internal conformational changes. The relatively low torsional energy values suggest minimal conformational penalty upon binding, indicating that the ligands adopt favourable geometries within the binding pocket [61].

8.3. Binding Mode and Interaction Analysis

The three-dimensional binding conformation of the most active compound is presented in Figure 23, while the detailed interaction profiles are discussed below.

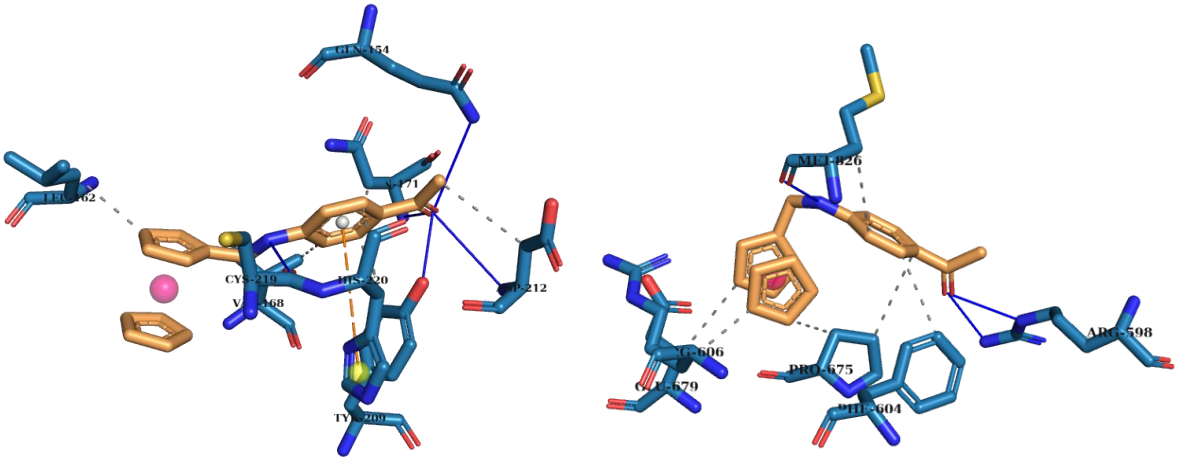

Figure II-23 Three-dimensional binding mode of FcMe4Ac within the active site of the target enzyme.

All ferrocenyl derivatives are located within the hydrophobic channel of the enzyme, where the ferrocenyl core establishes strong interactions with non-polar amino acid residues. This positioning is consistent with the lipophilic nature of the cyclopentadienyl rings.

The interaction network is dominated by:

- Hydrophobic interactions between the ferrocenyl unit and non-polar residues
- π–π stacking interactions involving the aromatic ring
- Hydrogen bonding interactions, mainly involving the carbonyl oxygen and surrounding residues

The interaction pattern varies among the three derivatives. FcMe2Ac exhibits a relatively limited interaction network, consistent with its lower binding affinity. FcMe3Ac shows improved stabilisation through additional interactions, including hydrogen bonding and aromatic contacts.

In contrast, FcMe4Ac displays the most extensive interaction network. Notably, it forms:

- Strong hydrogen bonds with polar residues (e.g., ASN)
- Multiple hydrophobic contacts along the binding channel
- Additional electrostatic interactions contributing to stability

This dense interaction network explains its superior binding affinity compared to the other derivatives and even the reference ligand [62].

8.4. Structure–Interaction Relationship

The observed differences in binding affinity can be rationalised by considering structural and electronic factors:

- The para substitution in FcMe4Ac allows better molecular extension and optimal accommodation within the active site
- Increased molecular polarity and polarizability enhance interaction potential
- Improved steric complementarity facilitates stronger contact with surrounding residues

In contrast, the ortho derivative (FcMe2Ac) may experience steric constraints that limit optimal positioning, while the meta derivative (FcMe3Ac) shows intermediate behaviour due to less effective electronic delocalisation.

These findings highlight the critical role of substitution pattern in modulating ligand–protein interactions and binding efficiency [63].

9. Molecular Dynamics Simulation

To further validate the stability and dynamic behaviour of the best-performing ligand, FcMe4Ac, molecular dynamics (MD) simulations were carried out for its complexes with the Xanathine Oxidase and NADPH Oxidase (PDB IDs: 1FIQ and 8WEJ). This analysis provides insight into structural stability, flexibility, intermolecular interactions and conformational adaptation under physiological conditions.

9.1. System Stability: RMSD Analysis

The time evolution of the backbone root-mean-square deviation (RMSD) was analysed to assess the global stability of the protein–ligand complexes. The results are presented in Figure 24A (1FIQ system) and Figure 24B (8WEJ system).

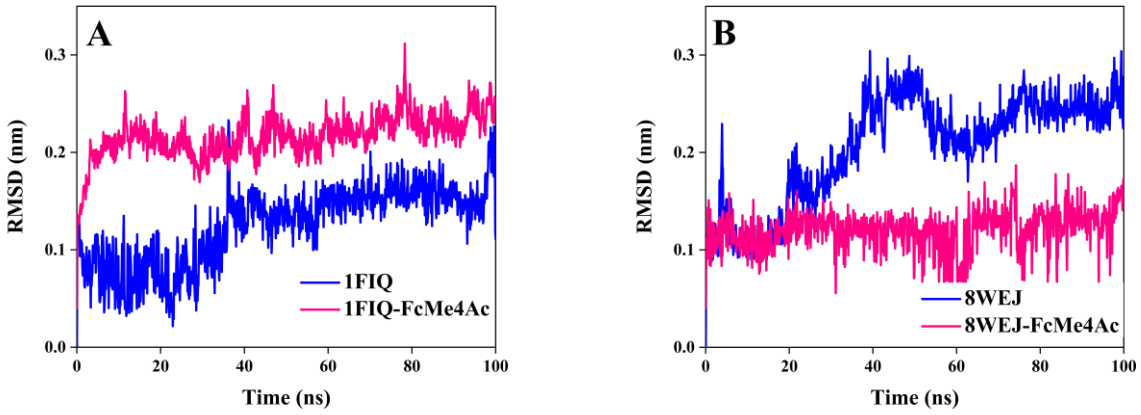

Figure II-24 RMSD profiles of protein and protein–FcMe4Ac complexes during 100 ns simulation: (A) 1FIQ and (B) 8WEJ systems.

As shown in Figure 24A, the apo form of 1FIQ stabilises around ~0.10–0.15 nm after an initial equilibration phase. Upon binding of FcMe4Ac, the RMSD increases moderately and stabilises around ~0.20–0.25 nm. This shift reflects a ligand-induced conformational adaptation, which remains stable over time without large structural deviations, indicating a well-equilibrated complex [64].

In contrast, the 8WEJ system (Figure 24B) exhibits a different behaviour. The apo protein shows larger fluctuations (~0.20–0.30 nm), suggesting higher intrinsic flexibility. However, upon ligand binding, the RMSD is significantly reduced (~0.10–0.15 nm) and remains stable throughout the simulation. This clearly indicates that FcMe4Ac stabilises the protein structure, reducing its dynamic fluctuations [64].

Overall, the RMSD results demonstrate that FcMe4Ac forms stable complexes with both targets, with a particularly strong stabilising effect observed in the 8WEJ system.

9.2. Residue Flexibility: RMSF Analysis

The root-mean-square fluctuation (RMSF) was calculated to evaluate residue-level flexibility. The results are shown in Figure 25A (1FIQ) and Figure 25B (8WEJ).

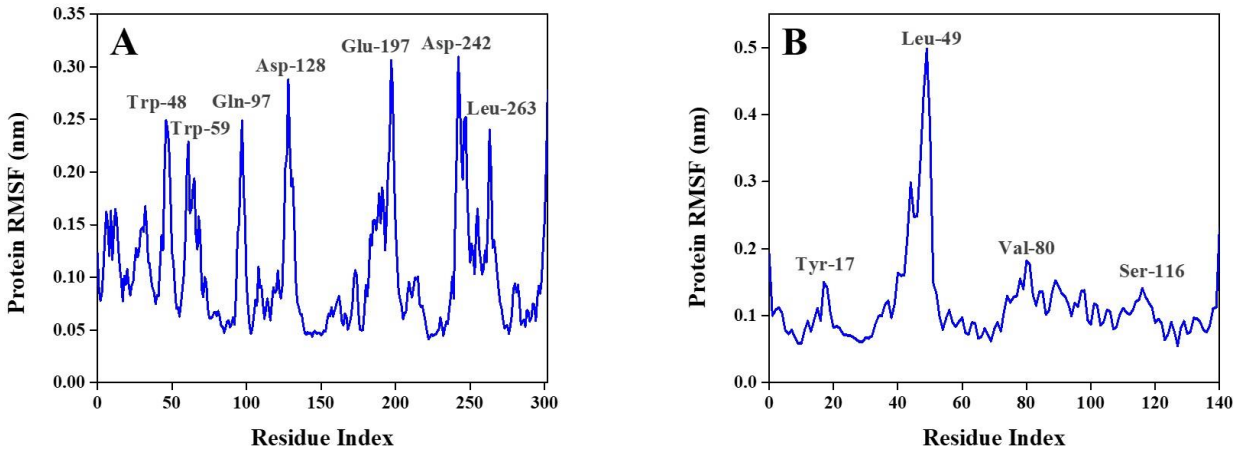

Figure II-25 RMSF profiles of protein residues in complex with FcMe4Ac: (A) 1FIQ and (B) 8WEJ systems.

For the 1FIQ system (Figure 25A), several peaks are observed, notably at residues such as Trp48, Trp59, Gln97, Asp128, Glu197 and Asp242. These fluctuations correspond mainly to loop regions and surface-exposed residues, which are inherently flexible. Importantly, residues involved in ligand binding show relatively moderate fluctuations, indicating stable interactions within the active site.

In the 8WEJ system (Figure 25B), overall fluctuations are significantly reduced. Only a limited number of residues, such as Leu49, exhibit higher mobility. The majority of residues remain below ~0.15 nm, confirming a more rigid and stabilised protein conformation upon ligand binding.

This comparison highlights that FcMe4Ac contributes to enhanced structural rigidity, particularly in the 8WEJ complex.

9.3. Ligand Stability: Ligand RMSF Analysis

The flexibility of FcMe4Ac within the binding pocket was further analysed through ligand RMSF, presented in Figure 26A (1FIQ) and Figure 26B (8WEJ).

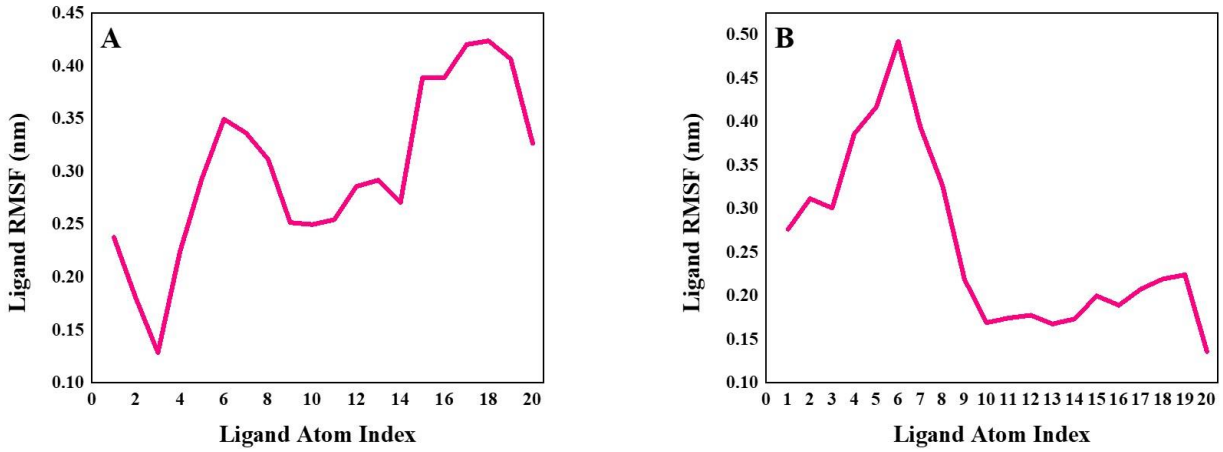

Figure II-26 Ligand RMSF profiles of FcMe4Ac: (A) 1FIQ and (B) 8WEJ complexes.

In the 1FIQ complex (Figure 26A), the ligand exhibits moderate fluctuations (~0.25–0.42 nm), particularly in terminal regions. These fluctuations indicate partial flexibility, likely associated with peripheral groups not directly involved in strong interactions.

Conversely, in the 8WEJ complex (Figure 26B), the ligand shows significantly lower fluctuations (~0.15–0.22 nm), indicating a more rigid and well-anchored conformation within the binding pocket.

These results confirm that FcMe4Ac is more tightly bound and conformationally constrained in the 8WEJ system, which correlates with its higher structural stability observed in RMSD analysis.

9.4. Interaction Profile Analysis

The interaction fractions between FcMe4Ac and protein residues during the simulation are presented in Figure 27A (1FIQ) and Figure 27B (8WEJ).

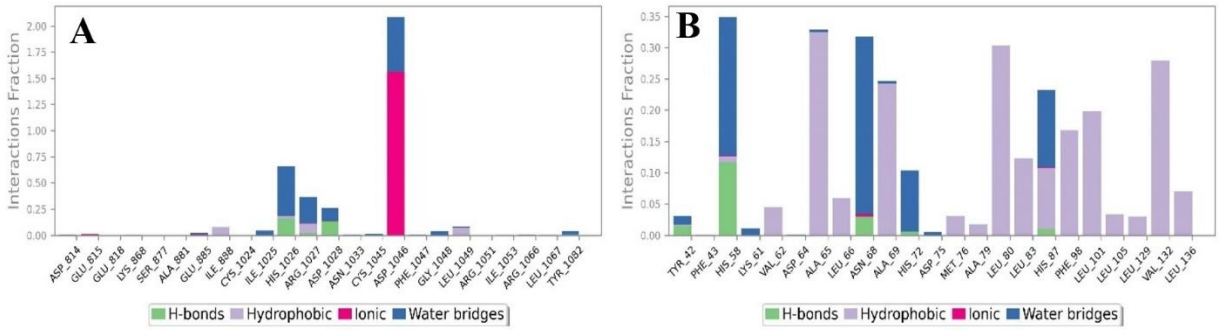

Figure II-27 Interaction fraction analysis showing hydrogen bonds, hydrophobic interactions, ionic contacts and water bridges: (A) 1FIQ and (B) 8WEJ complexes.

The interaction profiles reveal that the stabilisation of the complexes is dominated by:

- Hydrophobic interactions, particularly with residues such as PHE, LEU and VAL
- Hydrogen bonds, contributing to directional stabilisation
- Water-mediated bridges, enhancing interaction persistence

In the 1FIQ system, interactions are more localised, with significant contributions from residues such as HIS1025 and ARG1027, indicating a moderately stable interaction network.

In contrast, the 8WEJ complex exhibits a broader and more consistent interaction pattern involving multiple residues (e.g., TYR42, PHE43, LEU80 and LEU136), suggesting a more extensive and stabilised interaction network.

9.5. Global Structural Properties (Rg, SASA, PSA)

The evolution of global structural parameters is shown in Figure 28A (1FIQ) and Figure 28B (8WEJ).

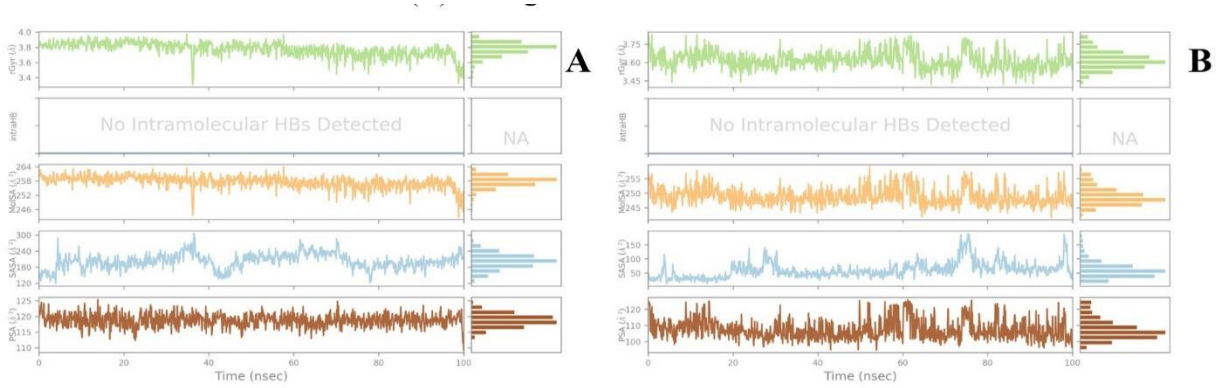

Figure II-28 Time evolution of radius of gyration (Rg), molecular surface area (MolSA), solvent-accessible surface area (SASA) and polar surface area (PSA): (A) 1FIQ and (B) 8WEJ systems.

The radius of gyration (Rg) remains relatively stable in both systems (~3.6–3.9 Å), indicating that no significant unfolding or structural collapse occurs during the simulation.

The SASA profiles show moderate fluctuations, reflecting normal solvent exposure dynamics without major conformational rearrangements.

The polar surface area (PSA) remains constant throughout the simulation, suggesting that ligand binding does not significantly alter the overall polarity of the system.

Notably, the 8WEJ system exhibits slightly more stable profiles across all parameters, further confirming its higher structural stability [65].

10. ADMET Prediction and Pharmacokinetic Evaluation

To complement the structural and dynamic analyses, the pharmacokinetic and toxicity profiles of the synthesised ferrocenyl acetylaniline derivatives were evaluated using in silico ADMET prediction tools. These analyses provide essential insights into drug-likeness, absorption, distribution, metabolism, excretion and toxicity, which are critical parameters for assessing the potential of small molecules as therapeutic agents.

10.1. Drug-Likeness and Physicochemical Properties

The fundamental physicochemical parameters governing drug-likeness are summarised in Table II-9.

Table II-9. Predicted physicochemical properties and drug-likeness parameters of ferrocenyl derivatives.

Parameter	FcMe2Ac	FcMe3Ac	FcMe4Ac
Molecular weight (g·mol^{-1})	335.2	335.2	335.2
LogP (consensus)	3.12	3.28	3.45
Lipinski violations	0	0	0

All three compounds comply with Lipinski's rule of five, indicating favourable oral drug-likeness. Their molecular weights remain well below the 500 g·mol^{-1} threshold, while LogP values (3.12–3.45) indicate balanced lipophilicity.

The slight increase in LogP from FcMe2Ac to FcMe4Ac reflects enhanced hydrophobic character due to substitution effects, which may influence membrane permeability and interaction with hydrophobic protein pockets [66].

10.2. Absorption and Distribution Properties

The predicted absorption and distribution profiles are presented in Table II-10.

Table II-10. Predicted absorption and distribution properties of the studied compounds**.**

Parameter	FcMe2Ac	FcMe3Ac	FcMe4Ac
Gastrointestinal absorption	High	High	High
Blood–brain barrier permeability	No	No	No

All compounds exhibit high gastrointestinal absorption, suggesting favourable oral bioavailability. This behaviour is consistent with their moderate lipophilicity and suitable molecular size.

The absence of predicted blood–brain barrier (BBB) permeability indicates that these compounds are unlikely to penetrate the central nervous system. This property is often desirable for compounds targeting peripheral enzymes, as it reduces the risk of central nervous system side effects [67].

10.3. Toxicological Profile

The toxicity predictions are summarised in Table II-11.

Table II-11. Predicted toxicity profiles of ferrocenyl acetylaniline derivatives.

Parameter	FcMe2Ac	FcMe3Ac	FcMe4Ac
Ames toxicity	No	No	No
Hepatotoxicity	No	No	No
Skin sensitisation	Low risk	Low risk	Low risk

All derivatives are predicted to be non-mutagenic (Ames test negative) and non-hepatotoxic, indicating a favourable safety profile. Additionally, the low risk of skin sensitisation further supports their potential as biologically compatible compounds [68].

10.4. Structure–Property Relationship and Comparative Analysis

The ADMET results reveal a consistent and favourable pharmacokinetic profile across the series. However, subtle differences can be observed:

- FcMe4Ac exhibits the highest lipophilicity, which may enhance membrane permeability and binding interactions
- Increased substitution correlates with enhanced polarizability and hydrophobicity, influencing distribution behaviour
- All compounds maintain a balanced physicochemical profile, avoiding excessive lipophilicity that could impair solubility

Importantly, the absence of toxicity alerts and compliance with drug-likeness rules indicate that structural modification of the ferrocenyl scaffold does not compromise safety [69].

CONCLUSION

General Conclusion

This work was devoted to the design, synthesis, characterisation and computational evaluation of a series of ferrocenyl acetylaniline derivatives, with the aim of exploring their structural features and understanding their behaviour through complementary experimental and theoretical approaches.

The synthetic strategy employed enabled the successful preparation of three regioisomeric compounds, namely FcMe2Ac, FcMe3Ac and FcMe4Ac, with satisfactory yields and good reproducibility. The molecular structures of the obtained derivatives were rigorously confirmed using a combination of spectroscopic techniques, including FT-IR, UV–Visible spectroscopy, and both one- and two-dimensional NMR analyses. These techniques provided consistent and complementary evidence supporting the successful functionalisation of the ferrocenyl scaffold and the correct positioning of substituents on the aromatic ring.

Electrochemical investigations highlighted the characteristic redox behaviour of the ferrocenyl moiety, with all compounds exhibiting a quasi-reversible Fe(II)/Fe(III) redox couple. The observed shifts in redox potentials confirmed the influence of the acetylaniline substituents on the electronic properties of the system. Furthermore, kinetic and diffusion analyses demonstrated that the electron-transfer processes are predominantly diffusion-controlled, while the variation in diffusion coefficients and rate constants reflected the impact of molecular structure on electrochemical behaviour.

Theoretical studies based on density functional theory provided detailed insight into the electronic structure and reactivity of the synthesised compounds. Frontier molecular orbital analysis revealed a donor–acceptor character within the molecules, characterised by electron density transfer from the ferrocenyl unit towards the aromatic moiety. Global reactivity descriptors, along with electrostatic potential and electron localisation analyses, confirmed the presence of well-defined reactive sites and highlighted the role of substitution in modulating electronic distribution and molecular properties.

Molecular docking studies demonstrated that the ferrocenyl derivatives are capable of interacting favourably with the selected biological targets, with binding affinities influenced by both structural and electronic factors. Among the studied compounds, FcMe4Ac consistently

exhibited the most favourable binding behaviour, attributed to improved steric accommodation and enhanced interaction capability within the active site.

The dynamic behaviour of the ligand–protein complexes was further investigated through molecular dynamics simulations, which confirmed the stability of the interactions over time. The FcMe4Ac complex, in particular, showed reduced structural fluctuations, enhanced rigidity and a well-maintained interaction network, especially with one of the investigated targets, indicating a strong and stable binding mode under dynamic conditions.

In addition, in silico ADMET predictions revealed that all compounds possess favourable pharmacokinetic profiles, characterised by good oral absorption potential, compliance with drug-likeness rules and low predicted toxicity. These properties further support the potential applicability of the studied compounds.

Taken together, the results obtained in this thesis demonstrate that the structural modification of ferrocenyl derivatives through acetylaniline substitution significantly influences their physicochemical, electronic and interaction properties. The combined experimental and computational approach adopted in this work provides a comprehensive understanding of these systems and highlights the importance of integrating multiple methodologies in the study of organometallic compounds.

Overall, FcMe4Ac emerges as the most promising derivative within the series, exhibiting optimal characteristics in terms of electronic properties, interaction stability and predicted pharmacokinetic behaviour. This compound represents a valuable scaffold for further investigations and potential optimisation in future studies.

This work thus contributes to the advancement of ferrocenyl-based compounds and provides a solid scientific basis for their continued exploration in the field of medicinal and bioinorganic chemistry.

REFERENCES

BIBLIOGRAPHY

References:

Part I: Bibliographic Study

[1] A. KEDADRA, *Etude théorique et comparative de quelques N-ferrocénylméthylamines à l'aide de la théorie de la fonctionnelle de la densité DFT et détermination de leurs activité biologique,* Eloued: Université Echahid Hamma Lakhdar, 2022/2023.

[2] A.SALZER, "NOMENCLATURE OF ORGANOMETALLIC COMPOUNDS OF THE TRANSITION ELEMENTS," INTERNATIONAL UNION OF PURE AND APPLIED CHEMISTRY, Printed in Great Britain, 1999.

[3] J. A. Dakeshwar Kumar Verma, Organometallic Compounds: Synthesis, Reactions, and Applications, British: Wiley Online Library, 2023.

[4] K. H. a. H. Lang, "Ferrocene - Beauty and Function," *ORGANOMETALLICS,* vol. 32, no. 20, pp. 5623-5625, October 28, 2013.

[5] P. D. G. G. Dr. Malay Patra, "Organometallic Compounds: An Opportunity for Chemical Biology?," 22 May 2012. [Online]. Available: https://doi.org/10.1002/cbic.201200159.

[6] D. Astruc, "Why is Ferrocene so Exceptional?," *EurJIC,* pp. 6-29, 05 October 2016.

[7] A. H. P. T. H. P. P. J. P. Sonia Coriani Dr., "The Equilibrium Structure of Ferrocene," *ChemPhysChem,* pp. 245-249, 11 January 2006.

[8] J. A. S. V. K. R. R. F. T. O. K. M. H.-B. K. &. N. I. Satoshi Takebayashi, "From 18- to 20-electron ferrocene derivatives via ligand coordination," *nature communications,* p. 11, 07 July 2025.

[9] E. Lanez, "Synthesis, characterization and in vitro and in silico study of biological activities of some ferrocenylmethyl-nucleic bases derivatives," November 2019. [Online]. Available: https://www.researchgate.net/publication/345984738_Synthesis_characterization_and_in_vitro_and_in_silico_study_of_biological_activities_of_some_ferrocenylmethyl-nucleic_bases_derivatives.

[10] A. T. C. V. Pedro Molina, "sciencedirect," 20 November 2001. [Online]. Available: https://doi.org/10.1016/S0022-328X(01)00913-5. [Accessed 20 04 2026].

[11] W.-T. W. Cindy Sze-Wai Lau, "Synthesis, structural characterisation and electrochemistry of ruthenium carbonyl clusters derived from ferrocenyl(formyl)acetylene," *Journal of Organometallic Chemistry,* pp. 113-124, 1 October 1999.

[12] J. Dolhun, "THE PREPARATION OF FERROCENE AND ACETYLFERROCENE," MASSACHUSETTS INSTITUTE OF TECHNOLOGY, Dec 2017.

[13] "FERROCENE," *Organic Syntheses,* vol. 4, p. 473, 1963.

[14] Q. O. G. M. I. A. Ibrohim Asqarov, "SYNTHESIS OF SOME FERROCENE DERIVATIVES," *American Journal of Technology and Applied Sciences,* vol. 21, pp. 40-48, February, 2024.

[15] E. L. Luis A. López, "Recent advances in transition metal-catalyzed C-H bond," *Dalton Transactions,* vol. 22, p. 8, 2015.

[16] S. M. a. M. K. Princi Gupta, "A Long Journey to the Unknown Chemical Space: Synthesis of Ferrocene 1,3−Derivatives by Distal C−H Activation by a Template Approach," Indian Institute of Science Education and Research, India, 2022.

[17] L. R. T. A. N. N. D. H. C. A. N. P. J. R. J.-C. H. Emmanuel Lerayer, "Highly Functionalized Ferrocenes," *European Journal of Inorganic Chemistry,* vol. 2020, no. 5, pp. 419-445, 2019.

[18] V. V. Mateja Toma, "Redoks-svojstva ferocenom supstituiranih nukleobaza," *Journal of Chemists and Chemical Engineers,* vol. 69, no. 13, pp. 21-29, 2020.

[19] L. W. M. G. Andrzej Lewandowski, "Ferrocene as a Reference Redox Couple for Aprotic Ionic Liquids," *Electroanalysis,* vol. 21, no. 20, pp. 2221-2227, 2009.

[20] K. P. Anvita Chaudhary, "The redox mechanism of ferrocene and its phytochemical and biochemical compounds in anticancer therapy: A mini review," *Inorganic Chemistry Communications,* 7 December 2021.

[21] N. N. S. A. K. Touhami Lanez, "Electrochemistry characterization of ferrocene/ferricenium redox couple at glassycarbon electrode," *Journal of Fundamental and Applied Sciences ,* September 2015.

[22] A. I. C. Laboratory, "Cyclic Voltammetry of Ferrocene, [Ru(bpy)3]2+, [Co(bpy)3]2+ and Iodide," UMass Boston, Boston.

[23] T. L. N. S .Neghmouche, "Electrochemical properties of ferrocene in aqueous and organic mediums at glassy carbon electrode," *Recent Trends in Physical Chemistry: An International Journal,* pp. 1-3, 07 February 2013.

[24] B. O. V. O. N. Ayomide H. Labulo, "Synthesis, crystal structures and electrochemical properties of ferrocenyl," *Heliyon,* 2 October 2019.

[25] E. M. S. P. S. a. J. E. R.-V. Claudia Y Acevedo-Morantes1, "Cytotoxicity and Reactive Oxygen Species Generated by Ferrocenium and," *Cance rScience & Therapy,* pp. 271-275, 2012.

[26] S. Y. J. K. ,. S. Y. ,. W. I. C. C. ,. J. K. ,. D. S. ,. B. S. K. Jiwon Kang, "Ferrocene-loaded glycerogel dressing for reactive oxygenspecies-modulated active wound healing," *Materials Today Advances,* 6 April 2026.

[27] F. A. L. A. S. T. A. F. U. M. P. A. Channar, "Recent advances in the synthesis, biological activities and various applications of ferrocene derivatives," *Applied Organometallic Chemistry,* p. 1–22, December 2016.

[28] A. a. N.S.Kochetkova, "Principal Practical Applications of Ferrocene and Its Derivatives," *Russian Chemical Reviews,* pp. 1513-1523, 1974.

[29] J. D. C. F. E. K. Beatrice S. Ludwig, "Ferrocene derivatives as anti-infective agents," *Coordination Chemistry Reviews,* pp. 22-48, 2019.

[30] J. S. K. S. N. S. V. B. M. D. I. K. D. S. Aleksandra Minić Jančić, "Ferrocene-containing tetrahydropyrimidin-2(1H)-ones: Antioxidant and antimicrobial activityThe Journal of Organometallic," *The Journal of Organometallic Chemistry,* 15 May 2022.

[31] P. D. G. F. Prof. Dr. Hans-Dieter Höltje, Molecular Modeling: Basic Principles and Applications, VCH Verlagsgesellschaft mbH, 24 October 1996.

[32] "Chapter 1 An Introduction to Molecular Modeling and Computer aided Drug Design," Universidad Politécnica de Cataluña, España.

[33] J. Boeyens, "Fundamentals of Molecular Modelling," Skukuza, South Africa, August 1996.

[34] N. M. Harrison, "An Introduction to Density Functional Theory," Department of Chemistry, Imperial College of Science Technology and Medicine, SW7 2AY, London, London.

[35] M. O. D. A. P. F. Neese, "Density functional theory," *Photosynth Res,* p. 443–453, 24 February 2009.

[36] D. SALAHUB, "Density Functional Theory, Methods, Techniques, and Applications," in *Atomic clusters and nanoparticles. Agregats atomiques et nanoparticules*, Springer Berlin Heidelberg, 2000, pp. 105-160.

[37] D. S. Aryal, "Microbe Notes," 22 December 2025 . [Online]. Available: https://microbenotes.com/molecular-docking/. [Accessed 23 04 2026].

[38] C. A. A. O. U. O. E. M. E. I. H. O. C. O. O. E. I. U. &. P. M. A. P. C. Agu, "Molecular docking as a tool for the discovery of molecular targets of nutraceuticals in diseases management," *Scientific Reports,* 17 August 2023.

[39] M. T. M. a. E. Aki-Yalcin, "Molecular Docking: Principles, Advances, and Its Applications in Drug Discovery," *Letters in Drug Design & Discovery,* pp. 480 - 495, January 2024.

[40] e. a. Mohammad Sufian Badar, "Molecular Dynamics Simulations: Concept, Methods, and Applications," in *Molecular Dynamics Simulations: Concept, Methods, and Applications*, USA, Springer Nature, 2020.

[41] M. M. G. B. a. A. C. Marco De Vivo, "Role of Molecular Dynamics and Related Methods in Drug Discovery," *Journal of Medicinal Chemistry,* p. 4035–4061, 25 January 2016.

[42] F. C. e. al, "In Silico ADMET Prediction: Recent Advances, Current Challenges and Future Trends," *Current Topics in Medicinal Chemistry,* May 2013.

[43] X. S. e. al, "Computational Approaches in Preclinical Studies on Drug Discovery and Development," *Frontiers in Chemistry,* vol. 8, no. 726, p. 32, 11 September 2020.

[44] M. K. e. al, "Quantitative Structure–Activity Relationship (QSAR): A Review for Beginners to Intermediate Researchers," *International Journal of Creative and Open Research in Engineering and Management,* pp. 1-9, March 2026.

[45] H. J. e. al, "Basic Concepts in Physiologically Based Pharmacokinetic Modeling in Drug Discovery and Development," *CPT: Pharmacometrics & Systems Pharmacology,* 14 August 2013.

[46] e. a. Thakor Rajkishan, "Computer-Aided Drug Designing," *Advances in Bioinformatics,* 2021.

[47] W. Z. e. al, "Current Trends and Challenges in Drug-Likeness Prediction: Are They Generalizable and Interpretable?," *Health Data Science,* 20 Oct 2023 .

[48] H. Z. M. S. Y. L. X. P. X. Y. B. L. Z. L. Guiling Zhang, "Substitution effect on the geometry and electronic structure of the ferrocene," Journal of Computational Chemistry, 02 July 2007. [Online]. Available: https://doi.org/10.1002/jcc.20629.

[49] G. A. N. a. A. Nicolaeva, "Transport in ferrocene single molecules for terahertz applications," *Physical Chemistry Chemical Physics,* pp. 18478-18482, 21 Jul 2014.

[50] D. Sarmah, "Ferrocene Structure and Bonding Analysis," *Scribd,* 17 05 2024.

[51] C. T. C. ,. G. F. W. Narges Mohammadi, "Differentiation of ferrocene D5d and D5h conformers using IR spectroscopy," *Journal of Organometallic Chemistry,* pp. 51-59, 15 August 2012.

[52] M. M. A.-E. R. A. A. A. A. L. Mohammad F. R. Fouda, "On the medicinal chemistry of ferrocene," *Bioorganometallic Chemistry,* p. 613–625, 11 April 2007.

[53] P. D. a. A. I. O. b. K. A. A. T. L. I. d. E. E. d. N. R. S. a. M. M. a. A. M. M. G. J. W. e. S. A. E. Samson O. Oselusi a, "The role and potential of computer-aided drug discovery strategies in the discovery of novel antimicrobials," *Computers in Biology and Medicine,* pp. 1-10, 1 January 2024.

[54] J. Z. ,. Z. C. Yi Fu, "Insights into the Molecular Mechanisms of Protein-Ligand Interactions by Molecular Docking and Molecular Dynamics Simulation: A Case of Oligopeptide Binding Protein," *Hindawi,* vol. 4, p. December, 2018.

[55] A. s. H. K. S. P. P. T. P. K. Avinash kumar1*, "Interaction of Protein- Ligand: Molecular Docking, A novel computational biology tool," *Annals of the Romanian Society for Cell Biology,* p. 20763 – 20775, 20 October 2021.

[56] S. O. O. e. al, "The role and potential of computer-aided drug discovery strategies in the discovery of novel antimicrobials," *Computers in Biology and Medicine,* February 2024.

[57] "BioChemCoRe," 30 Mar 2021. [Online]. Available: https://ctlee.github.io/BioChemCoRe-2018/rmsd-rmsf/. [Accessed 23 04 2026].

[58] Z. K. B. e. al, "Molecular dynamics and simulation analysis against superoxide dismutase (SOD) target of Micrococcus luteus with secondary metabolites from Bacillus licheniformis recognized by genome mining approach," *Saudi Journal of Biological Sciences,* September 2023.

PART II: EXPERIMENTAL

[1] I.U. Khand, T. Lanez, P.L. Pauson, Ferrocene derivatives. Part 24. Synthesis of dihydro-2-pyrindines and dihydro-3 H-2-cyclopent [c] azepines by photolysis of their cyclopentadienyliron derivatives, J. Chem. Soc. Perkin 1 (1989) 2075–2078.

[2] E. Lanez, L. Bechki, T. Lanez, Antioxidant Activities, Binding Parameters, and Electrochemical Behavior of Superoxide Anion Radicals Twords 1-Ferrocenylmethylthymine and 1-Ferrocenylmethylcytosine, Curr. Phys. Chem. 10 (2020) 10–22.

[3] E. Lanez, L. Bechki, T. Lanez, Ferrocenylmethylnucleobases: Synthesis, dft calculations, electrochemical and spectroscopic characterisation, Chemistry (Easton). 14 (2020) 146–153.

[4] E. Lanez, M. Saidi, T. Lanez, Assessment of antioxidant and DPPH free radical scavenging activity of 1,2-dithiole-3-thione derivatives by using cyclic voltammetry, spectroscopic, and molecular docking studies, Journal of Sulfur Chemistry 44 (2023) 542–558. https://doi.org/10.1080/17415993.2023.2200142.

[5] H. Benamara, T. Lanez, E. Lanez, Bsa-binding studies of 2-and 4-ferrocenylbenzonitrile: Voltammetric, spectroscopic and molecular docking investigations, Journal of Electrochemical Science and Engineering 10 (2020) 335–346. https://doi.org/10.5599/jese.861.

[6] E. Lanez, L. Bechki, T. Lanez, Antioxidant Activities, Binding Parameters, and Electrochemical Behavior of Superoxide Anion Radicals Twords 1-Ferrocenylmethylthymine and 1-Ferrocenylmethylcytosine, Curr. Phys. Chem. 10 (2019) 10–22. https://doi.org/10.2174/1877946809666190424143752.

[7] E. Lanez, L. Bechki, T. Lanez, Ferrocenylmethylnucleobases: Synthesis, dft calculations, electrochemical and spectroscopic characterisation, Chemistry and Chemical Technology 14 (2020) 146–153. https://doi.org/10.23939/chcht14.02.146.

[8] E. Lanez, L. Bechki, T. Lanez, N6, 9-bis (ferrocenylmethyl) adenine: synthesis, cyclic voltammetric, spectroscopic characterization, and DFT calculations, Scientific Study & Research. Chemistry & Chemical Engineering, Biotechnology, Food Industry 20 (2019) 509–519.

[9] M.J. Frisch, G.W. Trucks, H.B. Schlegel, G.E. Scuseria, M.A. Robb, J.R. Cheeseman, G. Scalmani, V. Barone, B. Mennucci, G.A. Petersson, Gaussian 09. Wallingford, CT: Gaussian, 2009.

[10] M.P. Andersson, P. Uvdal, New scale factors for harmonic vibrational frequencies using the B3LYP density functional method with the triple-ζ basis set 6-311+ G (d, p), J. Phys. Chem. A 109 (2005) 2937–2941.

[11] T. Lu, F. Chen, Multiwfn: A multifunctional wavefunction analyzer, J. Comput. Chem. 33 (2012) 580–592.

[12] P.W. Rose, A. Prlić, A. Altunkaya, C. Bi, A.R. Bradley, C.H. Christie, L. Di Costanzo, J.M. Duarte, S. Dutta, Z. Feng, R.K. Green, D.S. Goodsell, B. Hudson, T. Kalro, R. Lowe, E. Peisach, C. Randle, A.S. Rose, C. Shao, Y.P. Tao, Y. Valasatava, M. Voigt, J.D. Westbrook, J. Woo, H. Yang, J.Y. Young, C. Zardecki, H.M. Berman, S.K. Burley, The RCSB protein

data bank: Integrative view of protein, gene and 3D structural information, Nucleic Acids Res. 45 (2017) D271–D281.

[13] C. Steffen, K. Thomas, U. Huniar, A. Hellweg, O. Rubner, A. Schroer, AutoDock4 and AutoDockTools4: Automated Docking with Selective Receptor Flexibility, J. Comput. Chem. 31 (2010) 2967–2970.

[14] T. Lanez, M. Lanez, R. Lanez, E. Lanez, B. Talbi-Lanez, Computational Screening of Novel Nitroimidazole Candidates: Targeting Key Enzymes of Oral Anaerobes for Anti-Parasitic Potential, Curr. Drug Discov. Technol. (2024).

[15] E. Lanez, N. Zegheb, T. Lanez, In silico ADME, toxicological analysis, molecular docking studies and Molecular dynamics simulation of Afzelin with potential antibacterial effects against Staphylococcus aureus, Turkish Computational and Theoretical Chemistry 7 (2023) 10–16. https://doi.org/10.33435/TCANDTC.1196422.

[16] J. Huang, A.D. Mackerell, CHARMM36 all-atom additive protein force field: Validation based on comparison to NMR data, J. Comput. Chem. 34 (2013) 2135–2145. https://doi.org/10.1002/jcc.23354.

[17] K. Vanommeslaeghe, A.D. MacKerell, Automation of the CHARMM general force field (CGenFF) I: Bond perception and atom typing, J. Chem. Inf. Model. 52 (2012) 3144–3154. https://doi.org/10.1021/ci300363c.

[18] R. Kumari, R. Kumar, A. Lynn, G-mmpbsa -A GROMACS tool for high-throughput MM-PBSA calculations, J. Chem. Inf. Model. 54 (2014) 1951–1962. https://doi.org/10.1021/ci500020m.

[19] J. Dong, N.N. Wang, Z.J. Yao, L. Zhang, Y. Cheng, D. Ouyang, A.P. Lu, D.S. Cao, Admetlab: A platform for systematic ADMET evaluation based on a comprehensively collected ADMET database, J. Cheminform. 10 (2018) 1–11. https://doi.org/10.1186/s13321-018-0283-x.

[20] P. Banerjee, A.O. Eckert, A.K. Schrey, R. Preissner, ProTox-II: A webserver for the prediction of toxicity of chemicals, Nucleic Acids Res. 46 (2018) W257–W263. https://doi.org/10.1093/nar/gky318.

[21] Y. Ouennoughi, H.E. Karce, D. Aggoun, T. Lanez, R. Ruiz-Rosas, B. Bouzerafa, A. Ourari, E. Morallon, A novel ferrocenic copper (II) complex Salen-like, derived from 5-chloromethyl-2-hydroxyacetophenone and N-ferrocenmethylaniline: Design, spectral

approach and solvent effect towards electrochemical behavior of Fc+/Fc redox couple, J. Organomet. Chem. 848 (2017) 344–351.

[22] M. Chebbah, E. Lanez, S. Bouacida, H. Athmani, M.L. Ben Amor, R. Hafidi, A. Bouchemma, Synthesis, Characterization, Structural Analysis, Hirshfeld Surface Studies, and Molecular Docking of 1, 3, 5-Tris (P-Bromophenyl)-1, 3, 5-Triazacyclohexane, Hirshfeld Surface Studies, and Molecular Docking Of 1 (n.d.).

[23] M. Hanane, T. Lanez, I. Zafar, M.S. Afghan, N. Zegheb, N'-Ferrocenylmethyl-N'-phenylbenzohydrazide as a potential DNA binding compound: a combined experimental and computational study, J. Coord. Chem. 76 (2023) 1984–1998. https://doi.org/10.1080/00958972.2023.2275247.

[24] A. Adaika, Y. Bekkar, S. Youmbai, L. Bourougaa, E. Lanez, M.L. Ben Amor, K. Nesba, T. Lanez, L. Bechki, Synthesis, Antioxidant, and Antidiabetic Potential of Ferrocenylmethylnucleobase Compounds: In Vitro, In Silico Molecular Docking, DFT Calculation, and Molecular Dynamic Simulations, Appl. Organomet. Chem. 39 (2025) e7988.

[25] E. LANEZ, D. BENKHELIFA, F.Z. CHERIET, K. GORI, C. SLIMANI, S. KEBACHE, R. OUAKOUAK, O. ABDELLAOUI, Y. DJOUGHI, M.L. BENAMOR, Theoretical Investigation of Mitomycin Derivatives as Dual Inhibitors of HER2 and ER-α: Prospects for Novel Breast Cancer Treatment Strategies, Algerian Journal of Biosciences 6 (2025) 1–20.

[26] E. Lanez, Y. Bekkar, L. Bourougaa, M.L. Benamor, R. Bouraoui, O. Boudebia, A. Adaika, K. Nesba, H. Chaoua, L. Bechki, Antidiabetic potential of mentha piperita essential oil: GC-MS profiling, in vitro, in vivo and in silico analyses, J. Mol. Struct. (2025) 144239.

[27] C. Benine, D.A. Boutlelis, L.A. Touhami, E. Lanez, D.G. Amara, G. Rim, N. Hanen, W. Zahnit, M. Messaoudi, Green synthesis, characterization, antioxidant, interaction with DNA/BSA, and investigation of cytotoxicity against MCF-7 cancer cells of zinc oxide nanoparticles using Hammada scoparia (Pomel) Iljin extract, Int. J. Biol. Macromol. 295 (2025) 139709.

[28] M.L. Tlili, I. Laib, K. Salemi, I. Chetehouna, I. BenMoussa, E. Lanez, Phytochemical Analysis and Evaluation of the Antioxidant, Anti-Inflammatory, Hemolytic, and Antibacterial Effects of Astragalus gombo (L.) Leaves., Acta Chim. Slov. 71 (2024).

[29] M.L. Tlili, F. Alia, E. Bahri, T. Beyat, K. Redouan, E. Lanez, In vivo evaluations of the antidiabetic and antioxidant effects of Olea europaea L.(Chemlali variety) leaves, Acta Periodica Technologica (2025) 3.

[30] S. Khamouli, S. Belaidi, M. Ouassaf, T. Lanez, S. Belaaouad, S. Chtita, Multi-combined 3D-QSAR, docking molecular and ADMET prediction of 5-azaindazole derivatives as LRRK2 tyrosine kinase inhibitors, J. Biomol. Struct. Dyn. 40 (2022) 1285–1298.

[31] N. Zouaghi, E. Lanez, M.L. Benamor, S.N. Nacer, T. Lanez, Y. Bekkar, H. Haddad, K. Al-Abdallat, M. Zihlif, Y. Al-Abdallat, Targeting Alzheimer's Disease via Phytochemicals from Artemisia campestris L.: GC/MS Analysis with an Integrated Computational Approach, Food Biosci. (2025) 108128.

[32] N. Zegheb, C. Boubekri, T. Lanez, E. Lanez, T.T. Küçükkılınç, E. Öz, A. Khennoufa, S. Khamouli, S. Belaidi, In Vitro and In Silico Determination of Some N-ferrocenylmethylaniline Derivatives as Anti-Proliferative Agents Against MCF-7 Human Breast Cancer Cell Lines, Anticancer Agents Med. Chem. 22 (2021) 1426–1437. https://doi.org/10.2174/1871520621666210624141712.

[33] M.L.B.E.N. AMOR, E. LANEZ, Y. Bekkar, A. ADAIKA, T. LANEZ, K. NESBA, L. BECHKI, Exploring the Interactions of Ferrocenylmethylnucleobase Derivatives With BSA and HHb: Insights From Electrochemical, Spectroscopic, ADMET, in Silico Docking, and MD Simulations, ChemistrySelect 10 (2025) e202404678.

[34] A. Rebiai, T. Lanez, M.L. Belfar, Total polyphenol contents, radical scavenging and cyclic voltammetry of algerian propolis, Int. J. Pharm. Pharm. Sci. 6 (2014) 395–400.

[35] M.L. Ben Amor, E. Lanez, Y. Bekkar, A. Adaika, T. Lanez, K. Nesba, L. Bechki, EVALUATION OF FERROCENYLMETHYLNUCLEOBASES DERIVATIVES INTERACTING WITH DNA: INSIGHTS FROM ELECTROCHEMICAL, SPECTROSCOPIC, DFT CALCULATION, MOLECULAR DOCKING AND MOLECULAR DYNAMIC SIMULATIONS., Studia Universitatis Babes-Bolyai, Chemia 70 (2025).

[36] S. Khamouli, S. Belaidi, T. Lanez, Molecular doking and ADMET studies of amino-pyrimidine derivaties as mycobacterium tuberculosis Ser/Thr protein kinases B inhibitors, Journal of Fundamental and Applied Sciences 11 (2019) 914–939.

[37] H. Mouada, T. Lanez, I. Zafar, ROS scavenging, DNA binding and NADPH oxidase inhibition potential of N'-Ferrocenylmethyl-N'-phenylpropionohydrazide using cyclic voltammetry and molecular docking, J. Organomet. Chem. 1007 (2024) 123026.

[38] T. Lanez, M. Henni, H. Hemmami, Development of cyclic voltammetric method for the study of the interaction of antioxidant standards with superoxide anion radicals case of α-tocopherol, Scientific Study and Research: Chemistry and Chemical Engineering, Biotechnology, Food Industry 16 (2015) 161–168.

[39] Y. Bekkar, E. Lanez, T. Lanez, L. Bourougaa, A. Adaika, Z. Saada, A. Benine, Antidiabetic Potential of Synthesized Ferrocenylmethylaniline Derivatives: Insights From In Vitro Studies, Molecular Docking, ADMET, DFT Calculations, and Molecular Dynamics Simulation, Biotechnol. Appl. Biochem. (2025).

[40] Y. Bekkar, E. Lanez, T. Lanez, L. Bourougaa, A. Adaika, A. Benine, Z. Saada, Combined In Vitro and In Silico analysis of ferrocenylmethylaniline derivatives: Antibacterial potential, DFT calculations, and molecular dynamics insights, J. Organomet. Chem. (2025) 123618.

[41] E. Lanez, L. Zerrouk, L. Bechki, T. Lanez, A. Adaika, N. Zegheb, K. Nesba, Synthesis, molecular docking, drug-likeness analysis, and ADMET prediction of nickel and zinc tetraphenyl-porphyrin complexes as possible antioxidant agents, Journal of the Chinese Chemical Society (n.d.).

[42] S.N. Nacer, T. Lanez, Electrochemical properties of N'-ferrocenylmethyl-N'-phenylbenzohydrazide in aqueous and organic mediums, International Letters of Chemistry, Physics and Astronomy 5 (2013) 76–85.

[43] H. Laraoui, E. Lanez, N. Zegheb, A. Adaika, T. Lanez, M. Benkhaled, Anti-Diabetic Activity of Flavonol Glucosides From Fumana montana Pomel: In vitro Analysis, In Silico Docking, ADMET Prediction, and Molecular Dynamics Simulations, ChemistrySelect 8 (2023) e202204512. https://doi.org/10.1002/slct.202204512.

[44] T. Lanez, M. Henni, Dual Anti-Inflammatory and Antidiabetic Potential of Ferrocenylmethylcyanophenyl Derivatives: Integrated In Vitro and In Silico Evaluation, J. Organomet. Chem. (2025) 123956.

[45] A. Khelef, T. Lanez, In vitro assays of the antioxidant activities of ferrocene derivatives bearing amine, amide or hydrazine groups, . 7 (2015) 318–323.

[46] T. Zaiz, T. Lanez, Corrosion inhibition of carbon steel XC70 in H_2SO_4 solution by ferrocene derivative 3-(ferrocenylmethylamine)benzonitrile, Journal of Fundamental and Applied Sciences 4 (2015) 182. https://doi.org/10.4314/jfas.v4i2.8.

[47] T. Lanez, H. Hemmami, Antioxidant Activities of N-ferrocenylmethyl-2- and -3-nitroaniline and Determination of their Binding Parameters with Superoxide Anion Radicals, Curr. Pharm. Anal. 13 (2016) 110–116. https://doi.org/10.2174/1573412912666160831145524.

[48] N. Benyza, F. Allouche, S.W. Dammak, E. Lanez, T. Lanez, Chemical Reactivity, Topological Analysis, and Second-Order Nonlinear Optical Responses of M3O@ Al12N12: A Quantum Chemical Study, Russian Journal of Physical Chemistry A 96 (2022) 2909–2920.

[49] E. Lanez, A. Kedadra, T. Lanez, A. Adaika, N. Zegheb, In vitro antioxidant activity, QSAR, in silico toxicity prediction, molecular docking studies, and molecular dynamics of a series of N-ferrocenylmethylanilines as potent antioxidant agents, J. Organomet. Chem. (2024) 123284.

[50] C. Filote, E. Lanez, V.I. Popa, T. Lanez, I. Volf, Characterization and Bioactivity of Polysaccharides Separated through a (Sequential) Biorefinery Process from Fucus spiralis Brown Macroalgae, Polymers (Basel). 14 (2022) 4106. https://doi.org/10.3390/polym14194106.

[51] A. Boutarfaia, L. Bechki, T. Lanez, E. Lanez, M. Kadri, Synthesis, Antioxidant Activity, and Determination of Binding Parameters of Meso-Tetra-4-Actophenyl-Porphyrin and its Palladium (II) Complex with Superoxide Anion Radicals, Curr. Bioact. Compd. 16 (2019) 1063–1071. https://doi.org/10.2174/1573407215666191017105239.

[52] A. Yahiaoui, N. Benyza, A. Messai, T. Lanez, E. Lanez, Voltametric and molecular docking investigations of ferrocenylmethylaniline and its N-acetylated derivative interacting with DNA, Journal of Electrochemical Science and Engineering (2023). https://doi.org/10.5599/jese.2061.

[53] A. Kedadra, T. Lanez, E. Lanez, H. Hemmami, M. Henni, Synthesis and antioxidant activity of six novel N-ferrocenylmethyl-N-(nitrophenyl)and-N-(cyanophenyl)-acetamides: Cyclic voltammetry and molecular docking studies, Journal of Electrochemical Science and Engineering 12 (2022) 293–304. https://doi.org/10.5599/jese.1162.

[54] M. Meraghni, T. Lanez, E. Lanez, L. Bechki, A. Kennoufa, Experimental and theoretical study on corrosion inhibition of mild steel by meso-tetraphenyl-porphyrin derivatives in acid solution, Journal of Electrochemical Science and Engineering 13 (2023) 217–229. https://doi.org/10.5599/jese.1400.

[55] A. Khennoufa, L. Bechki, T. Lanez, E. Lanez, N. Zegheb, Spectrophotometric, voltammetric and molecular docking studies of binding interaction of N-ferrocenylmethylnitroanilines with bovine serum albumin, J. Mol. Struct. 1224 (2021) 129052. https://doi.org/10.1016/j.molstruc.2020.129052.

[56] Z. Nadjiba, B. Chérifa, T. Lanez, E. Lanez, In Silico Study on N-ferrocenylmethyl-N-phenylpropionohydrazide and N-ferrocenylmethyl-N-pheylbenzohydrazide as anticancer drugs for breast and prostate cancer, International Journal of Pharmacology, Phytochemistry and Ethnomedicine 11 (2018) 17–25.

[57] T. Lanez, M. Feizi-Dehnayebi, E. Lanez, Assessment of the electrostatic binding of ferrocenylmethyl-nitroaniline derivatives to DNA: A combined experimental and theoretical study, J. Mol. Struct. (2024) 138386.

[58] L. ZERROUK, L. BECHKI, E. LANEZ, T. LANEZ, Synthesis, characterization, cyclic voltammetry, and molecular docking studies of the antioxidant activities of superoxide anion radicals towards meso-tetramethophenyl-porphyrin and meso-tetrabiphenyl-porphyrin, Not. Sci. Biol. 16 (2024) 11823. https://doi.org/10.55779/nsb16211823.

[59] A. Adaika, A. Adaika, T. Lanez, E. Lanez, in Vitro and in Silico Evaluation of Anticancer Activity of N,N-Dimethylaminomethylferrocene, Journal of Fundamental and Applied Sciences 11 (2019) 748–768. https://jfas.info/index.php/JFAS/article/view/289.

[60] T. Lanez, H. Benaicha, E. Lanez, M. Saidi, Electrochemical, spectroscopic and molecular docking studies of 4-methyl-5-((phenylimino)methyl)-3H- and 5-(4-fluorophenyl)-3H-1,2-dithiole-3-thione interacting with DNA, Journal of Sulfur Chemistry 39 (2018) 76–88. https://doi.org/10.1080/17415993.2017.1391811.

[61] N. ZEGHEB, L. Elhafnaoui, T. Lanez, N-ferrocenylmethyl-derivatives as spike glycoprotein inhibitors of sars-cov-2 using in silico approaches, (2020).

[62] E. Lanez, T. Lanez, N. Zegheb, In silico ADMET, toxicological analysis, molecular docking studies and Molecular dynamics simulation of Afzelin with potential antibacterial effects

against Staphylococcus aureus, Turkish Computational and Theoretical Chemistry 7 (2023) 10–16.

[63] H. Mouada, T. Lanez, E. Lanez, Investigations of the binding parametres of the interaction of N'-ferrocenylmethyl-N'-phenylaceto-and propionohydrazide with DNA, Journal of Fundamental and Applied Sciences 11 (2019) 875–882.

[64] E. Lanez, L. Bechki, T. Lanez, Computational molecular docking, voltammetric and spectroscopic DNA interaction studies of 9N-(Ferrocenylmethyl)adenine, Chemistry and Chemical Technology 13 (2019) 11–17. https://doi.org/10.23939/chcht13.01.011.

[65] T. Lanez, E. Lanez, A molecular docking study of N-ferrocenylmethylnitroanilines as potential anticancer drugs, International Journal of Pharmacology, Phytochemistry and Ethnomedicine 2 (2016) 5–12.

[66] L. Guan, H. Yang, Y. Cai, L. Sun, P. Di, W. Li, G. Liu, Y. Tang, ADMET-score-a comprehensive scoring function for evaluation of chemical drug-likeness, Medchemcomm 10 (2019) 148–157. https://doi.org/10.1039/C8MD00472B.

[67] G. Xiong, Z. Wu, J. Yi, L. Fu, Z. Yang, C. Hsieh, M. Yin, X. Zeng, C. Wu, A. Lu, ADMETlab 2.0: an integrated online platform for accurate and comprehensive predictions of ADMET properties, Nucleic Acids Res. 49 (2021) W5–W14.

[68] D. Dascalu, D. Larisa Roman, M. Filip, A. Ciorsac, V. Ostafe, A. Isvoran, Solubility and Admet Profiles of Short Oligomers of Lactic Acid, ADMET DMPK 8 (2020) 425–436. https://doi.org/10.5599/admet.801.

[69] J. Hodgson, ADMET—turning chemicals into drugs, Nat. Biotechnol. 19 (2001) 722–726.